Development of Microfluidic Devices Incorporating Electrochemical Detection

Anne Regel

Submitted to the Department of Chemistry and the Graduate School of the University of Kansas in partial fulfillment of the requirements for the degree of Doctor of Philosophy

_____
Susan M. Lunte – Chair

_____
Craig Lunte

_____
Mario Rivera

_____
Timothy Jackson

_____
Karen Nordheden

Dissertation Defense: August 21, 2013

The Dissertation Committee for Anne Regel certifies that this is the

approved version of the following dissertation:

Development of Microfluidic Devices Incorporating Electrochemical Detection

_____

Susan Lunte − Chair

January 31, 2014

Date Approved

Abstract

Neurological disorders affect millions of people worldwide every day. These disorders range from issues affecting mental health, like depression to degenerative diseases such as Alzheimer's and Parkinson's disease. The neurotransmitters dopamine and nitric oxide are of particular interest.

Incorrect regulation of dopamine has been implicated in disorders such as depression, obsessive compulsive disorder, and attention deficit disorder as well as neurological degenerative diseases such as Parkinson's and Alzheimer's. Nitric oxide (NO) has been shown to affect sexual behavior and aggression in rats. NO has been identified as not just a neurotransmitter but also a neuromodulator and is associated with oxidative stress resulting in neurodegeneration. This small gaseous molecule has a short physiological half-life, so nitrite is commonly used for the indirect detection of nitric oxide.

In order to study neurological disorders methods often reduce or eliminate the *in vivo* concentrations of a compound of interest in order to determine its behavioral effect. However, dopamine and NO have complex metabolic pathways and functions, so the resulting behavior may be due to a series of chemical changes in the brain. In order to fully understand how these two neurotransmitters affect behavior both the *in vivo* concentration of multiple analytes and behavior need to be monitored simultaneously.

In this thesis, the development of a small and simple microchip electrophoresis device that can be used as a component of a portable analysis system, which is capable of functioning on an awake and freely moving animal, is described. The development of low cost polymer microchip electrophoresis (ME) devices capable of interfacing with microdialysis (MD)

sampling with electrochemical (EC) detection for the determination of dopamine and nitrite is described. Different fabrication processes were evaluated and optimized to create low cost polymer microchips. A polydimethylsiloxane (PDMS)/glass hybrid microchip capable of interfacing with the hydrodynamic flow from an on-line microdialysis probe was developed with an integrated carbon electrode for EC detection and used for the detection of nitrite. This microchip failed to inject sample into the separation channel when the conductivities of the sample and the BGE were significantly different. In order to understand the injection failure a finite element modeling program, COMSOL, was employed to simulate the sample injection method used for the PDMS/glass hybrid microchip. Also, a new microchip electrophoresis device, called a bow microchip, capable of injecting high conductivity samples while using a low conductivity BGE for electrophoretic separation was modeled. That bow microchip was then evaluated experimentally and made possible the injection of a plug of artificial cerebral spinal fluid into a separation channel containing low conductivity BGE.

In addition to the microchip fabrication and optimization, a graphite/polymethylmethacrylate (PMMA) composite electrode was developed and optimized. This electrode was integrated into a polymer substrate for EC detection and evaluated by both flow–injection analysis and microchip electrophoresis. Future directions include the further optimization of the bow microchip design to simplify the operation and increase the functionality of the microchip. Also, the addition of ionic liquids, which may increase the electron transfer rate, to the graphite/PMMA composite electrode (GPCE) and the use of electrode arrays, which should increase the signal without significantly increasing the background noise, may lower the limits of detection.

This thesis is dedicated to my parents, Carol and Roy Regel, for supporting me every step of the way and my sister, Jennifer Regel, for developing any engineering skills I have, (I bet Mom still regrets giving us those pulleys).

Acknowledgements

This work would not have been possible without the kindness and support of many people. First and foremost I would like to thank my advisor Dr. Susan Lunte for allowing me to work in her lab. Your enthusiasm for my project, no matter how many different materials I tried, made all of the difference. The opportunities you provided both for my scientific and personal development have been incredibly invaluable. I really cannot thank you enough.

I would like to thank my committee members Drs. Craig Lunte, Mario Rivera, Tim Jackson and Karen Nordheden for taking the time out of their busy schedules.

Thank you to Sonja Hall, Anne Smith, Deanne Arensberg and Janet Good for all of your help navigating forms, faxes and scantrons. A special thanks Gary Webber for help with formatting, posters, room reservations and being the official group photographer.

I was very fortunate to work with great people in the Lunte lab. Thank you Dr. Pradyot Nandi, Dr. David Fischer and Dr. Courtney Sloan for helping me get started in the lab, helping me make my first microchips and electrodes, and introducing me to all of the spicy food in Lawrence. I want to also thank all the current lab members Jessica Creamer, Dulan Gunasekara, Rachel Saylor, Abdullah Al-Hossaini, and Nate Oborny, Joe Siegel, Ryan Grigsby; undergraduates Emilie Mainz, Emer Duffy, Roy Meyler, Andrew Longanecker, Erin Reid, Erin Evans, and Pann Pichetsunnthorn; and visiting scientists Giuseppe Caruso, Dr. Fracassi da Silva, Diogenes Meneses dos Santos, Bruno Lucca and Christa Snyder.

To Courtney, Jessica, Rachel, and Erin thank you for your friendship, emotional support and awesome lunch conversation. Apparently, not everyone talks about weekend plans, why dopamine is the best looking CV, and how best to extract collagen out of rat tails over Thai food.

Thank you Jenny, Corey, Tina, Gill, Stacy and Swetha we might not be in the same group or even the same state, but we are united in our mutual geekiness. Dr. Melinda Toumi, thank you so much. You were both my friend and mentor. I don't think I would have made it through orals without you.

Table of Contents

List of Figures and Tables

Chapter One:

Research Objectives and Chapter Summaries

1.1 Research Objectives

Neurological disorders affect millions of people worldwide every day. These disorders range from issues affecting mental health, like depression, to degenerative diseases, such as Alzheimer's and Parkinson's disease. The neurotransmitters dopamine and nitric oxide are of particular interest.

Incorrect regulation of dopamine has been implicated in disorders such as depression, obsessive compulsive disorder, and attention deficit disorder as well as certain neurological degenerative diseases such as Parkinson's and Alzheimer's. Nitric oxide (NO) has been shown to affect sexual behavior and aggression in rats [1-3].

In order to understand how neurotransmitters affect behavior a common method is to reduce or eliminate the compound of interest's concentration in order to determine its behavioral effect. However, both dopamine and NO have complex metabolic pathways and functions, so the resulting behavior may be due to a series of chemical changes in the brain. Therefore, it is necessary to be able to monitor multiple compounds simultaneously to fully understand how these neurotransmitters affect behavior.

This thesis explores the many ways *in vivo* microdialysis sampling and microchip electrophoresis can be used to as monitor multiple analytes. It also explains the many fabrication, material and microchip design considerations that are necessary to couple on-line microdialysis sampling to microchip electrophoresis. The work presented here focused on the development of polymer-based microfluidic devices for the on-line electrochemical analysis of microdialysis samples. The goal is to develop an instrument that is small enough to function on a freely moving animal, so that both neurotransmitters and behavioral information can be obtained simultaneously.

1.2 Chapter Summaries

1.2.1 Chapter Two

This chapter is a review of the analytical considerations and common methods for the separation of microdialysis samples, including liquid chromatography, capillary electrophoresis and microchip electrophoresis (ME). Detection methods for microchip electrophoresis are discussed in detail as are methods for interfacing microdialysis to ME.

1.2.2 Chapter Three

The different fabrication procedures of polymer microchips are presented in detail. Many different master fabrication methods are presented and their relative strengths and weaknesses. Multiple procedures for the *in situ* polymerization of polydimethylsiloxane (PDMS) and polyethlyene glycol diacrylate (PEGDA) are described, as are embossing methods for polymethylmethacrylate (PMMA). The advantages and disadvantages of both materials and fabrication methods are discussed.

1.2.3 Chapter Four

The development of a graphite/PMMA composite electrode (GPCE) integrated into polymer microfluidic devices is presented. Optimization of the electrode composite is described in detail. Modification of the electrode using Cu- and Co-hexacyanoferrates was also explored. The optimal GPCE was evaluated using flow−injection analysis and microchip electrophoresis.

1.2.4 Chapter Five

The development of a microchip capable of coupling microdialysis sampling to microchip electrophoresis with electrochemical detection is presented. A double-T PDMS microchip was used with a pyrolyzed photoresist film (PPF) electrode. Amperometric detection

of nitrite was performed using a wireless electrically isolated potentiostat. Buffer optimization and electrode material are discussed in detail. Additionally, a fundamental weakness in the microchip design, the inability to inject high conductivity samples using a low conductivity background electrolyte, was discovered.

1.2.5 Chapter Six

This chapter focuses on using the finite element analysis software, COMSOL, to determine why the double-T microchip design used in chapter 5 fails to inject high conductivity sample when a low conductivity background electrolyte (BGE) is used. A new microchip design, called a bow microchip, was developed and evaluated with COMSOL to overcome the sample injection issues. The microchip was also evaluated experimentally and successfully injected artificial cerebral spinal fluid (high conductivity) into a low conductivity BGE.

1.2.6 Chapter Seven

This chapter provides a summary of this thesis and presents future directions of this work, including simplifying the bow microchip design. It also proposes modifications to the graphite/PMMA composite electrode developed in chapter four to improve limits of detection (LOD) by the addition of ionic liquids to the composite and the use of an array of electrodes instead of a single electrode.

Chapter Two:

Introduction

2.1 Analytical Methods for Monitoring Neurotransmitters and Behavior Concurrently

Neurological disorders and psychiatric diseases negatively affect people in all corners of the world. According to the World Health Organization, 35.6 million suffer from Alzheimer's disease and other dementias, 24 million people are affected by schizophrenia, and 4.5–19 per 100,000 people have Parkinson's disease globally. These numbers represent only a small number of the individuals afflicted by the many different neurological based diseases [1]. These diseases profoundly affect behavior and although there have been many breakthroughs in the field of neurology there is still much unknown about the underlying neurochemistry of these disorders and their corresponding behavior.

A common method for investigating the link between neurochemistry and behavior is to alter the brain chemistry in an animal, have specific tasks performed by the animal and observe changes in the animal's behavior compared to previous behavior or a control group's behavior. The animals are later sacrificed and the brains analyzed utilizing a multitude of methods including histology and liquid chromatography (LC) with electrochemical (EC), ultraviolet (UV), and/or fluorescence detection [2-4]. This methodology has been used extensively with animal models for research involving memory and cognition as there are many behavioral assessments for evaluating memory and problem solving ability [5, 6].

Manipulation of brain chemistry can be accomplished by genetically altering the animal [7, 8] and/or local administration of chemicals that reduce or enhance neurochemical activity [9-11]. These methods can be very effective for studying diseases but are limited to disorders that have an animal model. However, even in these cases, the animal must be sacrificed before any

quantitative analysis of neurotransmitters in the brain tissue can be performed, which means a large number of animals are needed for each study to get statistically meaningful results.

2.2 *In vivo* Methods for Neurological Research

2.2.1 Sensors

Sensors are one way circumvent the limitations of performing chemical analysis post mortem by making it possible to monitor neuroactive compounds in awake animals. Sensors can be placed in two broad categories: chemical sensors and biosensors. There are many different ways they can function, which will be addressed in this Section, but *in vivo* sensors are generally implemented in a similar way. The sensor(s) is (are) implanted directly into the animal brain to detect a neurotransmitter(s) and/or a compound(s). The dimensions and type of sensor determine the spatial and temporal resolution that can be achieved. Most sensors are small enough that it is possible to simultaneously monitor behavior and neurochemistry in an awake and freely moving animal.

Many chemical sensors use electrochemical detection, most commonly amperometry or voltammetry. Small electrodes that function as the working and reference electrode, typically 10 – 500 μm in diameter are implanted into the region of interest. Smaller working electrodes provide better spatial resolution. Auxiliary electrodes can also be used to improve the stability of the system. However, they are often omitted because of the low current being generated by the microelectrodes [12]. Also, by implanting fewer electrodes, tissue damage is minimized. In the case of electrochemical sensors, the analyte must be electroactive and undergo a redox reaction at the working electrode surface in order to be detected.

Sensors employing amperometric detection use a fixed working electrode potential (vs. a reference electrode) and monitor the current vs. time. Selectivity is often difficult to achieve with this method, as multiple endogenous compounds may be oxidized (or reduced) at similar potentials. This is especially true for analytes that require a high potential to be detected, such as nitrite, which can require a potential of 1 V (vs. Ag/AgCl) or higher. At this potential, endogenous compounds that oxidize at lower potentials, such as ascorbic acid and most catecholamines, will interfere with detection.

The material used for the fabrication of the working electrode is an important factor in the selectivity and sensitivity of a sensor. Platinum is popular due to its inert surface and has been shown to exhibit a low overpotential and good current response for inorganic compounds, especially hydrogen peroxide [13-15]. Gold electrodes are often used for the detection of compounds with thiol functional groups, such as glutathione [16]. However, during amperometric detection many metals suffer from fouling due to the formation of oxides at the surface, especially when high oxidation potentials are used [17]. Carbon electrodes are less prone to fouling as it takes a much higher potential to form an oxide layer in comparison to metal.

Voltammetric methods work by changing the potential of the working electrode (vs. a reference electrode) as a function of time and monitoring the subsequent current. Fast scan cyclic voltammetry (FSCV) is the most common voltammetric method employed for *in vivo* sensors. The shape of the cyclic voltammogram can be used to determine/confirm the identity of an analyte, which has the important advantage of increasing selectivity over amperometric methods [18]. However, like with amperometry, endogenous compounds may interfere with detection.

FSCV has been used to detect many different neurotransmitters including, dopamine [19-21], serotonin [22, 23], adenosine [24] and norepinephrine [25] *in vivo*. This technique exhibits sub-second temporal resolution and has enabled the monitoring of dopamine release from dopaminergic neurons in the striatum of a rat while observing the resulting motor activity [26]. Unfortunately, as scan rate increases so does the background capacitive current. This is normally eliminated by background subtraction [27]. However, when using this method for *in vivo* measurements, the background current also includes the response for endogenous levels of the analyte of interest. Thus, *in vivo* background subtraction can only measure changes in analyte concentration.

Analyte selectivity can be improved for both voltametric and amperometric detection by modifying the working electrodes. Nafion®, a negatively charged material, is often used exclude negatively charged analytes such as ascorbate [28]. Park *et al.* modified a carbon fiber electrode by coating the electrode with a mixture of *m*-phenylenediamine, resorcinol, and Nafion® creating an electrochemical sensor that was selective for nitric oxide (NO). Using this sensor, they were able to amperometrically monitor the extracellular fluid concentration of NO in the parietal cortex of anesthetized rats following an ischemic event [29]. Carbon nanotubes [30] and metal nanoparticles have also been used to modify carbon fiber microelectrodes. These materials add surface area and can lead to unique analyte-material interactions that lead to lower overpotential and higher sensitivity and selectivity [31].

Fiber optics have also been used to fabricate chemical sensors for spectrometric detection. Volkan *et al.* modified a fiber optic probe by coating it with a sol-gel that contained iron (III) ions [32]. Catecholamines formed iron (III) –catecholate complexes and were detected using surface-enhanced Raman spectroscopy. Three analytes, namely dopamine,

norepinephrine, and 4-(2-methylaminoethyl)benzene-1,2-diol were simultaneously detected *in vitro*. However, these probes have not been used *in vivo,* where the number of catecholamines present and matrix affects may lower selectivity. Fluorescence detection has also been used to monitor the pH *in vivo* by implanting an optical fiber, coated with a pH sensitive fluorescent dye, into the brain of an adult rat [33].

Biosensors are similar to chemical sensors except they have at least one biological recognition element, such as an enzyme, that can increase selectivity and in some cases improve limits of detection (LOD) [34]. Glucose biosensors are frequently used to assess the overall metabolic activity in the brain [35, 36]. They are normally fabricated through the immobilization of glucose oxidase on to a platinum microelectrode. The enzyme converts glucose to hydrogen peroxide (H_2O_2), which is detected amperometrically. Similarly, H_2O_2 is generated by the enzyme glutamate oxidase (GluOx), shown in Equation 2.1; GluOx has been utilized to create glutamate specific amperometric biosensors [37-42].

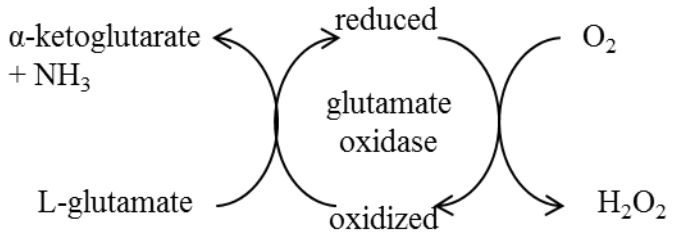

Eq. 2.1

Optical sensors have utilized a different byproduct of the glutamate oxidase reaction, ammonia, to monitor glutamate. In this application, a hydrogel containing glutamate oxidase and an ammonia sensitive florescent dye was used to coat the tip of a fiber-optic probe. This probe had a 100 nM limit of detection (LOD) for glutamate [43].

Chemical- and bio- sensors have many advantages over the more traditional post−mortem analysis of neurotransmitters; however there are also some disadvantages, chiefly, the number of analytes that can be detected simultaneously. In order to maintain selectivity, most sensors can only detect one or two analyte(s). It is possible to implant multiple sensors into the brain to increase the amount of neurochemical information that is obtained. Unfortunately, with each additional probe an increasing amount of tissue damage and inflammation occurs. Fouling, especially bio−fouling is also a problem when sensors are used *in vivo*. Long term implantation can trigger an inflammatory response that reduces sensitivity and makes quantitative studies difficult [44].

2.2.2 Microdialysis Sampling

Another method that can be used to monitor neurotransmitters and behavior simultaneously is microdialysis (MD). MD is a method for sampling the extracellular fluid (ECF) of the brain *via* diffusion through a semipermeable membrane implanted into the brain or other tissue. The resulting samples can be analyzed by a number of analytical methods including LC with electrochemical or fluorescence detection. Since the sampling method relies on the diffusion of small molecules (> 100 kDa) based on their concentration gradient across a semipermeable membrane, the sample collected will contain the non-protein bound molecules in the ECF. Therefore, it is possible to measure multiple analytes in a single microdialysis sample. However, temporal and/or spatial resolution is often inferior in comparison to sensors and behavioral information can also be reduced. These issues will be addressed in detail Section 2.3.

Microdialysis sampling is one of the few ways to sample multiple analytes *in vivo* from the brain. It is especially important in the field of neurology because most disorders involve

more than one neurotransmitter. Often the associated metabolic and/or degradation pathways are also affected. Microdialysis sampling has been used extensively for the monitoring of catecholamines [45, 46], peptides [47-49], amino acid neurotransmitters [50, 51], nitric oxide metabolites [52], and other neuroactive substances in the brain ECF.

Microdialysis sampling works by implanting small probe(s) into the tissue of interest. The diameters of typical microdialysis probes are on the order of 100-300 μm, which makes them minimally invasive. A linear microdialysis probe, shown in Figure 2.1, consists of a semi-permeable membrane that is connected to both inlet and outlet capillary tubing. A solution, with a composition similar to that of the ECF of interest, is perfused through the probe. The semi-permeable membrane allows for small molecules to diffuse across the membrane. Due to the concentration gradient between the ECF and the perfusate, analyte(s) will enter the probe and the resulting analyte-enriched perfusate can then be collected and analyzed [53-55]. Compounds can also move from the perfusate to the ECF, enabling localized delivery. Water moves freely across the membrane, which means there is no net flux of fluid.

Relative recovery of analyte from the extracellular space is defined as the ratio of the concentration of analyte in the perfusate to the *in vivo* concentration, and is often represented as a percent, as shown in Equation 2.2.

$$\text{Recovery } (\%) = 100 * \frac{\text{analyte concentration in perfusate}}{\text{analyte concentration } \textit{in vivo}} \quad \textbf{Eq. 2.2}$$

The flow rate used for sampling influences the recovery. Generally, flow rates less than 0.1 μL/min allow enough time for the perfusate and extracellular fluid to come to equilibrium, resulting in recoveries close to 100% for many analytes [56]. At higher flow rates, there is less time for equilibration between the perfusate and the ECF, leading to lower recoveries. Therefore,

probes need to be calibrated at each flow rate to determine analyte recovery. Techniques for probe calibration have been covered extensively for many different types of analytes and probes [57-61].

Microdialysis sampling is often used for animal studies. This is because each animal can act as its own control [62] and microdialysis probes can be implanted into most tissues [63]. Also, multiple probes can be used with one animal so that blood, spinal fluid and different tissues, such as brain and muscle can be investigated at the same time [64], all of which reduces the number of animals needed for a study. This technique generates no net fluid loss, so sampling can take place over long periods of time (hours to days) and multiple measurements can be performed on a single animal.

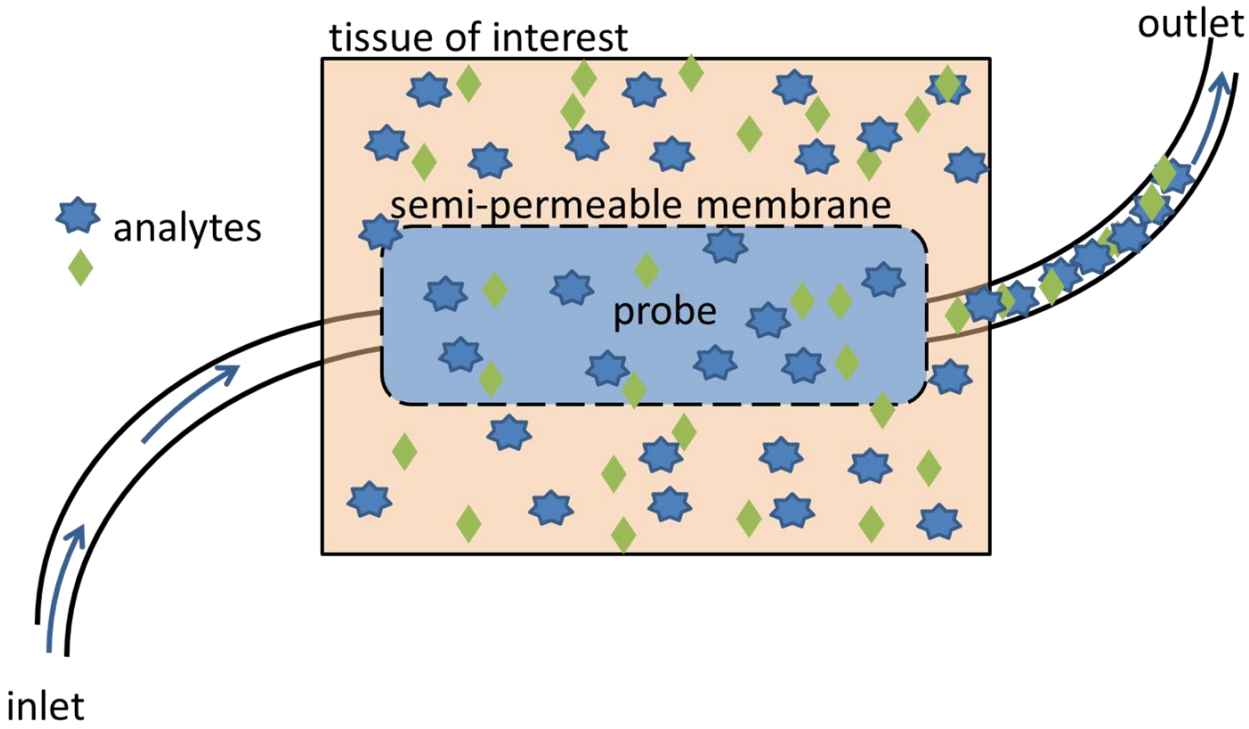

Figure 2.1: Schematic of microdialysis sampling with a linear probe.

2.2.2.1 Microdialysis probes

The two most common probe styles for microdialysis sampling *in vivo* are linear and cannula probes. Linear probes, shown in Figure 2.1, are often used when sampling from a large homogeneous area, such as muscle tissue or skin [65]. Linear probes can have a variety of dialysis membrane lengths, which are commercially available up to 10 mm, but can also be customized in-house. Cannula style probes, shown in Figure 2.2, have smaller sampling areas and are generally used for brain sampling. Commercially available probes use membranes from 1 to 4 mm in length. Flexible cannula type probes are also available and are often used for blood sampling in awake and freely moving animals [66-68].

Westerink *et al.* recently described a relativity new MD probe, the MetaQuant probe. Figure 2.3 shows how the probe functions [69]. This modified cannula microdialysis probe has two separate flows. There is the sampling flow that is perfused through the dialysis portion at a slow flow rate (~200 nL/min), and a second make-up flow, which is much faster (1-2 μL/min), and only goes through the cannula portion of the probe. The low sampling flow rate has been shown to have ~ 100% recovery, which can simplify or even eliminate the need for probe calibration while still having reasonable temporal resolution [70]. However, secondary flow dilutes the sample significantly, which can be problematic for the determination of analytes that exist at low endogenous concentrations.

The material used for the dialysis membrane determines the molecular weight cut-off and influences analyte recovery [71]. Specifically, the charge and hydrophobic properties of the membrane can also influence the recovery of the analyte. Table 2.1 lists some common polymers used for dialysis membranes, along with their material properties and molecular weight (mw) cut-off values; commercially available probes typically have 6-100 kDa mw cutoffs.

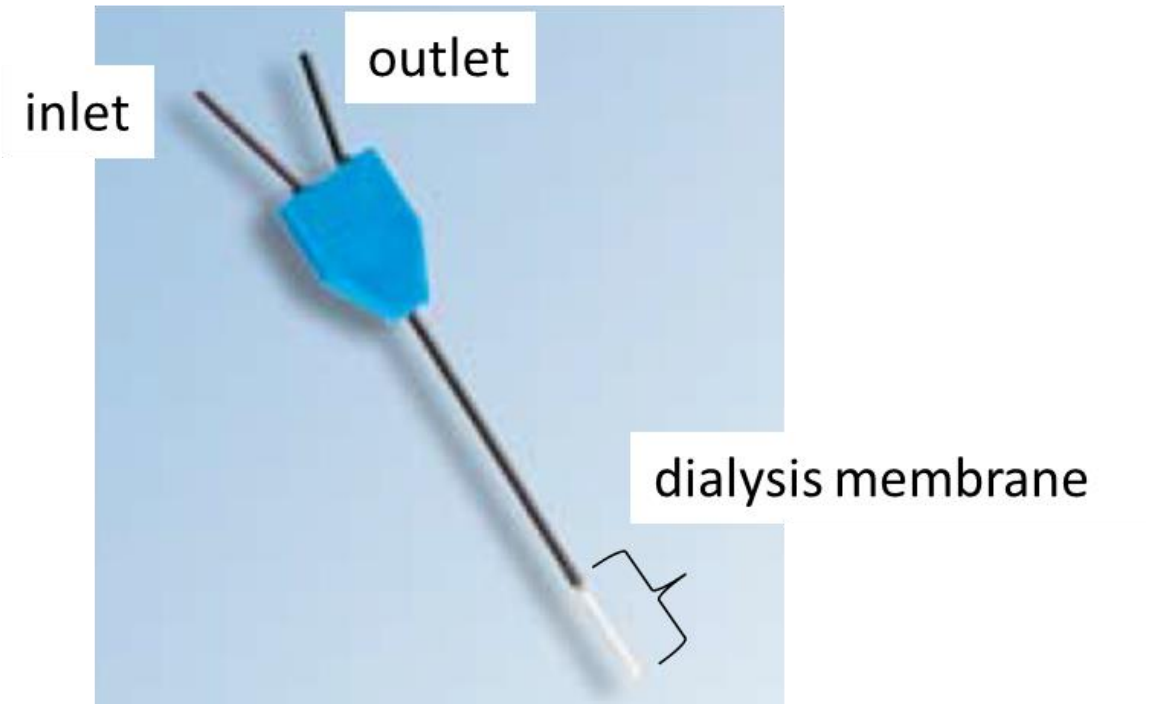

Figure 2.2: Schematic of a cannula probe design for microdialysis sampling of the brain (CMA 12 microdialysis probe).

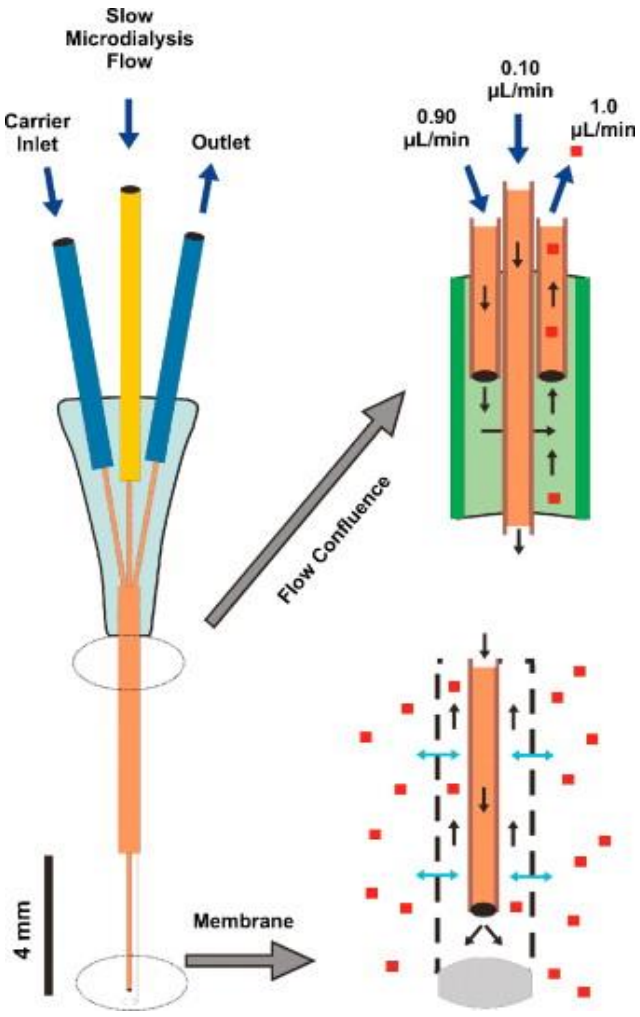

Figure 2.3: Schematic of how the MetaQuant probe functions. (reproduced with permission from [69])

Table 2.1: Physicochemical characteristics of commonly employed microdialysis polymers

Polymer Types	Physicochemical Properties	Typical MW Cutoff (kDa)
DOW (cellulose acetate)[40]	Hydrophilic, slightly negative	5
Cuprophane Regenerated Cellulose[40, 41]	Hydrophilic, neutral	12
polyacrylanitrile (PAN)[40, 41]	Hydrophilic, highly negative	29
Polycarbonate-polyether (PCE)[41]	Hydrophilic, neutral	20
Polyether Sulfone (PES)[42]	Hydrophilic, neutral	100

(adapted with permission from [72])

2.3 Analysis of Microdialysis Samples

Microdialysis samples can be analyzed either off-line or on-line. Off-line samples are generally collected in a vial using a fraction collector and analyzed at a later time and/or location. Microdialysis samples do not contain protein and therefore samples do not undergo enzymatic degradation. The collection process is usually automated so that each sample vial collects perfusate for a fixed amount of time.

As stated earlier in Section 2.2.2, the relative recovery is dependent on the perfusate flow rate for MD sampling. Therefore, when choosing a flow rate (and collection times) for the MD experiment, the following factors must be taken into consideration: (a) the concentration of the analyte in the ECF, (b) the sample volume requirements of the analytical method and (c) the LOD of the analytical method that is used. Faster flow rates provide better temporal resolution (more sample volume over a shorter time), but lower the relative recovery. An example of how flow rate, temporal resolution, and relative recovery influence each other is shown in Figure 2.4 [73]. Practical limitations may also need to be taken into consideration as it can be difficult to manually transfer and inject sub-microliters of sample volume [54, 74].

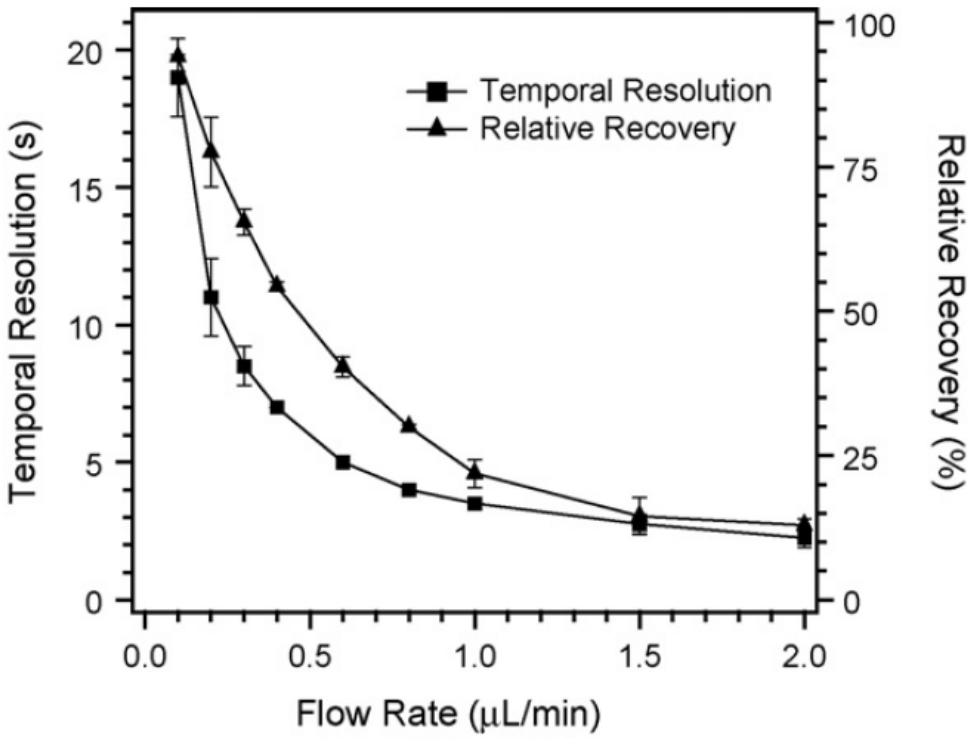

Figure 2.4: A graph depicting the relationship between temporal resolution, MD flow rate and relative analyte recovery for MD sampling (reproduced with permission from [73]

When using separation based analytical methods and on-line MD, a new sample cannot be injected until the previous sample has been analyzed, which can affect temporal resolution. However, for analytical methods that have very fast analyses and sub-microliter sample volumes, near-real time monitoring to be achieved. On-line methods can be fully automated which helps mitigate sample handling issues. Sub-microliter sample volumes can be analyzed without sample loss, mislabeling, evaporation, and surface tension being a problem. Also, sample degradation by exposure to air (e.g., oxidation of ascorbic acid and catecholamines) can be avoided [75, 76].

In order to correlate behavior with specific neurotransmitter activity, microdialysis sampling (both on- and off-line) can be performed in awake and freely moving animals. This is possible because microdialysis probes are relatively non-invasive and can be implanted in specific regions of the brain, allowing the animal to be awake after surgery. One of the disadvantages of using microdialysis for behavior studies in small animals is that the animal is tethered to the syringe pump and the fraction collector or analysis system by tubing. That tubing limits the area in which the animal can move around and also produces a time delay between sample and behavior. Commercial systems for these types of awake microdialysis studies are available from CMA (Holliston, MA, USA) and Bioanalytical Systems, Inc. and are depicted in Figure 2.5.

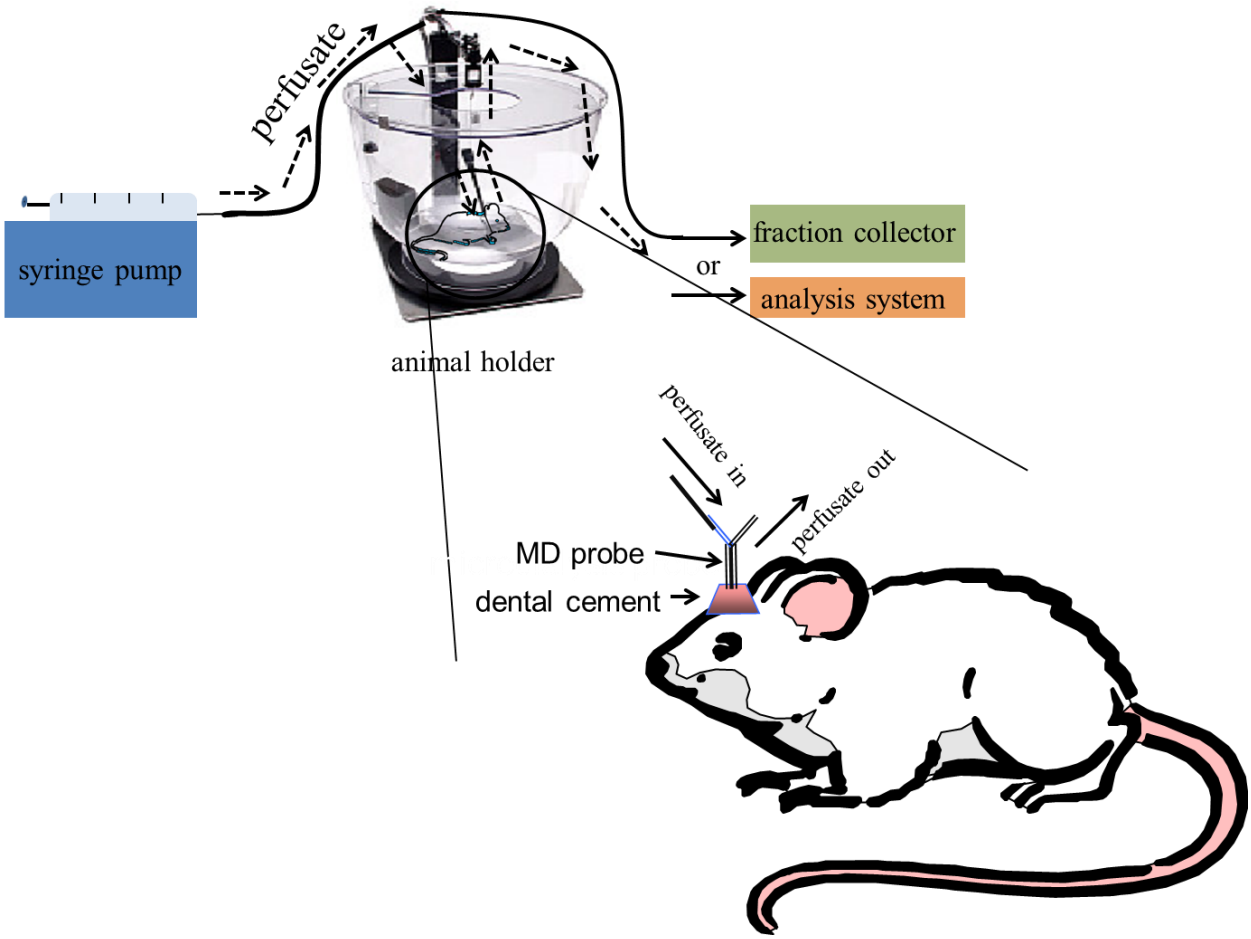

Figure 2.5: Schematic of "RatTurn" system (BASi) for microdialysis sampling of an awake moving small animal (images courtesy of BASi and Dr. Susan Lunte).

2.3.1 Liquid chromatography

Liquid chromatography (LC), including high performance liquid chromatography (HPLC), and capillary chromatography are the most commonly used separation methods for the analysis of MD samples. LC is a very versatile separation method as many different column materials and particle sizes can be used, as well as different detection methods. Due to the aqueous nature of microdialysis samples and the semi-polar nature of many of the analytes examined, reversed-phase systems with alkyl columns are often used [77]. Other types of stationary phases, such as ion exchange [78], mixed mode [79], phenyl [80], amino [81], and carbohydrate [82] columns have also been used for unique applications. The column (length, particle size, and internal diameter) affects the pressure and separation time and should be chosen with respect to the required sensitivity and detection limits. The detection method employed for LC analysis is chosen based on the properties of the analyte(s) or interest and its relative concentration in the dialysate [83, 84]. Typical detectors include UV, fluorescence, electrochemical, and mass spectrometers.

One of the biggest advantages of using a separation-based analysis is the number of analytes that can be monitored [85]. However, LC methods often have poor temporal resolution as typical injection volumes for conventional columns are on the order of 2-10 μL. If the flow rate is 1 μL/min, then the temporal resolution will be 2-10 min. In order to increase temporal resolution microbore and capillary columns have been used. The use of the small diameter (3-4 μm) packing materials also improves separation efficiency. These column modifications lower the sample volume requirements and have improved chromatographic resolution [86]. The smaller diameter columns (<2.1 mm i.d.) provide separations equivalent to those obtained with larger i.d. conventional analytical columns. Capillary columns have very small internal diameters

(150 – 300 μm) and offer the advantage of low consumption of sample and reagents. Typical injection volumes are 50 nL and typical flow rates are on the order of 1-100 μL/min. These aspects make capillary columns particularly well suited for microdialysate analysis [87, 88].

Short microbore columns and capillary columns provide both high sensitivity and rapid analysis (<10 min), and therefore have increased temporal resolution for on-line methods. Unfortunately, these types of columns do present several analytical challenges including the need for low flow rates [89], pulse-free pumps and minimal dead volume [90]. Dead volumes can be reduced by minimizing the length and the internal diameter of all tubing and by employing low volume flow detection cells. Also, in general, capillary LC columns are not as robust as conventional LC columns as they are prone to clogging and require nanoliter volume injectors [89].

2.3.2 Capillary electrophoresis

Capillary electrophoresis (CE) has three basic components, a separation capillary, a power supply and a detector. Figure 2.6 shows a schematic of a typical CE system. The sample is introduced into a capillary filled with a background electrolyte (BGE) using either electrokinetic or pressure injections and can be used for both off-line and on-line analysis. A potential is then applied to both sides of the capillary by a power supply, which induces an electric field. The charged species in the sample will then separate base on charge. Lastly, a detector is interfaced at/close to the end of the capillary; detectors are addressed in more detail in Section 2.4.

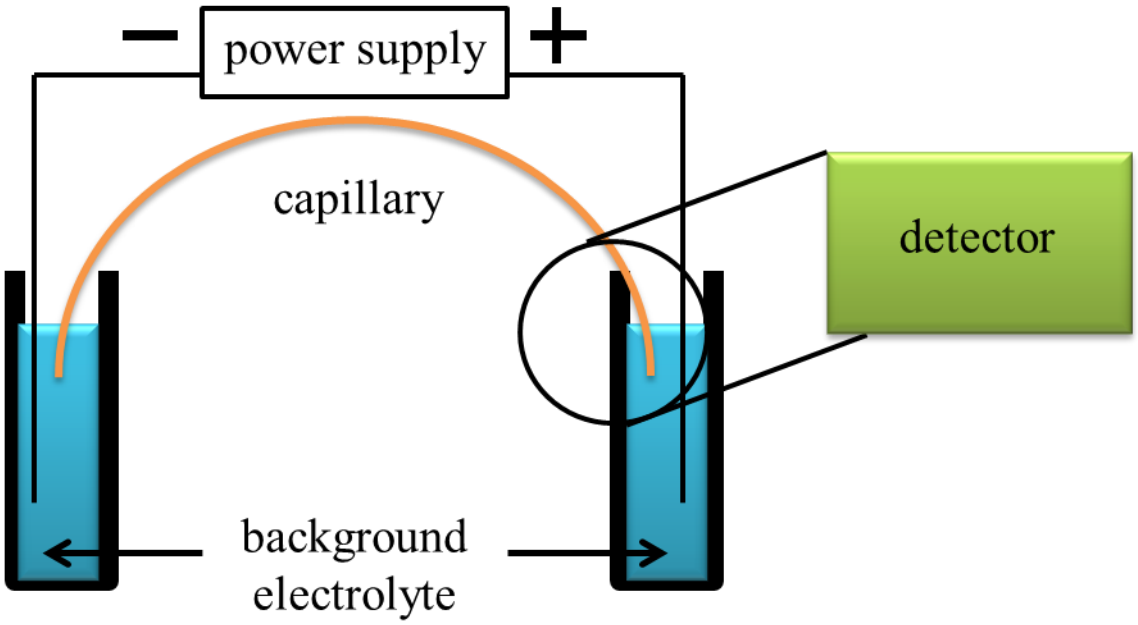

Figure 2.6: Schematic of the basic components of a CE system

CE separates charged compounds in the microdialysis sample based on their electrophoretic mobility in an electric field. An analyte's mobility (μ_a) in this field is based on its charge-to-hydrodynamic radius. A second force, electroosmotic flow (EOF), can cause bulk flow of the BGE toward the cathode. The EOF is caused by the electric double layer's (EDL) movement in an electric field. The EDL is generated by the ionized groups at the capillary surface as shown in Figure 2.7 A. For fused silica capillaries, the silanol groups are ionized above pH 3 and as the pH increases the EOF increases, until it plateaus around pH 10. The EOF flow exhibits a plug profile that is due to the sum of the BGE flow and frictional forces at the walls of the capillary as shown in Figure 2.7 A. The EOF influences the direction and velocity in which the analytes move toward the cathode as shown in Figure 2.7 B. The apparent mobility (μ_{app}) of a charged analyte is the sum of its electrophoretic mobility (μ_a) and the force of the EOF (μ_{EOF}). In capillary zone electrophoresis, neutral species are not affected by the electric field (electrophoretic mobility = 0) and will migrate with the EOF.

The magnitude and/or direction of the EOF can be modified by altering the charge of capillary wall. By coating the wall with an uncharged polymer, such as polyethylene glycol, the EOF can be suppressed. EOF direction can also be reversed so that fluid moves from the cathode to the anode, by making the wall positively charged. This is most commonly accomplished using quaternary ammonium cations, such as cetyltrimethylammonium bromide (CTAB) or tetradecyltrimethylammonium bromide (TTAB).

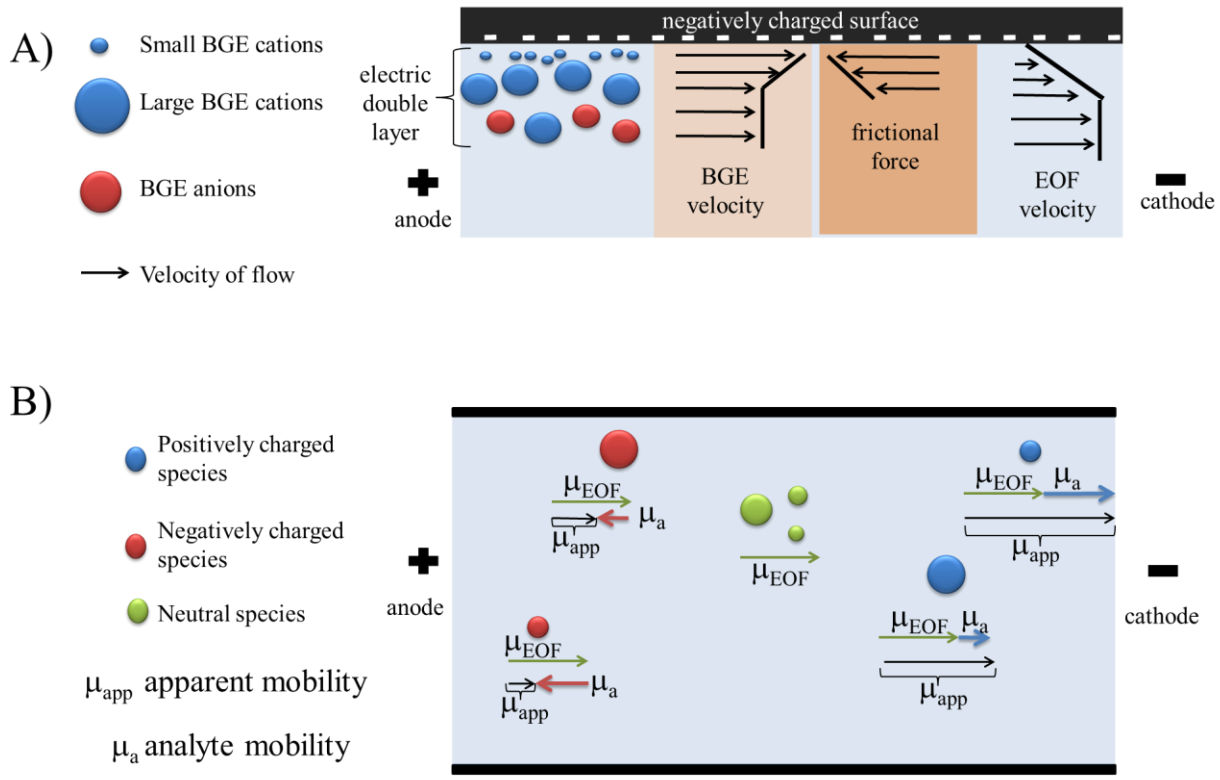

Figure 2.7: A diagram of A) the different components of EOF and B) the apparent electrophoretic motilities (μ_{app}) for differently sized and charged analytes.

CE has some advantages over LC for the analysis of microdialysis samples, specifically very low sample volume requirements (1-10 nL injection volumes), and the ability to perform fast separations (< 1 min). Increasing the field strength in CE increases both the separation speed and efficiency (in the absence of Joule heating). Separations with theoretical plates in the millions have been achieved by capillary zone electrophoresis (CZE) by using high voltages. CE, like LC, can be coupled to a wide variety of detectors and both off-line and on-line analysis methods for microdialysis have been developed [91-93]. However, because such small sample volumes are required in comparison to LC, CE often provides better temporal resolution. This is especially true for on-line methods because of the faster analysis time.

Analysis of microdialysis samples by CE is not without challenges. Microdialysis samples are very high in ionic strength, which increases their conductivity significantly. If the BGE also has a high conductivity, then Joule heating can become problematic, causing bubbles to form as well as band broadening. Thus, for high conductivity BGEs, lower field strengths must be used. This leads to a loss of separation efficiency and increased analysis times. If the BGE has a lower conductivity than the sample, Joule heating is less of a problem. However, this will cause the field strength across the sample plug to decrease, which negatively affects the separation efficiency. This phenomenon is called analyte de-stacking.

Despite its limitations, CE is one of the very few techniques that can monitor multiple analytes (1-30 analytes) in microdialysis samples on-line with near-real time temporal resolution [94-96]. However, the behavioral data that can be collected using on-line microdialysis-CE systems is still limited due to the physical tethering of the animal to the instrumentation that must be used in order to perform microdialysis sampling.

2.3.3 Microchip Electrophoresis (ME)

Microchip electrophoresis (ME) is the corner−stone of the miniaturized total analysis system (μTAS) concept that was first introduced in 1990 by Manz *et al.* [97]. This separation technique needs only μL-mL of supporting reagents and requires less sample volume (pL-nL) than even CE. The advances made in the electronics industry regarding photolithography have been utilized by the ME community to create multi-functional devices that integrate sampling, separation and detection.

A typical format for ME is the simple T design (Figure 2.8 A). The cross injection and gated injection are the most common means of introducing a plug of sample into the separation channel (Figures 2.8 B and 2.8 C, respectively). The cross injection is performed by placing sample in one of the side arms manually, as shown in dark gray in reservoir 4 (Figure 2.8 B i). Voltage is applied between reservoir 4 and reservoir 2 so that the EOF will move the sample from 4 to 2 (Figure 2.8 B ii). Voltage is then applied to reservoir 1 and 2, so that EOF of the background electrolyte (BGE) is reestablished. The sample that was in the injection T is then moved into the separation channel, where separation by electrophoresis occurs (Figure 2.8 B iii).

Gated injection is accomplished by placing sample, shown in dark gray, in reservoir 1 and BGE, shown in light gray, in reservoir 2; see (Figure 2.8 C i). Voltage is applied between reservoir 1 and 4 to establish EOF of sample, and between reservoir 2 and 3 to establish EOF of the BGE; see (Figure 2.8 C ii). This establishes a “gate”, shown by the dotted line. In order to inject sample into the separation channel, the voltage for the EOF of the BGE is turned off and sample is allowed to fill the T area (Figure 2.8 C iii). The BGE EOF voltage is then turned back on to re-form the gate (Figure 2.8 C iv). A sample plug is now in the separation channel where

electrophoresis occurs. Many approaches exist for coupling microchip electrophoresis; these approaches are discussed in the next Section.

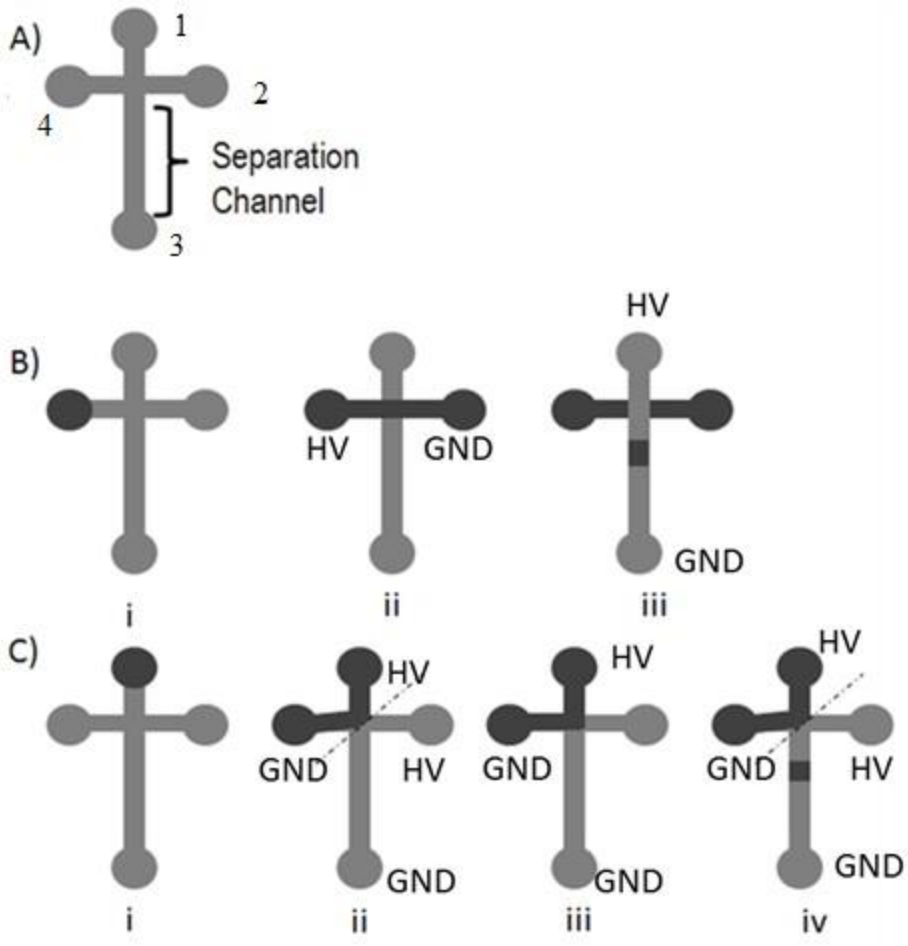

Figure 2.8: Diagram of common injection methods for ME. A) Simple T microchip B) (i) Cross injection method (ii) Reservoir 4 is filled with sample. High voltage is applied and sample flows using EOF into the cross section. (iii) High voltage is applied to BGE in reservoir 1 and sample plug is electrophoresed C) Gated injection method (i) Reservoir 1 is filled with sample. (ii) High voltage is applied to sample and BGE while reservoirs 4 and 3 are grounded; this establishes a gate, shown by the dotted line. (iii) Reservoir 2 high voltage is stopped and sample fills the cross section. (iv) High voltage is replaced in reservoir 2, the gate is re-established (dotted line) and sample plug is electrophoresed. Reproduced with permission from [72].

2.4 Interfacing Microdialysis Sampling to Microchip Electrophoresis

2.4.1 Droplet-based methods

Air based segmented flow was developed in the 1950s for clinical analyzers [56]. More recently, research using liquid phase segmented flow, or droplet based sampling, has increased [98, 99]. Segmented flow is a low volume sample handling technology that has been shown to be very useful for the introduction microdialysis samples into microfluidic devices [100, 101]. This droplet sample collection method has been used for both on- and off-line analysis.

Segmented flow employs a continuous phase and a dispersed phase. The two phases have different hydrophobicities so that they are immiscible with one another. In the case of microdialysis sampling, a hydrophobic liquid is the continuous phase and the aqueous microdialysis sample is the disperse phase, as shown in Figure 2.9. The resulting droplets can be made to have a very controlled and small volume (fL-nL), which means each droplet is in essence a single precise time point. If a 1 µL/min flow rate is used, then each droplet translates into time points in the 60 ns- 60 ms range. At this time scale, temporal resolution is actually determined by diffusion of analytes across the dialysis membrane, which can take a few seconds. The droplets can also be generated very close to the point of sampling, which minimizes sample dispersion and dilution due to diffusion.

Droplet generation is commonly accomplished using either T-junctions [101, 102], shown in Figure 2.9 A, or flow focusing 2.9 B [103]. T-junctions have the continuous phase perpendicular to the disperse phase. The geometry of the junction, the flow rates of the microdialysis perfusate and immiscible phase, and composition of the immiscible phase all determine the volume and the rate at which the drops are being generated [104]. Droplets can be collected during the experiment and analyzed off-line at a later time and/or at another location

without sacrificing temporal resolution [73]. On-line analysis of droplets is also possible. In order to perform on-line ME of droplets the aqueous portion needs to be first de-segmented so that only the aqueous portion enters the separation channel.

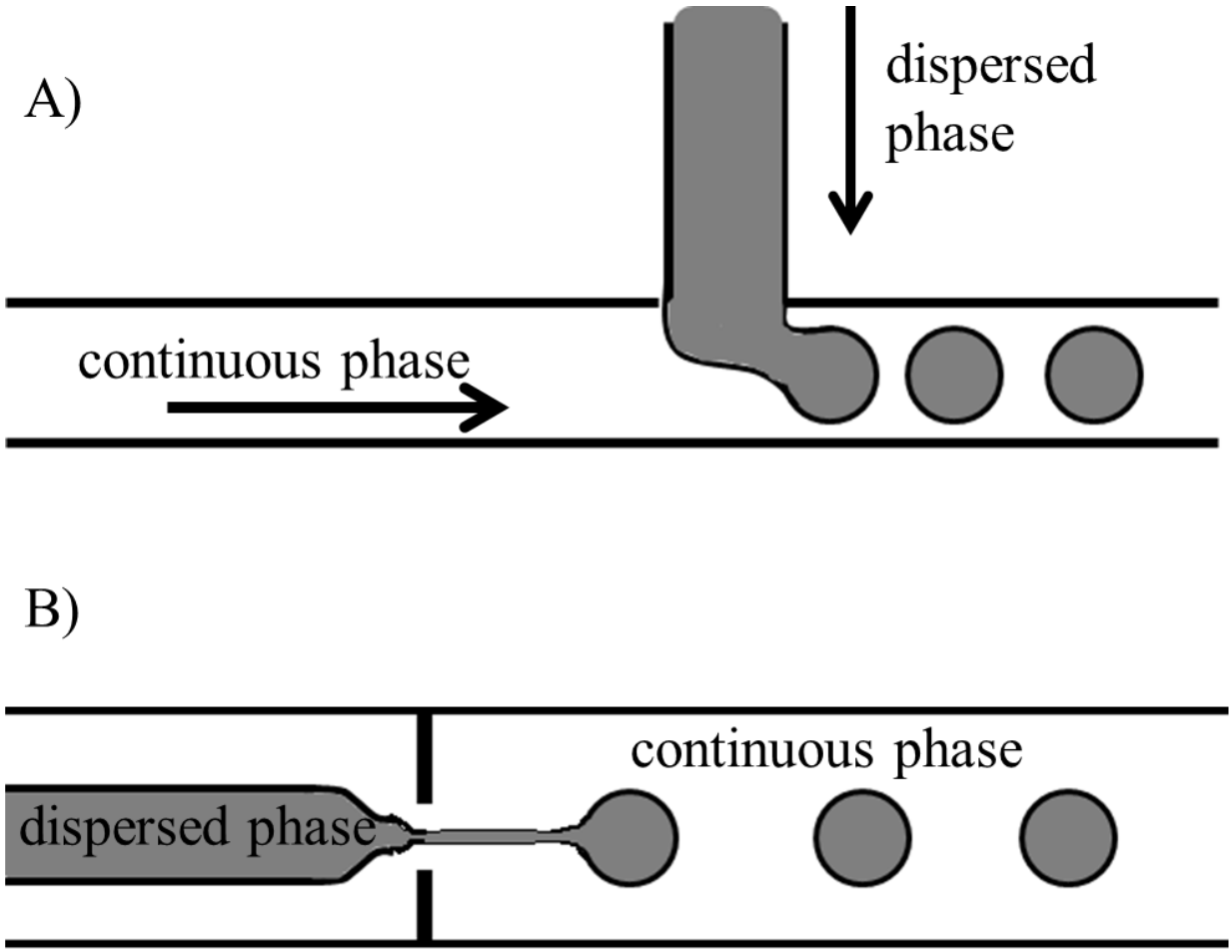

Figure 2.9: A schematic droplet generation using A) T-junction and B) flow-focusing. (adapted with permission from [103])

De-segmenting droplets for electrophoretic analysis has been accomplished by a few different schemes; using T-junctions, K-shaped interfaces and narrow channel "bridges". Edgar *et al.* developed a method that utilized PDMS microchips to de-segment droplets using a T-junction. After the droplet was formed (also using a T-junction), the entire droplet was hydrodynamically pushed into a larger aqueous separation channel, as shown in Figure 2.10 A [105].

Roman *et al.* developed a method for de-segmenting droplets using a K-shaped interface. The continuous phase channel carrying the droplets is hydrophobic and has a K-shaped hydrophilic aqueous channel filled with electrophoresis buffer that connects with one wall of the continuous phase as shown in Figure 2.10 B. The droplet enters the interface and coalesces with the aqueous buffer [106]. Wang *et al.* used a small hydrophilic channel or "extraction bridge" that connected the channel carrying the droplets with the electrophoresis sampling channel, shown in Figure 2.10 C. As the droplets pass the extraction bridge the aqueous content is drawn through it to the electrophoresis sampling channel due to capillary action and hydrophilicity [107].

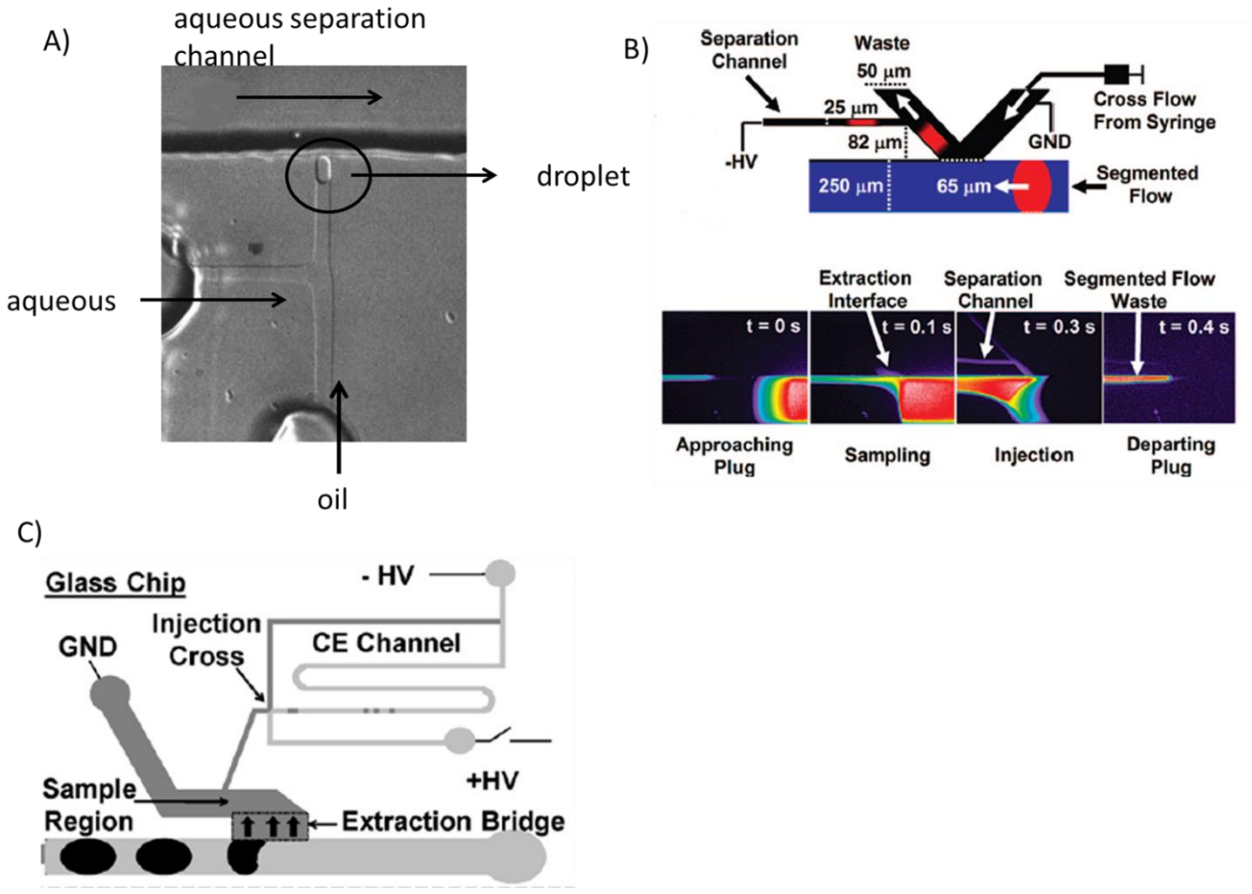

Figure 2.10: A) A micrograph of a droplet being pushed into an electrophoretic separation channel for ME (adapted with permission from [105]) B) A schematic and micrographs of de-segmenting a droplet into an electrophoretic separation channel (adapted with permission from [106]) C) A schematic of de-segmenting a droplet using an extraction bridge into an electrophoretic separation channel (adapted with permission from [107])

2.4.2 Direct coupling to microchip electrophoresis

Achieving our goal of placing an autonomous analytical system on-animal requires microdialysis sampling to be directly coupled to the ME device. Microdialysis samples have been analyzed on-line using microchip electrophoresis through the use of modified versions of the cross and gated injection schemes. Nandi *et al.* developed a modified cross injection method that worked by having the dialysate fill a reservoir using the hydrodynamic pressure produced by the microdialysis flow (Figure 2.11 A). Microdialysis sample was then introduced into the T-section by applying voltage to the filled sample reservoir (Figure 2.11 B). The sample plug was then electrophoresed in the separation channel by applying voltage to the top buffer reservoir, Figure 2.11 C, similar to the standard cross injection [108].

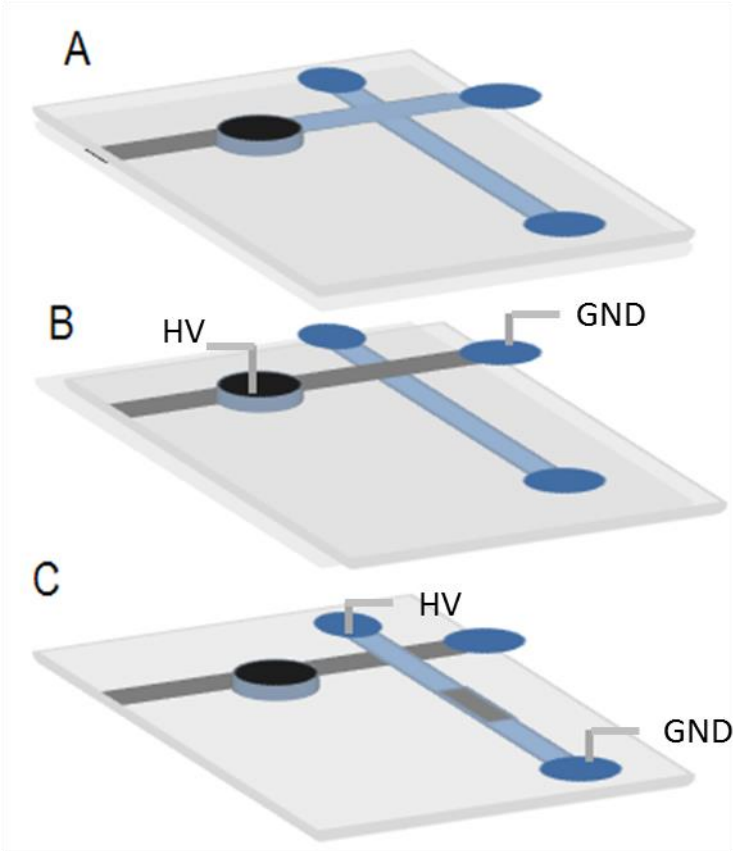

Figure 2.11: Schematic of a simple injection of microdialysis sample to a microchip (adapted with permission from [72])

Simplicity is the main advantage of injecting sample directly from a reservoir. The main disadvantages of this approach are loss of temporal resolution and the need for manual fluid handling. If the volume of the reservoir is 10 µL, and the MD flow rate is 1 µL min^{-1}, then the temporal resolution cannot be less than ten minutes. Also, the sample needs to be manually removed from the reservoir before a new sample can be injected.

An alternative to this method is to inject discreet portions from the continuous microdialysis flow. To accomplish this, the Martin group integrated valves into PDMS microchips to perform pressure injections of dialysate samples into the electrophoresis channel, shown in Figure 2.12 [109]. The microdialysate flows through a channel from the sample inlet (S) to the sample waste outlet (SW). Two PDMS pneumatic valves (1 and 2) are engaged to inject a sample into the electrophoresis channel. Valve 1 closes so that the path to sample waste is blocked and valve 2 is opened to allow the MD sample to enter the separation channel. Once the injection is accomplished the valve positions are reversed and the MD sample is again diverted to waste (Figure 2.12) [109, 110]. This method works extremely well but the pneumatically controlled valves can be difficult to fabricate and require an external gas source for activation, which make the system too large to be placed on an animal.

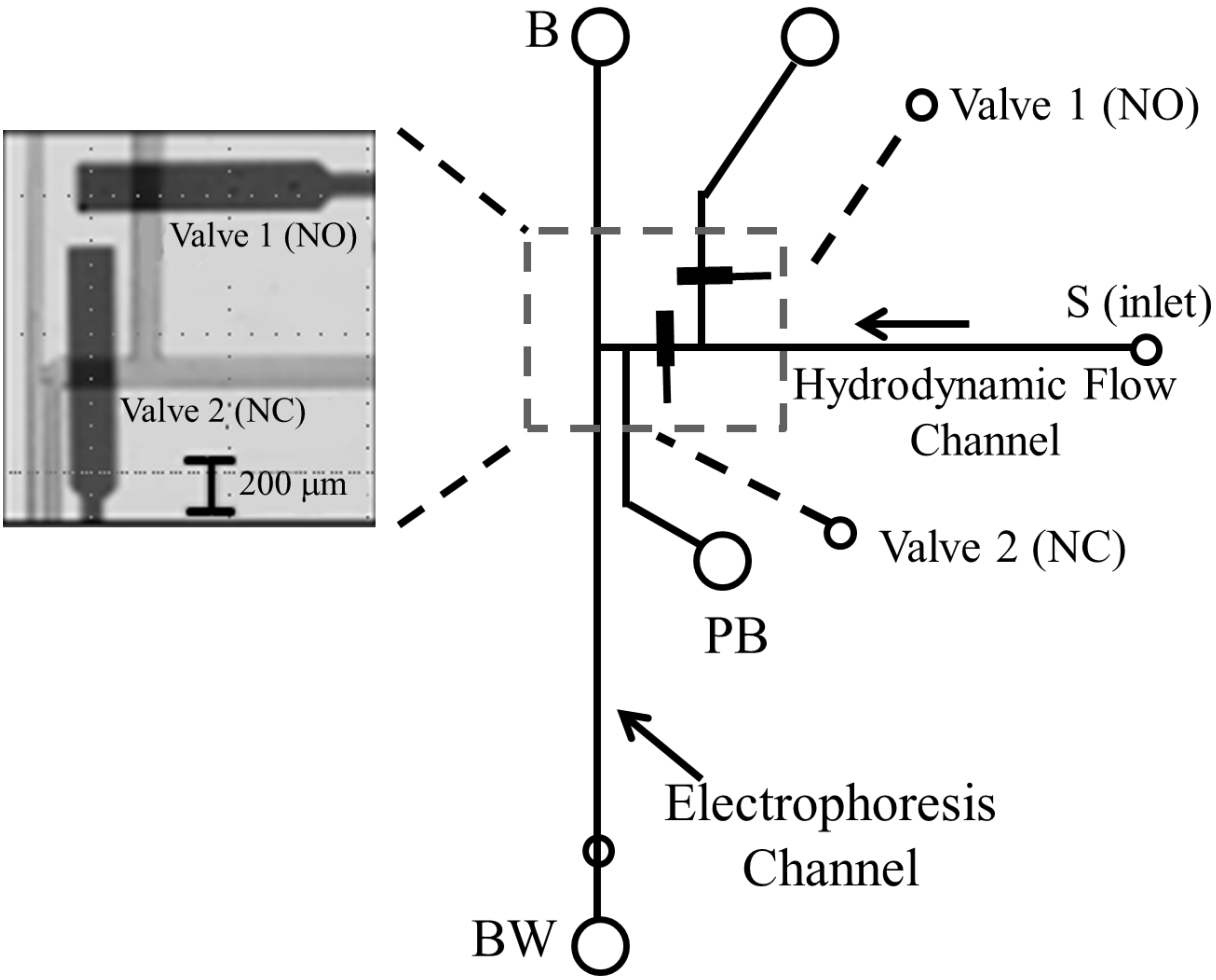

Figure 2.12: PDMS valves pneumatically controlled injection (reproduced with permission from [109])

Huynh *et al.* used a modified gated injection scheme, originally developed by Chen's group [54], in order to perform electrokinetic injections of microdialysate [111]. The steps involved in sample injection with the double-T microchip design are shown in Figure 2.13. First the microdialysate filled the top channel (Fig. 2.12 A), and then a portion of the sample enters into the T-junction and was diverted to the grounded side-arm by EOF. When the high voltage was floated, the microdialysis sample filled the T-junction (Figure 2.13 C), and finally the HV was re-applied and the "gate" re-established. The analytes present in the discreet sample plug were then separated using ME [112].

This type of gated injection approach has several advantages. The sample injection process occurs on a sub-second time scale and can be automated. Additionally, this microchip is smaller and easier to fabricate than the valve-based microchip. However, with this approach, the forces generated by the hydrodynamic and electrophoretic flows need to be balanced in order to establish a gate. It may not be possible to use this approach at very low MD flow rates in conjunction with very high separation voltages because a gate will not form.

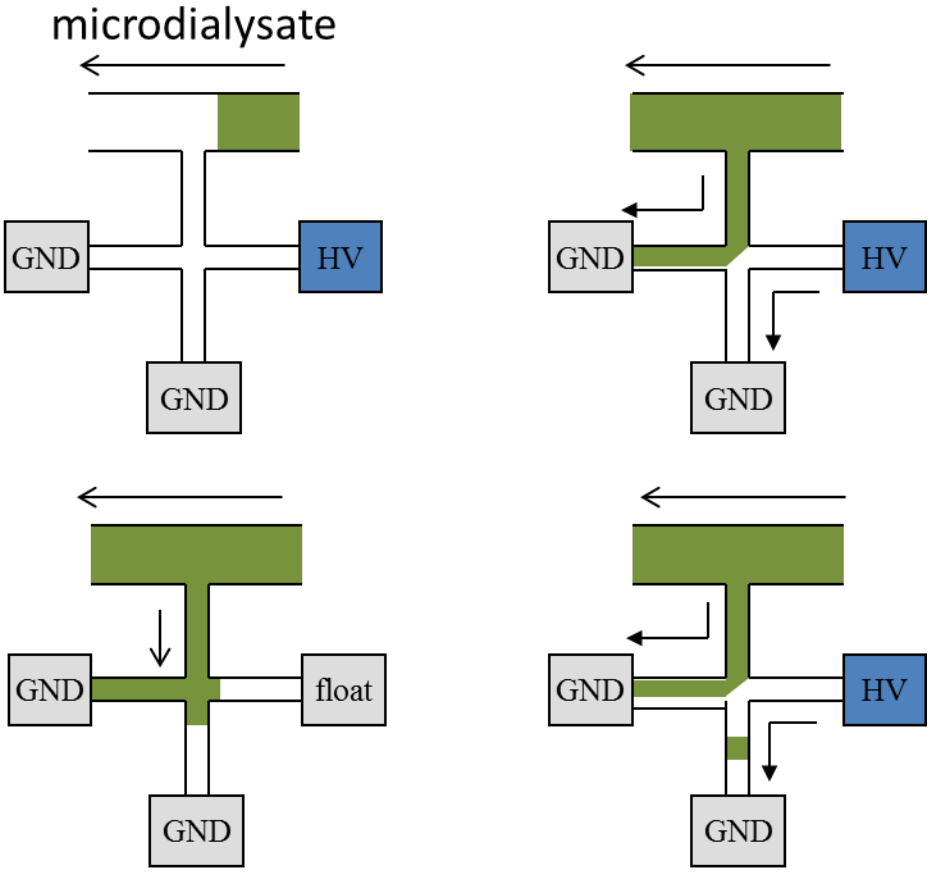

Figure 2.13: Sample injection using a double-T microchip; A) microdialysate fills top channel, B) a portion of the sample enters into the T-junction and is diverted to the grounded side-arm by EOF generated using high voltage (HV), C) the HV is floated and the microdialysis sample was allowed to fill the T-junction and D) the HV is re-applied the gate is again established and a discreet sample plug enters the separation channel. (adapted with permission from [112])

2.5 Detection Methods for Microchip Electrophoresis

2.5.1 Fluorescence detection

Fluorescence is one of the most common detection method employed for microchip electrophoresis [113-115]. Since the laser, optics, and detector are all external to the microchip, this detection method can be used for virtually any microchip analytical system. However, most analytes are not natively fluorescent and therefore need to be derivatized with a fluorescent reagent in order to be detected. This can be a detriment to the analysis since derivatization requires an additional sample preparation step and often causes dilution of the sample. The additional mass and charge of the fluorescent tag can affect the mobility of the analytes, which may help or hurt the separation. Derivatization can also provide selectivity such that the reagent only derivatizes the analyte or class of analytes that are of interest.

One of the most common applications of on-line microdialysis microchip electrophoresis is monitoring amino acid neurotransmitters [116]. Presently, naphthalene-2, 3-dicarboxaldehye (NDA) and o-phthaldehyde (OPA) are the most popular derivatization reagents. Amines that have been derivatized with NDA/CN are more stable and have a higher quantum yield than those derivatized with OPA/RSH [117]. However, the reaction kinetics of the OPA derivatization are faster [118].

2.5.2 Amperometric detection

One advantage of using electrochemical detection in conjunction with microchip electrophoresis is that the supporting hardware, such as potentiostats and function generators, are relatively inexpensive. Also, due to the advances made by the electronics industry, much of the hardware has been miniaturized, which is amenable to the development of portable analysis systems. Amperometry is one of the most commonly used techniques for electrochemical

detection with microchip electrophoresis. This is due in part to its simplicity and sensitivity. Amperometric detection uses a potentiostat to apply a potential (vs. a reference electrode) to the working electrode and monitor the resulting current. The amount of current that is generated by oxidation or reduction of the analyte at the working electrode is directly proportional to the number of moles of analyte being oxidized or reduced, as seen in Equation 2.2.

$$i_t = \frac{dQ}{dt} = nF\frac{dN}{dt} \qquad \textbf{Eq.2.2}$$

Where i_t is the current generated at the working electrode at time t, Q is the charge at the electrode surface, t is time, n is the number of moles of electrons transferred to the electrode surface per mole of analyte, F is Faraday's constant, and N is the number of moles of analyte being oxidized (or reduced).

Since the potential is fixed, there is no capacitive current, leading to lower backgrounds than voltammetric methods. When using amperometry with ME, the separation voltage needs to be decoupled from the potentiostat in order to avoid damage to the instrumentation. Placing the working electrode 5–20 μm away from the end of the separation channel is the most common and a very effective way to decouple the current [119-120]. This arrangement is called end-channel detection and is shown in Figure 2.14 A. However, analytes can diffuse in the small space between the end of the channel and the electrode, which leads to band broadening, poor peak shape, and diminished resolution.

If better resolution is needed, then off-channel detection should be considered. This method utilizes a decoupler, which is a band of metal (or other conductive material) placed in the separation channel before the working electrode. The separation voltage is grounded through the metal, which decouples the separation voltage from the potentiostat [121]. However, electrolysis of water can occur at this ground and will cause bubbles to form in the channel. This

arrangement, depicted in Figure 2.14 B, has been shown to reduce band broadening. However, it has also been shown to decrease sensitivity [122].

One way to preserve both separation resolution and sensitivity is in-channel electrode alignment, shown in Figure 2.14 C. This method uses an electrically isolated potentiostat. Thus, the electrode can safely be placed in the electric field created by separation voltage without grounding the high voltage through the potentiostat [123], which would be very damaging. However, because the working electrode is not decoupled from the electric field, the actual potential at the electrode is the sum of both the potential applied to the electrode using a potentiostat and the potential induced by the electric field. Therefore, the potential at the working electrode for normal polarity is depressed, and in reverse polarity it is increased, by the electric field [124]. This phenomenon makes it difficult to determine exactly what potential needs to be applied to effectively oxidize or reduce the analytes of interest. That information must be experimentally determined for every separation voltage and BGE by generating hydrodynamic voltammograms [125]. In-channel detection also exhibits more background noise due to the instability in the power supply used for the separation voltage. Any small fluctuation in the power will change the potential being applied to the electrode, which in turn will induce capacitive current resulting in more background noise.

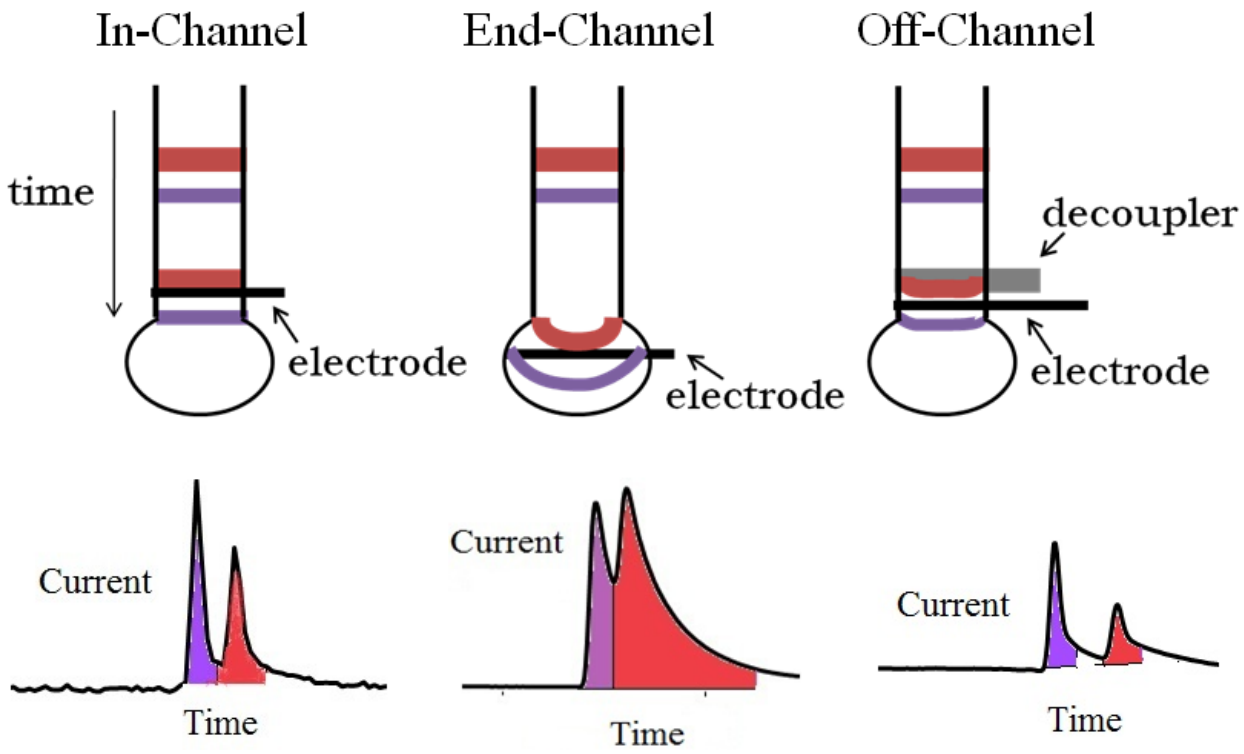

Figure 2.14: The working electrode placement for amperometry and how it affects separation resolution and signal intensity; A) End-channel alignment, B) Off-channel alignment and C) In-channel alignment (reproduced with permission from [122])

2.6 Conclusions and Overall Objective of Thesis

Over the past eight years, the Lunte group has been developing analytical instrumentation and hardware for the simultaneous monitoring of behavior and *in vivo* neurochemistry. Instead of using conventionally sized hardware for small animal studies, the goal is to miniaturize the instrumentation and place it on a larger animal (sheep), shown in Figure 2.15. This approach would allow complex behavior, such as social behavior and/or cognitive tasks to be evaluated while simultaneously monitoring compounds near-real time *in vivo*. In this thesis, methods to couple microdialysis sampling to microchip electrophoresis with electrochemical detection of dopamine and nitrite are described. The next chapter will discuss fabrication of polymer chips that can be used for microchip electrophoresis, an essential component of the overall on-animal MD-ME-EC system.

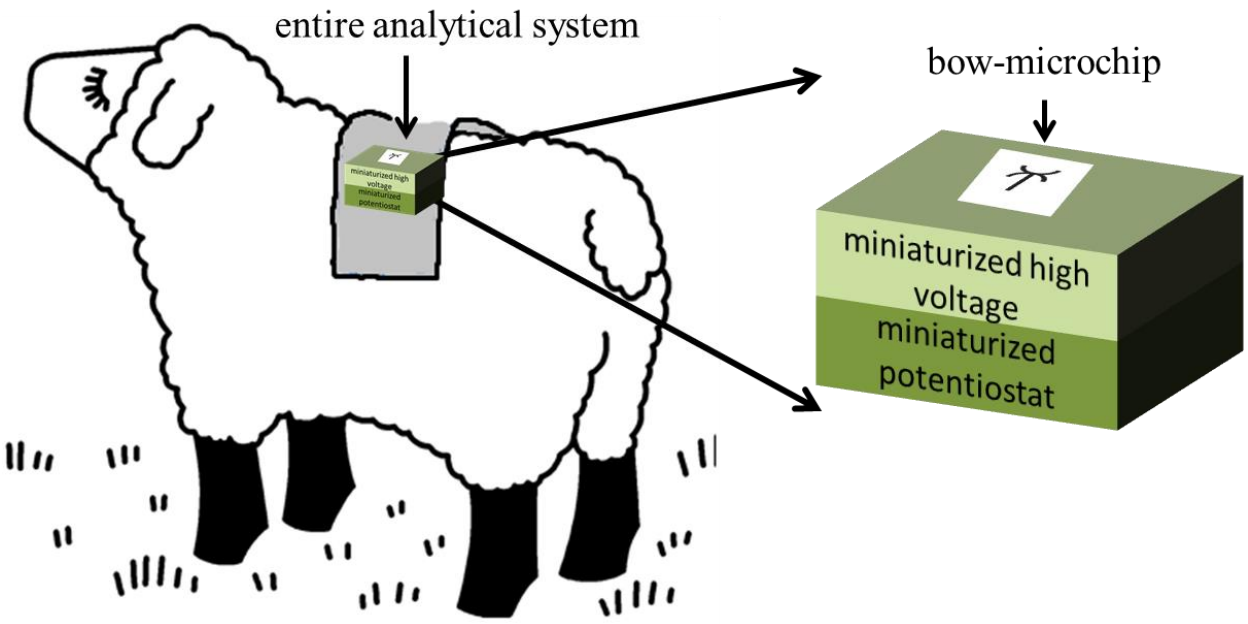

Figure 2.15: Picture of proposed system on a sheep.

2.7 References

[1] Baker, M., Gershanik, O., in: Aarli, J., Dua, T., janca, A., Muscetta, A. (Eds.), *Neurological disorders: public health challenges*, World Health Organization 2006, pp. 140-150.

[2] Murphy, B. L., Arnsten, A. F. T., Goldman-Rakic, P. S., Roth, R. H., *Proceedings of the National Academy of Sciences of the United States of America* 1996, *93*, 1325-1329.

[3] Lim, J. H., Wen, T. C., Matsuda, S., Tanaka, J., Maeda, N., Peng, H., Aburaya, J., Ishihara, K., Sakanaka, M., *Neuroscience Research* 1997, *28*, 191-200.

[4] Berger-Sweeney, J., Stearns, N. A., Murg, S. L., Floerke-Nashner, L. R., Lappi, D. A., Baxter, M. G., *J. Neurosci.* 2001, *21*, 8164-8173.

[5] Leanza, G., Nilsson, O. G., Wiley, R. G., Bjorklund, A., *European Journal of Neuroscience* 1995, *7*, 329-343.

[6] Ramos-Rodriguez, J. J., Pacheco-Herrero, M., Thyssen, D., Murillo-Carretero, M. I., Berrocoso, E., Spires-Jones, T. L., Bacskai, B. J., Garcia-Alloza, M., *Journal of Neuropathology and Experimental Neurology* 2013, *72*, 272-285.

[7] Levine, M. S., Cepeda, C., Hickey, M. A., Fleming, S. M., Chesselet, M.-F., *Trends in Neurosciences* 2004, *27*, 691-697.

[8] Lee, M. K., Price, D. L., *Clinical Neuroscience Research* 2001, *1*, 456-466.

[9] Denys, D., Zohar, J., Westenberg, H. G. M., *J. Clin. Psychiatry* 2004, *65*, 11-17.

[10] Obrenovitch, T. P., Sarna, G. S., Millan, M. H., Lok, S.-Y., Kamauchi, M., Ueda, Y., Symon, L., in: Krieglstein, J., Oberpichler, J. (Eds.), *Pharmacology of Cerebral Ischemia*, Wissenschaftliche Verlagsgesellschaft, Stuttgart 1990, pp. 23-31.

[11] Mani, S. K., Allen, J. M., Rettori, V., McCann, S. M., O'Malley, B. W., Clark, J. H., *Proceedings of the National Academy of Sciences* 1994, *91*, 6468-6472.

[12] Kawagoe, K. T., Zimmerman, J. B., Wightman, R. M., *Journal of Neuroscience Methods* 1993, *48*, 225-240.

[13] Hall, S. B., Khudaish, E. A., Hart, A. L., *Electrochim. Acta* 2000, *45*, 3573-3579.

[14] Zhang, Y., Wilson, G. S., *J. Electroanal. Chem.* 1993, *345*, 253-271.

[15] GonzÁLez-SÁNchez, M. I., GonzÁLez-Macia, L., PÉRez-Prior, M. T., Valero, E., Hancock, J., Killard, A. J., *Plant, Cell & Environment* 2013, *36*, 869-878.

[16] Hiraku, Y., Murata, M., Kawanishi, S., *Biochimica Et Biophysica Acta-General Subjects* 2002, *1570*, 47-52.

[17] McCreery, R. L., *Chem. Rev.* 2008, *108*, 2646-2687.

[18] Fang, H., Pajski, M. L., Ross, A. E., Venton, B. J., *Analytical Methods* 2013, *5*, 2704-2711.

[19] Cheer, J. F., Heien, M. L. A. V., Garris, P. A., Carelli, R. M., Wightman, R. M., *Proceedings of the National Academy of Sciences of the United States of America* 2005, *102*, 19150-19155.

[20] Clark, J. J., Sandberg, S. G., Wanat, M. J., Gan, J. O., Horne, E. A., Hart, A. S., Akers, C. A., Parker, J. G., Willuhn, I., Martinez, V., Evans, S. B., Stella, N., Phillips, P. E. M., *Nat Meth* 2010, *7*, 126-129.

[21] Peairs, M. J., Ross, A. E., Venton, B. J., *Analytical Methods* 2011, *3*, 2379-2386.

[22] Hashemi, P., Dankoski, E. C., Petrovic, J., Keithley, R. B., Wightman, R. M., *Anal. Chem.* 2009, *81*, 9462-9471.

[23] Jacobs, C. B., Vickrey, T. L., Venton, B. J., *Analyst* 2011, *136*, 3557-3565.

[24] Swamy, B. E. K., Venton, B. J., *Anal. Chem.* 2006, *79*, 744-750.

[25] Park, J., Kile, B. M., Mark Wightman, R., *European Journal of Neuroscience* 2009, *30*, 2121-2133.

[26] Robinson, D. L., Hermans, A., Seipel, A. T., Wightman, R. M., *Chem. Rev.* 2008, *108*, 2554-2584.

[27] Howell, J. O., Kuhr, W. G., Ensman, R. E., Wightman, R. M., *J. Electroanal. Chem.* 1986, *209*, 77-90.

[28] Finnerty, N. J., O'Riordan, S. L., Brown, F. O., Serra, P. A., O'Neill, R. D., Lowry, J. P., *Analytical Methods* 2012, *4*, 550-557.

[29] Park, J. K., Tran, P. H., Chao, J. K. T., Ghodadra, R., Rangarajan, R., Thakor, N. V., *Biosens. Bioelectron.* 1998, *13*, 1187-1195.

[30] Santos, R. M., Rodrigues, M. S., Laranjinha, J., Barbosa, R. M., *Biosensors and Bioelectronics* 2013, *44*, 152-159.

[31] Lin, L., Yang, J., Lin, R., Yu, L., Gao, H., Yang, S., Li, X., *Journal of Pharmaceutical and Biomedical Analysis* 2013, *72*, 74-79.

[32] Volkan, M., Stokes, D. L., Vo-Dinh, T., *Applied Spectroscopy* 2000, *54*, 1842-1848.

[33] Grant, S. A., Bettencourt, K., Krulevitch, P., Hamilton, J., Glass, R., *Sensors and Actuators B: Chemical* 2001, *72*, 174-179.

[34] Wilson, G. S., Gifford, R., *Biosensors and Bioelectronics* 2005, *20*, 2388-2403.

[35] Calia, G., Rocchitta, G., Migheli, R., Puggioni, G., Spissu, Y., Bazzu, G., Mazzarello, V., Lowry, J. P., O'Neill, R. D., Desole, M. S., Serra, P. A., *Sensors (14248220)* 2009, *9*, 2511-2523.

[36] Kealy, J., Bennett, R., Lowry, J. P., *Journal of Neuroscience Methods* 2013, *215*, 110-120.

[37] Qin, S., van der Zeyden, M., Oldenziel, W. H., Cremers, T., Westerink, B. H. C., *Sensors* 2008, *8*, 6860-6884.

[38] Hu, Y. B., Mitchell, K. M., Albahadily, F. N., Michaelis, E. K., Wilson, G. S., *Brain Research* 1994, *659*, 117-125.

[39] Tolosa, V. M., Wassum, K. M., Maidment, N. T., Monbouquette, H. G., *Biosensors and Bioelectronics* 2013, *42*, 256-260.

[40] Jamal, M., Xu, J., Razeeb, K. M., *Biosensors and Bioelectronics* 2010, *26*, 1420-1424.

[41] Frey, O., Holtzman, T., McNamara, R. M., Theobald, D. E. H., van der Wal, P. D., de Rooij, N. F., Dalley, J. W., Koudelka-Hep, M., *Biosensors and Bioelectronics* 2010, *26*, 477-484.

[42] Burmeister, J. J., Davis, V. A., Quintero, J. E., Pomerleau, F., Huettl, P., Gerhardt, G. A., *ACS Chemical Neuroscience* 2013, *4*, 721-728.

[43] Kar, S., Arnold, M. A., *Anal. Chem.* 1992, *64*, 2438-2443.

[44] Wisniewski, N., Moussy, F., Reichert, W. M., *Fresenius Journal of Analytical Chemistry* 2000, *366*, 611-621.

[45] Olive, M. F., Koenig, H. N., Nannini, M. A., Hodge, C. W., *J. Neurosci.* 2001, *21*, art. no.-RC184.

[46] Boileau, I., Assaad, J. M., Pihl, R. O., Benkelfat, C., Leyton, M., Diksic, M., Tremblay, R. E., Dagher, A., *Synapse* 2003, *49*, 226-231.

[47] Weber, M., Birklein, F., Neundorfer, B., Schmelz, M., *Pain* 2001, *91*, 251-257.

[48] Ide, S., Hara, T., Ohno, A., Tamano, R., Koseki, K., Naka, T., Maruyama, C., Kaneda, K., Yoshioka, M., Minami, M., *J. Neurosci.* 2013, *33*, 5881-5894.

[49] Maidment, N. T., Brumbaugh, D. R., Rudolph, V. D., Erdelyi, E., Evans, C. J., *Neuroscience* 1989, *33*, 549-557.

[50] Reinhoud, N. J., Brouwer, H.-J., van Heerwaarden, L. M., Korte-Bouws, G. A. H., *ACS Chemical Neuroscience* 2013, *4*, 888-894.

[51] Greco, S., Danysz, W., Zivkovic, A., Gross, R., Stark, H., *Anal. Chim. Acta* 2013, *771*, 65-72.

[52] Wang, J., Lu, M., Yang, F., Zhang, X., Bayens, W. R. G., Campana, A. M. G., *Anal. Chim. Acta* 2001, *428*, 173-181.

[53] Nandi, P., Lunte, S. M., in: Pawliszyn, J., Lord, H. L. (Eds.), *Handbook of Sample Preparation*, John Wiley & Sons, Inc., Hoboken 2010, pp. 103-123.

[54] Schultz, K. N., Kennedy, R. T., *Annual review of analytical chemistry* 2008, *1*, 627-661.

[55] Krebs-Kraft, D. L., Frantz, K. J., Parent, M. B., in: Lajtha, A. (Ed.), *Handbook of Neurochemistry and Molecular Neurobiology: Practical Neurochemistry Methods* Springer, New York 2007, pp. 219-256.

[56] Menacherry, S., Hubert, W., Justice, J. B., Jr., *Anal. Chem.* 1992, *64*, 577-583.

[57] Song, Y., Lunte, C. E., *Anal. Chim. Acta* 1999, *379*, 251-262.

[58] Scheller, D., Kolb, J., *Journal of Neuroscience Methods* 1991, *40*, 31-38.

[59] Kehr, J., *J. Neurosci. Methods* 1993, *48*, 251-261.

[60] Davies, M. I., Cooper, J. D., Desmond, S. S., Lunte, C. E., Lunte, S. M., *Advanced Drug Delivery Reviews* 2000, *45*, 168-188.

[61] Whitaker, G., Lunte, C. E., *Journal of Pharmaceutical and Biomedical Analysis* 2010, *53*, 490-496.

[62] Ault, J. M., Riley, C. M., Meltzer, N. M., Lunte, C. E., *Pharm. Res.* 1994, *11*, 1631-1639.

[63] de la Peña, A., Liu, P., Derendorf, H., *Advanced Drug Delivery Reviews* 2000, *45*, 189-216.

[64] Kaul, S., Williams, T. D., Lunte, C. E., Faiman, M. D., *J Pharm Biomed Anal* 2010, *51*, 13.

[65] Zuo, H., Ye, M., *Current Separations* 1995, *14*, 54-57.

[66] Yang, H., Wang, Q., Elmquist, W. F., *Pharm. Res.* 1997, *14*, 1455-1460.

[67] Telting-Diaz, M., Scott, D. O., Lunte, C. E., *Anal. Chem.* 1992, *64*, 806-810.

[68] Huff, J. K., Davies, M. I., *Journal of Pharmaceutical and Biomedical Analysis* 2002, *29*, 767-777.

[69] Cremers, T. I. F. H., de Vries, M. G., Huinink, K. D., Loon, J. P. v., Hart, M. v. d., Ebert, B., Westerink, B. H. C., De Lange, E. C. M., *Journal of Neuroscience Methods* 2009, *178*, 249-254.

[70] Sood, P., Cole, S., Fraier, D., Young, A. M. J., *J Neurosci Methods* 2009, *185*, 39-44.

[71] Zhao, Y., Liang, X., Lunte, C. E., *Anal. Chim. Acta* 1995, *316*, 403-410.

[72] Ducey, M. W., Regel, A. R., Nandi, P., Lunte, C. E., Lunte, S. M., in: Pawliszyn, J. (Ed.), *Comprehensive Sampling and Sample Preparation*, Academic Press, Oxford 2012, pp. 535-557

[73] Wang, M., Slaney, T., Mabrouk, O., Kennedy, R. T., *Journal of Neuroscience Methods* 2010, *190*, 39-48.

[74] Rossell, S., Gonzalez, L. E., Hernández, L., *Journal of Chromatography B* 2003, *784*, 385-393.

[75] Jin, G., Cheng, Q., Feng, J., Li, F., *J. Chrom. Sci.* 2008, *46*, 276-287.

[76] Tsai, P.-J., Wu, J.-P., Lin, N.-N., Kuo, J.-S., Yang, C.-S., *Journal of Chromatography, B: Biomedical Applications* 1996, *686*, 151-156.

[77] Faro, L. R. F., Ferreira Nunes, B. V., Alfonso, M., Ferreira, V. M., Durán, R., *Toxicology* 2013, *311*, 154-161.

[78] Heidbreder, C. A., Lacroix, L., Atkins, A. R., Organ, A. J., Murray, S., West, A., Shah, A. J., *Journal of Neuroscience Methods* 2001, *112*, 135-144.

[79] Motoyama, A., Xu, T., Ruse, C. I., Wohlschlegel, J. A., Yates, J. R., *Anal. Chem.* 2007, *79*, 3623-3634.

[80] Tsai, T.-H., *Journal of Chromatography A* 2005, *1073*, 317-322.

[81] Berthemy, A., Newton, J., Wu, D., Buhrman, D., *Journal of Pharmaceutical and Biomedical Analysis* 1999, *19*, 429-434.

[82] Mannino, S. I., Cosio, M. S., Zimei, P., *Electroanalysis* 1996, *8*, 353-355.

[83] Perry, M., Li, Q., Kennedy, R. T., *Anal. Chim. Acta* 2009, *653*, 1-22.

[84] Nandi, P., Lunte, S. M., *Anal. Chim. Acta* 2009, *651*, 1-14.

[85] Devall, A. J., Blake, R., Langman, N., Smith, C. G. S., Richards, D. A., Whitehead, K. J., *Journal of Chromatography B* 2007, *848*, 323-328.

[86] Schultz, K. N., Kennedy, R. T., *Annual Review of Analytical Chemistry* 2008, *1*, 627-661.

[87] Baseski, H. M., Watson, C. J., Cellar, N. A., Shackman, J. G., Kennedy, R. T., *Journal of Mass Spectrometry* 2005, *40*, 146-153.

[88] Shackman, H. M., Shou, M., Cellar, N. A., Watson, C. J., Kennedy, R. T., *J. Neurosci. Methods* 2006, *159*, 86-92.

[89] Column Guide, in: Brucker-Microchrom, *4*

[90] Cooley, J. C., Ducey, M. W., Regel, A. R., Nandi, P., Lunte, S. M., Lunte, C. E., in: Mueller, M. (Ed.), *Microdialysis in Drug Deveopment*, Springer 2012.

[91] Parrot, S., Bert, L., Mouly-Badina, L., Sauvinet, V., Colussi-Mas, J., Lambas-Senas, L., Robert, F., Bouilloux, J. P., Suaud-Chagny, M. F., Denoroy, L., Renaud, B., *Cell. Mol. Neurobiol.* 2003, *23*, 793-804.

[92] Bowser, M. T., Kennedy, R. T., *ELECTROPHORESIS* 2001, *22*, 3668-3676.

[93] Lada, M. W., Kennedy, R. T., *Anal. Chem.* 1996, *68*, 2790-2797.

[94] Nandi, P., Scott, D. E., Desai, D., Lunte, S. M., *ELECTROPHORESIS* 2013, *34*, 895-902.

[95] Zhou, S. Y., Zuo, H., Stobaugh, J. F., Lunte, C. E., Lunte, S. M., *Anal. Chem.* 1995, *67*, 594-599.

[96] Hogan, B. L., Lunte, S. M., Stobaugh, J. F., Lunte, C. E., *Anal. Chem.* 1994, *66*, 596-602.

[97] Manz, A., Graber, N., Widmer, H. M., *Sens. Actuators B* 1990, *1*, 244-248.

[98] Baroud, C. N., Gallaire, F., Dangla, R., *Lab on a Chip* 2010, *10*, 2032-2045.

[99] Subramanian, B., Kim, N., Lee, W., Spivak, D. A., Nikitopoulos, D. E., McCarley, R. L., Soper, S. A., *Langmuir* 2011, *27*, 7949-7957.

[100] Jensen, E. C., Bhat, B. P., Mathies, R. A., *Lab on a Chip* 2010, *10*, 685-691.

[101] Schneider, T., Burnham, D. R., VanOrden, J., Chiu, D. T., *Lab on a Chip* 2011, *11*, 2055-2059.

[102] Thorsen, T., Roberts, R. W., Arnold, F. H., Quake, S. R., *Physical Review Letters* 2001, *86*, 4163-4166.

[103] Ralf, S., Martin, B., Thomas, P., Stephan, H., *Reports on Progress in Physics* 2012, *75*, 016601.

[104] Garstecki, P., Fuerstman, M. J., Stone, H. A., Whitesides, G. M., *Lab on a Chip* 2006, *6*, 437-446.

[105] Edgar, J. S., Pabbati, C. P., Lorenz, R. M., He, M., Fiorini, G. S., Chiu, D. T., *Anal. Chem.* 2006, *78*, 6948-6954.

[106] Roman, G. T., Wang, M., Shultz, K. N., Jennings, C., Kennedy, R. T., *Anal. Chem.* 2008, *80*, 8231-8238.

[107] Wang, M., Roman, G. T., Perry, M. L., Kennedy, R. T., *Anal. Chem.* 2009, *81*, 9072-9078.

[108] Nandi, P., Desaias, D. P., Lunte, S. M., *ELECTROPHORESIS* 2010, *31*, 1414-1422.

[109] Mecker, L. C., Martin, R. S., *Anal. Chem.* 2008, *80*, 9257-9264.

[110] Li, M. W., Martin, R. S., *ELECTROPHORESIS* 2007, *28*, 2478-2488.

[111] Chen, S. H., Lin, Y. H., Wang, L. Y., Lin, C. C., Lee, G. B., *Anal. Chem.* 2002, *74*, 5146-5153.

[112] Huynh, B. H., Fogarty, B. A., Martin, R. S., Lunte, S. M., *Anal. Chem.* 2004, *76*, 6440-6447.

[113] Kuswandi, B., Nuriman, Huskens, J., Verboom, W., *Anal. Chim. Acta* 2007, *601*, 141-155.

[114] Johnson, M. E., Landers, J. P., *ELECTROPHORESIS* 2004, *25*, 3513-3527.

[115] Uchiyama, K., Nakajima, H., Hobo, T., *Anal. Bioanal. Chem.* 2004, *379*, 375-382.

[116] Huynh, B. H., Fogarty, B. A., Nandi, P., Lunte, S. M., *J. Pharm. Biomed. Anal.* 2006, *42*, 529-534.

[117] Roach, M. C., Harmony, M. D., *Anal. Chem.* 1987, *59*, 411-415.

[118] Toyo'oka, T., *Anal. Chim. Acta* 2002, *465*, 111-130.

[119] Wu, C.-C., Wu, R.-G., Huang, J.-G., Lin, Y.-C., Chang, H.-C., *Anal. Chem.* 2003, *75*, 947-952.

[120] Wallingford, R. A., Ewing, A. G., *Anal. Chem.* 1987, *59*, 1762-1766.

[121] Osbourn, D. M., Lunte, C. E., *Anal. Chem.* 2003, *75*, 2710-2714.

[122] Fischer, D. J., Hulvey, M. K., Regel, A. R., Lunte, S. M., *Electrophoresis* 2009, *30*, 3324-3333.

[123] Chen, C., Hahn, J., *Environ Chem Lett* 2011, *9*, 491-497.

[124] Gunasekara, D. B., Hulvey, M. K., Lunte, S. M., *ELECTROPHORESIS* 2011, *32*, 832-837.

[125] Martin, R. S., Ratzlaff, K. L., Huynh, B. H., Lunte, S. M., *Anal. Chem.* 2002, *74*, 1136-1143.

Chapter 3:

Polymer Microchip Fabrication

3.1 Introduction

An on-line microdialysis (MD) sampling system coupled to a microchip electrophoresis (ME) device with an integrated working electrode(s) for amperometric detection could simultaneously monitor neurochemistry and behavior on an animal. A key component of this on-line system would be the microchip used to perform an ME separation of the MD sample. The material and fabrication techniques used to produce microfluidic devices are intimately tied to their function, cost, and over-all performance. In this thesis, polymer based microfluidic devices were of particular interest due to their relatively low cost, simple fabrication methods and diverse material available [1, 2].

Historically, ME devices were fabricated from glass do to its outstanding separation qualities and ruggedness [3, 4]. It is a very hydrophilic, and thus adsorption of many biological analytes is minimal. An exception to this is proteins or peptides with many basic residues because they can electrostatically interact with the ionized silanol groups [5]. Most glass microchips are constructed using thermal bonding which allows them to withstand very high pressures without leaking. Also, the procedures for chemical modification of glass, such as functionalization and antibody immobilization are well established, which makes integrating multiple functions onto glass easier [6]. Glass also exhibits very high optical transmission and low background fluorescence, which makes it ideal for fluorescence detection. However, integrating electrodes into glass microchips can be expensive and often limits the electrode material to a metal, which is not ideal for many organic analytes [7-9]. Also, the fabrication of glass microchips is difficult, time consuming and expensive.

Due to the drawbacks associated with glass microchip fabrication, the use of polymer substrates for ME has increased significantly over the last 10 years [10-13]. Compared to glass,

polymer microchips are inexpensive, easy to fabricate, and more amenable to mass production [14-18]. Polydimethlysiloxane (PDMS) is one of the most commonly used polymers because it is inexpensive and easy to use. This also makes it ideal for prototyping new designs. Unfortunately, PDMS is very hydrophobic, which makes adsorption of organic molecules, especially when using biological samples, very problematic. Adsorption can lead to unstable electroosmotic flow (EOF) and can drastically change the migration time of analytes [19]. This inconsistent EOF often leads to poor chip-to-chip reproducibly. Therefore, internal standards are normally needed to achieve acceptable precision for migration time, peak area and/or peak height. PDMS can swell or constrict depending on the humidity and light manual pressure can deform the channels, which means shipping and storing these devices can be problematic. Thus, more and more research has been dedicated to acrylate based substrates, such as polymethylmethacrylate (PMMA) [20-25].

Acrylate based microchips are not only easier and less expensive to fabricate than glass but are also more amenable to shipping and long-term storage, as this material is more rigid and less absorptive. PMMA [26-28], polyurethane methacrylate (PUMA) [29] and polyethylene glycol diacrylate (PEGDA) [30] have all been used for the construction of microchips for ME. For example, Liu *et al.* fabricated microchips resistant to protein adsorption by using a mixture of poly (ethylene glycol), methyl ether methacrylate (PEGMEMA), PEGDA and methyl methacrylate (MMA) [31]. Acrylate based materials are also very attractive for mass production because the monomers used and the resulting material properties, such as hydrophobicity, can be changed without changing the fabrication method.

This chapter describes the fabrication methods for both PDMS and acrylate based microchips. The advantages and disadvantages of different polymer materials and fabrication method are also discussed. The PDMS microchips were used for development and prototyping of new microchips. Acrylate based microchips can be used for more long term applications and point-of-care instrumentation because they can be produced in mass, are relatively inexpensively, and can be stored for long period of times. However, they do require more complex fabrication.

3.2. Reagents

The following chemicals were used as received: S1818 positive photoresist and Microposit 351 developer (Microchem Corp., Newton, MA, USA); SU-8 10 negative photoresist and SU-8 developer (MicroChem Corp., Newton, MA, USA); 100 mm and 127 mm Si n-type wafers (Silicon, Inc., Boise, ID, USA);100 mm p-type wafers (University Wafers, Boston, MA, USA); Sylgard 184 (Ellsworth Adhesives, Germanton, WI, USA); polyethylene glycol diacrylate (PEGDA, MW 258), 2,2-dimethoxy-2-phenylacetophenone (DMPA), (Sigma-Aldrich, St. Louis, MO, USA); 2-propanol (IPA), acetone, 30% H_2O_2, H_2SO_4, NH_4OH, 1 mL syringes, and Pt wire (22 gauge) (Fisher Scientific, Fairlawn, New Jersey, USA); high temperature fused silica glass plates (4 in. × 2.5 in. × 0.085 in.; Glass Fab, Inc., Rochester, NY, USA); colloidal silver (Ted Pella Inc., Redding, CA, USA); 0.22 μm Teflon filters (Osmonics, Inc., Minnetonka, MN, USA); deionized water (18.2 MΩ water, Millipore, Kansas City, MO, USA); quick set epoxy and Cu wire (22 gauge; Westlake Hardware, Lawrence, KS, USA).

3.3 Master Fabrication

3.3.1 Silicon wafer/SU-8 10 masters

Masters with SU-8 10 photoresist features patterned onto 4 in. silicon wafers were fabricated using the following previously optimized steps, which are depicted in Figure 3.1 [32, 33] SU-8 10 (4 mL) was spin coated on a 4 in. diameter silicon (Si) wafer using a Cee 100 spincoater (Brewer Science, Rolla, MO, USA), which resulted in 25 ± 1 μm thick layer. The wafer was soft baked on a hot plate and heated to 65°C for 3 min, then 95°C 5 min. A design containing the desired structures was created using AutoCAD LT 2004 (Autodesk, Inc., San Rafael, CA, USA) and transferred to a transparency film at a resolution of 50,000 dpi (Infinite Graphics Inc., Minneapolis MN, USA). The appropriate negative film mask was placed over the coated wafer, brought into hard contact, and exposed to a near-UV flood source at 21.5 mW/cm^2 (ABM, San Jose CA, USA) for 14 s. Following the UV exposure, both wafers were postbaked at 65°C for 1 min. then 95°C for 5 min. and allowed to cool to room temperature. The wafers were then developed in SU-8 developer, rinsed with IPA, and dried under nitrogen. A final hard-curing bake was performed at 200 °C for 2hr. The thickness of the raised photoresist, which corresponded to the depth of the PDMS channels, was measured with a surface profiler (Alpha Step-200, Tencor Instruments, Mountain View, CA, USA).

The Si wafer must be very clean or the photoresist will not adhere to the surface. Re-used Si wafers were cleaned by first manually removing any material on the wafer with a razor blade and acetone. Wafers were then placed in an acid piranha solution (70% conc. H_2SO_4, 30% conc. H_2O_2) heated to ~ 80°C for 20 min., rinsed with water, and submerged for 20 min. into a heated (~ 80°C) base piranha solution (70% conc. NH_4OH, 30% conc. H_2O_2). The wafer was then rinsed with deionized (DI) water, dried with nitrogen, and heated to 200°C on a hot plate for 2 h. to drive off any residual water. (**Caution: acid and base piranhas are very dangerous and should be handled with care.)* New Si wafers are used as received.

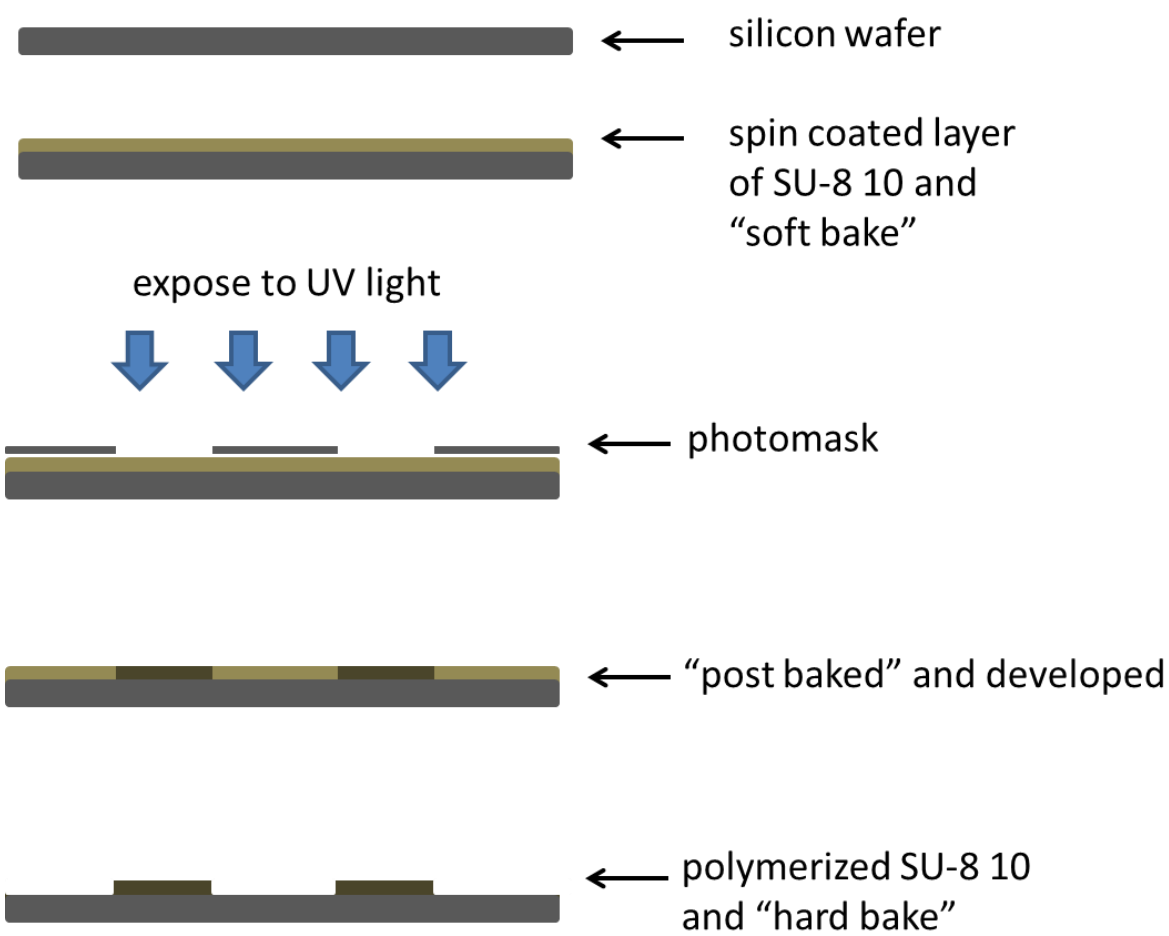

Figure 3.1: Schematic of SU-8 10 master fabrication.

3.3.2 Silicon/Silicon nitride wafer masters

Masters made from silicon wafers were fabricated using silicon nitride as a resist and KOH etching. Figure 3.2 depicts the fabrication process. Bare Si wafers were coated with a very thin layer (nanometers) of silicon nitride. Negative SU-8 10 photoresist was then used to pattern microchip features using the same photolithography steps (coating, soft bake, UV exposure, post bake, develop and hard bake) described in Section 3.3.1. An inductively-coupled plasma reactive ion etch (ICP-RIE) system (Oxford Instruments, Abingdon, Oxfordshire UK) was used to remove the silicon nitride that was not protected by the SU-8 10. Etching conditions were O_2 at 3.1 SCCM, CF_4 at 25 SCCM, 100 W, and 100 mTorr. The SU-8 10 was then removed by dipping the wafer into a cold KOH etching solution. Manually applied friction may be necessary to completely remove the photoresist. The silicon nitride patterned wafer was submerged in a heated KOH etching solution, and then rinsed with water and N_2 dried.

The height of the silicon features was dependent on the amount of silicon etched away. The parameters for specific etch depths were determined by varying the % KOH, temperature, and time in etching solution. The depth was determined using a profilometer (Alpha-Step 200, Tencor, Milpitas, CA, USA). The parameters and resulting feature heights are shown in Table 3.1. Increasing the temperature will increase the etching rate. Decreasing the % KOH will also increase the etching rate. The addition of IPA will decrease the etching rate.

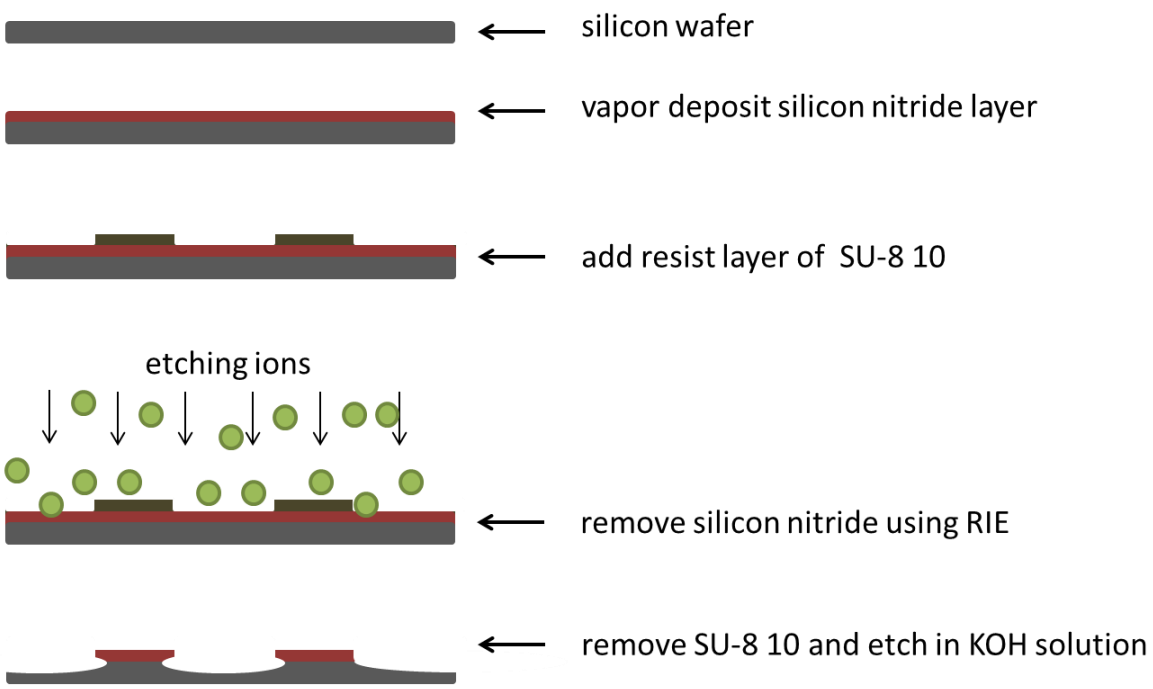

Figure 3.2: Silicon/silicon nitride wafer master fabrication steps.

Table 3.1: Etching conditions and resulting depth

KOH%(w/w)	IPA%(w/w)	time (min)	temp (°C)	depth (μm)
53	-	24	25	6
53	-	36	25	7.4
45	-	44	40	13
45	-	60	40	25
20	20	9.5	40	1.6
20	20	29.5	40	5.9
20	20	76	40	20.1

3.3.3 Polyethylene glycol diacrylate (PEGDA) masters

Polyethylene glycol diacrylate (PEGDA) masters were fabricated by photopolymerization of a thin layer of pre-polymer solution using a photomask and a collimated UV light flood source. The fabrication steps are shown in Figure 3.3. The pre-polymer solution was made by mixing a photoinitiator 2,2-dimethoxy-2-phenylacetophenone (DMPA) with PEGDA. That solution was syringed into a holder consisting of two glass plates, which were spaced ~ 0.5 mm apart using layers of Parafilm. As the pre-polymer solution was less viscous than water, the plates needed to be clamped together with binder clips to sufficiently seal the holder. A photomask with 40 μm wide features was then placed on top of the holder and exposed to columnated UV light (ABM Mask Aligner, Scotts Valley, CA, USA). The resulting polymerized features were rinsed with a 70% ethanol water mixture.

The width and depth of the PEGDA features are dependent on the percent DMPA and exposure time. Using two different % DMPA solution concentrations, the resulting height and width were determined, as shown in Tables 3.2 and 3.3. The resulting features are too large to create channels that can be used for microchip electrophoresis. However, for applications such as flow-injection analysis or flow cytometry this is a quick, simple, inexpensive method to fabricate masters.

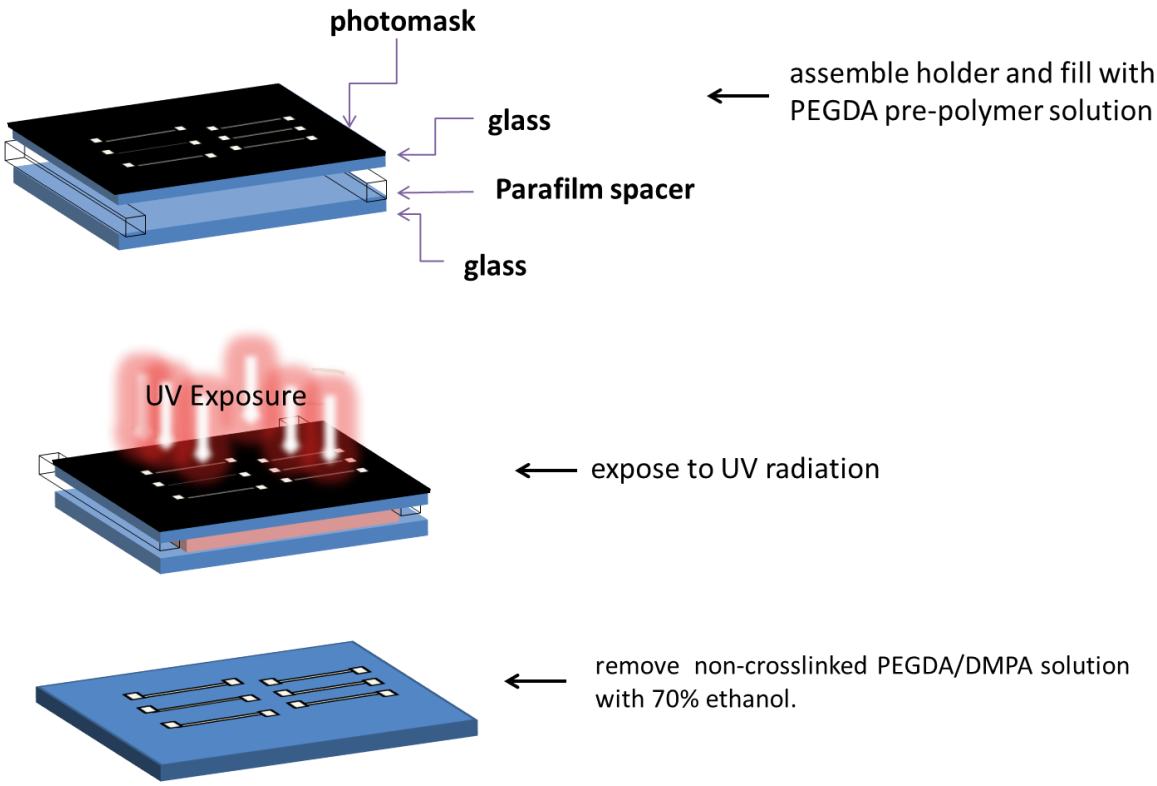

Figure 3.3: Fabrication process for PEGDA masters.

Table 3.2: PEGDA solution with 2.7%(w/v) DMPA

Exposure time (s)	5	10	15	20
Width (µm)	330 ± 10	330 ± 27	321 ± 3	360 ± 17
Height (µm)	64 ± 14	74 ± 8	59 ± 9	97 ± 10

Table 3.3: PEGDA solution with 3.7%(w/v) DMPA

UV exposure time (s)	**5**	**10**	**15**	**20**
Width (µm)	300 ± 8	350 ± 26	382 ± 55	322 ± 47
Height (µm)	137 ± 6	137 ± 4	86 ± 6	89 ± 12

3.3.4 PDMS masters

PDMS masters were fabricated from siloxane coated PDMS molds. The fabrication steps are shown in Figure 3.4. The PDMS mold was fabricated by pouring a pre-polymer mixture of un-cured PDMS and curing agent on top of a SU-8 10 master and placing it in an oven to polymerize. The cured PDMS was then peeled off of the SU-8 10 master, placed channel side up on a glass plate and moved into a plastic air tight container. One or two drops of a silanization reagent (tridecafluoro-1, 1, 2, 2-tetrahydrooctyl trichlorosilane) were added to the container. The container (Tupperware, Dillions, Lawrence, KS, USA) was then sealed for ~ 12 hours allowing the PDMS to be vapor coated with silanol. A pre-polymer PDMS mixture was then poured onto the silanol coated PDMS (recessed features) mold and cured in an oven at 85°C. The resulting cured PDMS master (raised features) can easily be peeled from the mold.

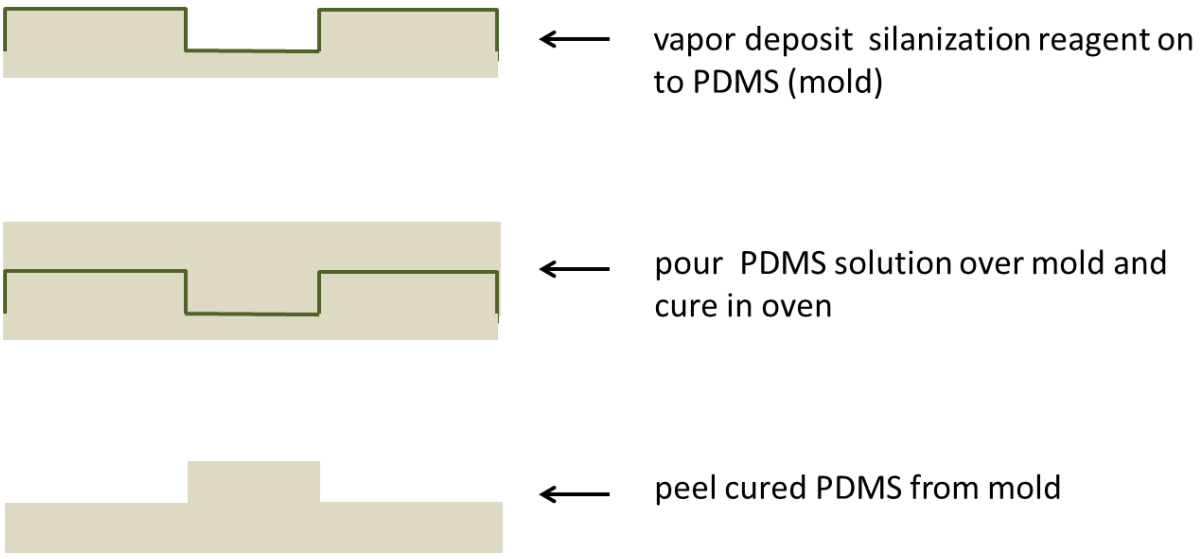

Figure 3.4: PDMS master fabrication steps.

3.3.5 Comparing Master Fabrication Processes

The silicon wafer SU-8 10 master fabrication process produces high quality micron sized features. The minimum feature size is directly related to the type and resolution of the photomask that is used. For these experiments, a printed toner photomask that had a minimum feature size of 10 microns was used. The depth was controlled by the spin coating procedure and type of photoresist that was employed as discussed in Section 3.2.1. This master type was used for PDMS microchip fabrication 10-30 times until a defect in a feature occurred. If a feature did detach from the wafer, all of the SU-8 10 was manually removed and the wafer could be reused. These masters were also used for hot-embossing thermoplastics but, in this case, the de-molding process often caused the removal of features so the number of replicates that could be produced was reduced to 2-5 times. Silicon/silicon nitride wafers had similar minimum feature sizes to the silicon wafer SU-8 10 masters since SU-8 10 was used to define the masking material. However, the KOH etching process leads to anisotropic features. The severity of the anisotropy increases as the depth increases.

Silicon masters can theoretically be used with PDMS microchip fabrication an infinite number of times, as PDMS will not cause the Si features to detach. However, the etching process makes the silicon wafer thinner and more likely to break, limiting the number of PDMS replicates that can be made. The features on silicon/silicon nitride masters were robust when used for hot-embossing, but again the wafer itself was fragile. Also, once silicon/silicon nitride masters are etched they cannot be re-processed to have different features, like the SU-8 10 masters.

The silicon nitride masters are both more expensive per master, as the gases used for depositing and etching the layer of silicon nitride are expensive, and in instrumentation, as PECVD and ICP-RIE instruments are extremely expensive. PEGDA masters were the least

expensive to fabricate as PEGDA, DMPA and the photomask were the only consumables needed and a UV flood source the only instrumentation. However, these masters had the lowest reproducibility, highest minimum feature size and lowest fidelity when used for hot-embossing. The major applications for such large features are flow−injection analysis and flow cytometry.

PDMS masters require a primary master (any of the masters described could be used), which is the main cost as the consumables used are silanization reagent, PDMS monomer and curing agent. These masters were used 10-30 times with PUMA microchip fabrication, but were incompatible with PEGDA microchip fabrication as the oxygen introduced by the gas permeable PDMS inhibited the polymerization. Table 3.4 gives a condensed comparison of the master fabrication processes.

Table 3.4: Comparison of different master fabrication processes

Master Type	Feature Size	Cost	Time	Other Considerations
silicon wafer/SU-8 10	≤ 10 μm	$$	2-4 h	requires expensive specialty equipment
silicon/silicon nitride wafer	≤ 10 μm	$$$$	4-6 h	requires expensive specialty equipment
PEGDA	> 100 μm	$	~2 h	poor reproducibility
PDMS	≤ 10 μm	$	~24 h	requires a primary master

3.4 Fabrication of PMMA Microchips

3.4.1 Microchannel fabrication

Microchannels were fabricated into PMMA using two different methods; hot-embossing and laser etching. Fabrication of microchips using hot-embossing, shown in Figure 3.5, consists of pressing a master into a softened thermal plastic [34, 35]. The hot-embossing process heated the PMMA to 80°C and held at that temperature until the entire substrate was heated thoroughly. The substrate and master (metal, SU-8 10, silicon, or PEGDA masters can be used) were then placed in a hydraulic press (Carver, Wabash, IN, USA) and pressed into light contact so that there was resistance to additional pressure, but no pressure registered on the pressure gauge. The temperature was then increased to 120°C, PMMAs glass transition temperature (T_g); the temperature at which the polymer softens. The T_g can vary with the manufacturer, but has been reported between 100 - 122°C [1]. That temperature was held constant as a master, was pressed into the polymer using a pressure of 0.5 metric tons for 30 min. The PMMA was then cooled to 80°C under pressure, and removed from the press. The master and polymer were separated, so that a three-sided channel is formed in the PMMA. The channel substrate was then bonded to a cover substrate to create a complete microchannel. The bonding procedures are addressed in Section 3.4.2.

Hot-embossing of PMMA channels was simple, with the major cost being the initial purchase of the heated press. PMMA has a relatively low glass transition temperature (T_g), and all of the masters described in this chapter are compatible with the hot-embossing process. However, the pressure required by this process can often break delicate masters such as those made using silicon wafer and deform the features of PDMS masters. In general, metal masters

are used in these processes that can cost $100-$300 each and have limited feature sizes (≥ 50 μm). Also, hot-embossing was time consuming due to heating and cooling of the press.

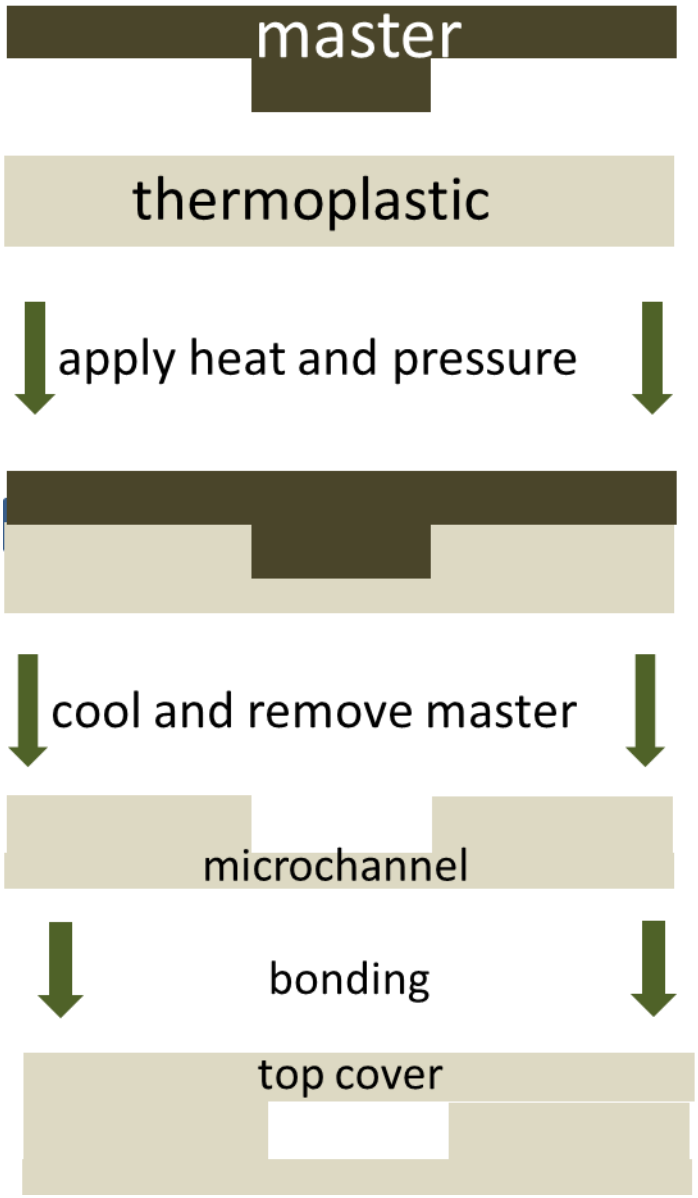

Figure 3.5: A schematic of the hot-embossing process.

For the etching procedures, a CO_2 laser (Universal, Scottsdale, AZ, USA) was used to etch channels in PMMA, shown in Figure 3.6. The channel design was drawn with CorelDraw (Corel Corporation of Ottawa, Canada), then "printed" to the laser system. The depth of the channels was controlled by adjusting the rate at which the laser moves and laser power. These parameters also influenced the width of the channel, along with the optics, which controlled the laser spot diameter. This laser system pulses the laser at a high frequency, which results in channels that have uneven widths [22]. In order to avoid that, the same feature was etched three times, adjusting the starting point by 0.01 in. each time. This created a more consistent width. Channels approximately 100 microns wide and 100 microns deep channels were etched using 3% power, 0.8% speed, at 1000 dpi settings (CorelDraw). *Note: it is important to allow all fumes to be removed by air handling before opening the laser system, as toxic gas is created by lasering PMMA.* Laser ablation of PMMA was very simple and extremely fast ($\leq$ 1 min.), but had very limited feature sizes ($\geq$ 100 μm).

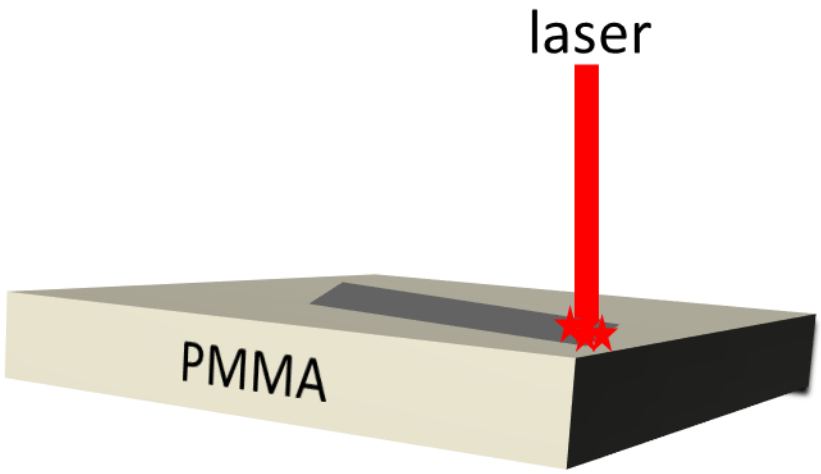

Figure 3.6: A schematic of rastering features using a laser.

3.4.2 Substrate bonding

3.4.2.1 Thermal bonding

The process of thermally bonding PMMA channel substrates to another PMMA substrate is similar to the hot-embossing process. The two substrates were placed in contact with the hydraulic press and heated to 80°C. The temperature was increased to 130°C and the pressure was increased until a firm resistance to increasing pressure is felt (< 0.1 metric tons). The temperature and pressure are held for 30 min then the temperature was decreased to 80°C. The bonded microchip was removed from the press. In this approach, the temperature and pressure must be carefully controlled since even small fluctuations (1-2°C) can lead to unbounded or collapsed channel.

3.4.2.2 Solvent bonding

To solvent bond PMMA a laser etched PMMA substrate was placed on top of a blank PMMA substrate. A thin layer of a mixture of acetone (75%) and IPA (25%) was placed between the two substrates. This was accomplished by adding a few drops of the solvent mixture to the area where the substrates met. Capillary action then drew the solvent solution into the interface. Drops were added until the entire interface between the two substrates was coated, which took less than a minute. Weight (approx. 1 lb.) was placed on top of the substrates for about 2 hours. It was important to allow enough time for all of the solvent to evaporate in order to achieve fully bonded substrates.

3.4.2.3 Solvent assisted thermal bonding

To bond PMMA using this method a PMMA substrate with laser cut channels was placed on a blank PMMA substrate. A thin layer of IPA was formed at the interface of the two substrates, using capillary action. The substrates were then placed in a heated press at 110°C and

pressure was added so that the two substrate surfaces were in hard contact for 15 min. The bonded microchip could then be removed from the press and cooled to room temperature.

3.4.2.4 Comparison of different substrate bonding methods

Thermal bonding is simple and straight forward, but requires very tight temperature and pressure control. A temperature difference of a few degrees can mean the either an unbounded microchip or a microchip with collapsed channels. The bond strength is also weaker relative to other methods [36]. One advantage of that weak bond is if a microchip does not properly bond the substrates can be pulled apart and re-bonded.

Solvent bonding, done correctly, dissolves a very thin layer of the surface of two PMMA substrates. When the two layers are pressed in contact with one another, the dissolved polymers mix. When the solvent evaporates the two substrates become permanently bonded. Acetone and acetonitrile are both very good solvents for PMMA. However, for bonding purposes, they dissolve too much of the surface and cause parts of the channel to collapse. The optimal conditions were obtained by diluting acetone with isopropanol (IPA), which is not a good solvent for PMMA at room temperature. This made it possible to use lower concentrations of acetone while increasing the amount of time the solvent was in contact with the substrates before it evaporated. This method creates very strong bonds. However, this method also had a low success rate where one part of the microchip may have collapsed channels and the other part not bonded at all.

Solvent assisted thermal bonding is a combination of solvent and thermal bonding. At elevated temperatures and pressures the ability of IPA to dissolve PMMA is increased. Therefore, only where the IPA and PMMA meet at the interface, will the PMMA dissolve. Thus, bonding can occur below the T_g and the bulk of the material will not soften. This lessens the chance of collapse or deformation of the channels. This method has the added benefit of being

faster than thermal or solvent bonding since the temperature does not need to be ramped slowly and the solvent evaporates faster than it does using the traditional solvent bonding procedure described above. This method was also much faster than thermal bonding, as there is no waiting for heating and cooling and created a very strong bond that can withstand high flow rates (20 μL/min) without any leaking.

3.5 Fabrication of Acrylate Based Microchips

3.5.1 Polyurethane methacrylate (PUMA)

Polyurethane methacrylate (PUMA) was purchased as a viscous UV active pre-polymer solution (Dymax adhesives, Orrington, CT, USA). Exposure to UV light fully polymerized the solution to a hard polymer but the photopolymerization agent was not disclosed by the manufacturer. However, it was observed that oxygen inhibited the polymerization, so it is postulated that it is radical induced polymerization since oxygen is a known quencher of this type of reaction. Initially, the fabrication was based on a method developed by Kuo *et al.* [42]. PUMA was poured on silicon wafer/SU-8 10 masters (described in section 3.2.2.1), then covered with a sheet of fluorinated ethylene propylene (FEP) plate using PDMS as a spacer (~ 1 mm) and then exposed to UV light until it was almost completely cured (6 s). However, this method often damaged the master and/or the PUMA channels. Therefore, PDMS masters were used instead. A diagram of the fabrication process is shown in Figure 3.7. A ~ 1 mm thick slab of semi-cured PUMA was first fabricated by placing the PUMA solution between two sheets of FEP, spaced with PDMS, and exposed to UV light at 21.5 mW/cm^2 power (ABM, San Jose CA, USA) for 2 s. The mold was then flipped over and exposed from the other side for an additional 2 s. The resulting PUMA was hard enough to be handled with tweezers but soft enough to

conform to the PDMS master. The semi-cured PUMA was placed on the PDMS master and pressed gently and covered by a sheet of FEP then exposed to UV light until the PUMA was almost completely cured (5 s). Blank PUMA substrates were fabricated by placing PUMA solution between two sheets of FEP separated using PDMS (~ 1 mm thick) and exposing both sides to UV light for 3 s. Blank and channel PUMA substrates were bonded together by placing them in contact using manual pressure. The substrates were then pressed together by placing them in a vacuum sealed bag (FoodSaver, Sunbeam Inc., Boca Raton, FL, USA) and exposed to UV light for 15 s.

The use of FEP to enclose the mold, instead of glass, was necessary because PUMA is such a good adhesive that it adhered to glass. The removal of polymerized PUMA from a mold using SU-8 10 master often damaged the features and new masters needed to be fabricated for every 2-3 PUMA channel substrates made. Even if the removal of the PUMA left the master intact, the force used to remove the polymer would deform the channels. Thus, PDMS masters were used as they can be peeled off without disturbing the channels or permanently deforming the PDMS. However, directly pouring the PUMA solution into a mold with a PDMS master was problematic because the polymer solution easily leaked out of the mold if no pressure was applied. However, the use of pressure caused the deformation of the soft PDMS and resulting in deformed channels. Therefore, the semi-cure method was used, which successfully allowed PDMS masters to be used, without deforming the channels.

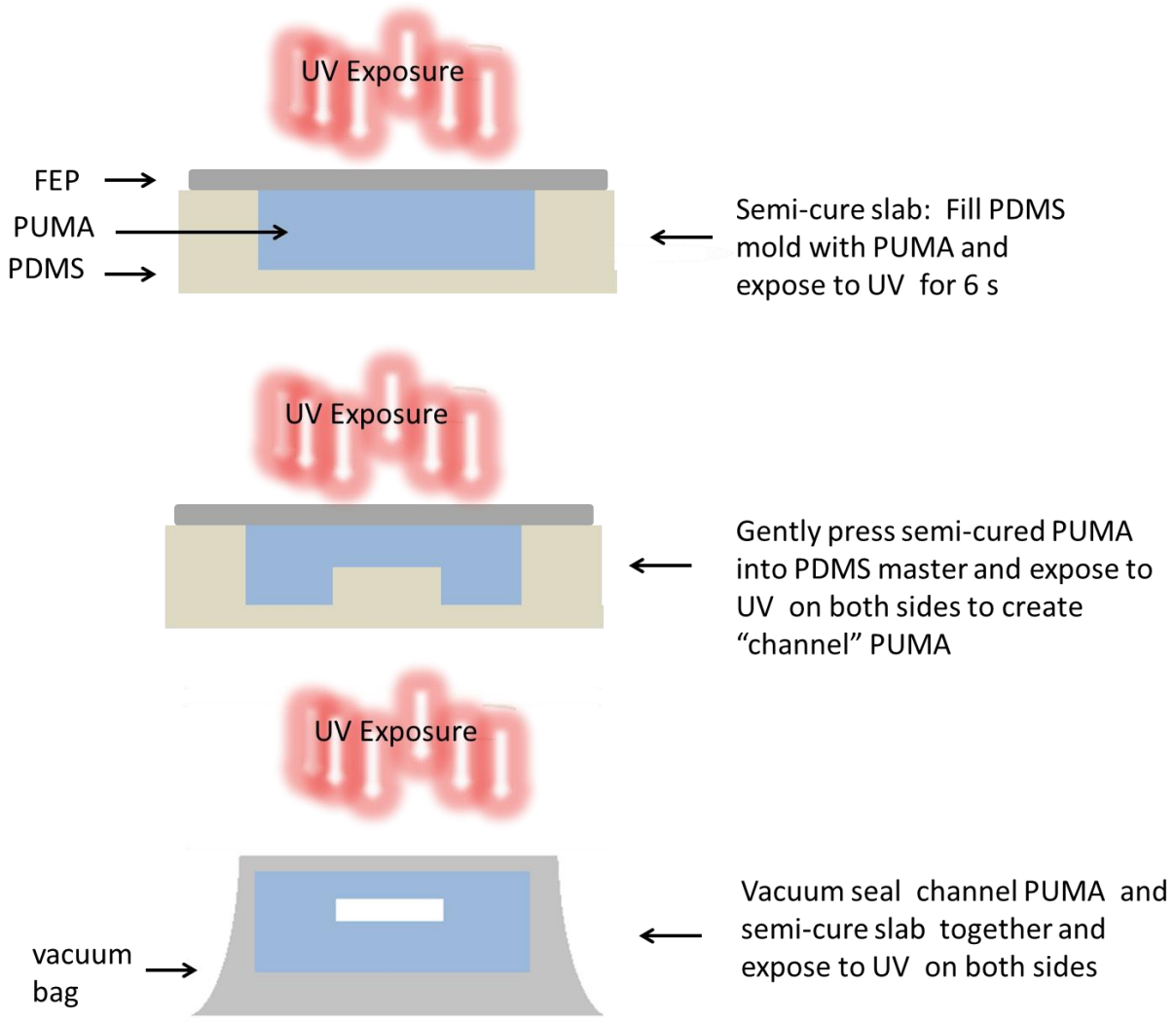

Figure 3.7: The fabrication steps for PUMA microchips.

3.5.2 Polyethylene glycol diacrylate (PEGDA)

To produce PEGDA microchips *in situ* fabrication, depicted in Figure 3.8, was used. A mold was made by placing Parafilm on a glass substrate and heated till soft. A silicon wafer/SU-8 10 master and spacer were pressed onto the warm Parafilm, which sealed them to the glass. A layer of petroleum jelly (Vaseline, Unilever, USA) was spread around the outside of the wafer and on top of the spacer to prevent leaking. Polyethylene glycol diacrylate (PEGDA) was mixed with 1% (w/v) photoinitiator 2,2-dimethoxy-2-phenylacetophenone (DMPA) and the solution was pipetted onto the master, then a glass substrate was placed over the solution and pressed into the top of the spacer and secured using binder clips (Office Depot, Lawrence, KS, USA). The petroleum jelly created a tight seal that prevented solution from leaking out as well as oxygen from entering. The mold was then exposed to UV light using either ambient light through a window (~ 4 h.) or a 51 LED bulb UV flashlight (LED wholesalers, Amazon, USA) for ~ 1 h. Once the PEGDA solution was fully polymerized, the mold was disassembled and the resulting PEGDA channel substrate was removed from the master, cleaned by sonication in a mixture of water and IPA, and then dried with $N_{2(g)}$. Reservoirs were made with a biopsy punch (Harris Uni-Core, Redding, CA, USA) in double sided acrylic based adhesive (ARcare 92712, Adhesives Research Ltd, Limerick, Ireland). The protective cover was removed from one side and placed on a PMMA substrate. The second protective cover was removed from the tape and the PEGDA channel substrate was placed channel side to sticky side, then pressed gently until a tight seal with the channel was formed.

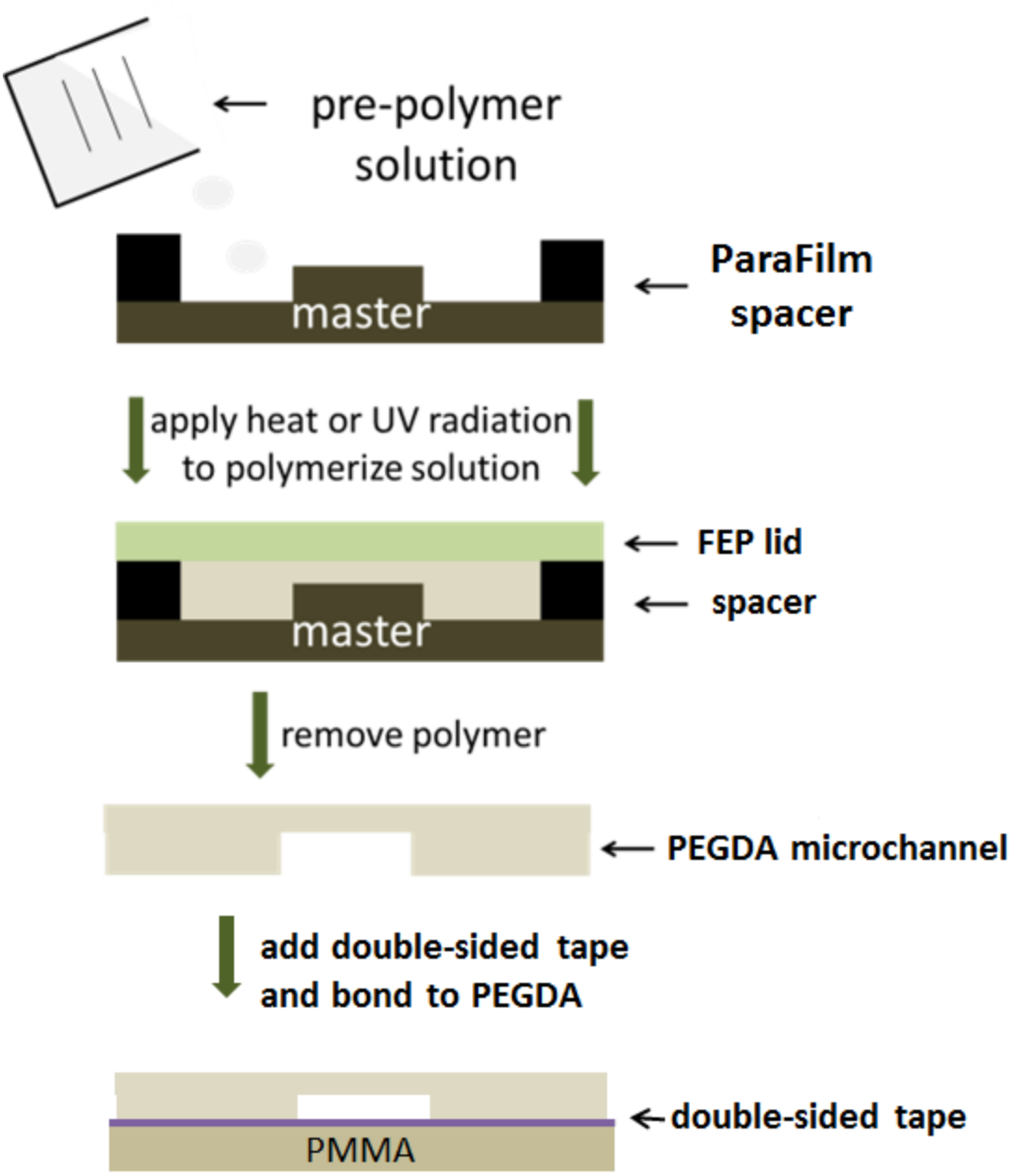

Figure 3.8: The fabrication steps for a PEGDA microchip.

3.6 Fabrication of PDMS Microchips

PDMS micro-channels were fabricated using *in situ* polymerization with silicon wafer/SU-8 10 masters. The PDMS monomer and polymerization reagents were mixed in a weight-to-weight ratio of either 10:1 or 20:1. The mixture was then de-gassed using a vacuum chamber. Once all bubbles were visibly gone the mixture was poured onto the master and cured overnight. In order to decrease curing time PDMS can be heated at 90°C, 80°C, and 70°C for 30 min, 2 h, and 3 h, respectively. Once it was fully cured, the PDMS was peeled off of the master. Reservoirs to address the channels were created by punching an area through the PDMS with a biopsy punch (Harris Uni-Core, Redding, CA, USA). The channel substrate was then reversible bonded by to PDMS, glass or PMMA by simply placing the substrates into direct contact.

A semi-cure method was used to irreversibly bond PDMS channels to a PDMS substrate. In this case, both substrates were fabricated using the 20:1 monomer to polymerization reagent ratio and were heated for ~10 min at 90°C, so that the surface of each substrate was sticky. The substrates were then placed together and heated overnight at 80°C.

The PDMS microchip for the reversibly bonded fabrication method was easier than any of the other microchips and can be used with EOF. Unfortunately, these microchips leak when used with hydrodynamic pressure. The semi-cure method created a stronger bond that can be used with pressure. However, the channels could easily be deformed when in the semi-cured state which increased the difficulty of the fabrication. Also, because there are more steps these microchips took longer to make compared to the reversibly bonded microchips.

3.7 Conclusions

There are many different ways to fabricate polymer microchips. Each process has distinct advantages and disadvantages so that there really is not one "best" method. When choosing a method the application, cost, time, and degree of difficulty must all be taken into account. PDMS methods are easy to learn and due to the silicon/SU-8 10 master are moderately expensive and have very small feature sizes. Laser etching of PMMA is the easiest and least expensive method, but has larger feature sizes (>100 μm), and the associated bonding methods require expertise. The next chapter will describe how to fabricate a graphite/PMMA composite electrode into a polymer substrate.

3.8 References

[1] Tsao, C.-W., DeVoe, D., *Microfluid. Nanofluid.* 2009, *6*, 1-16.

[2] Yang, S., Devoe, D. L., *Methods in molecular biology (Clifton, N.J.)* 2013, pp. 115-123.

[3] Manz, A., Graber, N., Widmer, H. M., *Sens. Actuators B* 1990, *1*, 244-248.

[4] Jacobson, S. C., Hergenroder, R., Koutny, L. B., Warmack, R. J., Ramsey, J. M., *Anal. Chem.* 1994, *66*, 1107-1113.

[5] Kuhnline, C. D., Lunte, S. M., *Journal of Separation Science* 2010, *33*, 2506-2514.

[6] Phillips, T. M., Wellner, E. F., *ELECTROPHORESIS* 2009, *30*, 2307-2312.

[7] Ghanim, M. H., Abdullah, M. Z., *Talanta* 2011, *85*, 28-34.

[8] Noh, J., Kim, H. C., Chung, T. D., in: Lin, B. C. (Ed.), *Microfluidics: Technologies and Applications*, Springer-Verlag Berlin, Berlin 2011, pp. 117-152.

[9] Lacher, N. A., Garrison, K. E., Martin, R. S., Lunte, S. M., *Electrophoresis* 2001, *22*, 2526-2536.

[10] Nge, P. N., Rogers, C. I., Woolley, A. T., *Chem. Rev.* 2013, *113*, 2550-2583.

[11] Njoroge, S. K., Chen, H. W., Witek, M. A., Soper, S. A., in: Lin, B. C. (Ed.), *Microfluidics: Technologies and Applications* 2011, pp. 203-260.

[12] Jin, L. J., Ferrance, J., Landers, J. P., *Biotechniques* 2001, *31*, 1332-+.

[13] Chen, Y., Zhang, L., Chen, G., *ELECTROPHORESIS* 2008, *29*, 1801-1814.

[14] McDonald, J. C., Whitesides, G. M., *Accounts Chem. Res.* 2002, *35*, 491-499.

[15] Duffy, D. C., McDonald, J. C., Schueller, O. J. A., Whitesides, G. M., *Anal. Chem.* 1998, *70*, 4974-4984.

[16] Chabinyc, M. L., Chiu, D. T., McDonald, J. C., Stroock, A. D., Christian, J. F., Karger, A. M., Whitesides, G. M., *Anal. Chem.* 2001, *73*, 4491-4498.

[17] Anderson, J. R., Chiu, D. T., Jackman, R. J., Cherniavskaya, O., McDonald, J. C., Wu, H. K., Whitesides, S. H., Whitesides, G. M., *Anal. Chem.* 2000, *72*, 3158-3164.

[18] McDonald, J. C., Duffy, D. C., Anderson, J. R., Chiu, D. T., Wu, H. K., Schueller, O. J. A., Whitesides, G. M., *ELECTROPHORESIS* 2000, *21*, 27-40.

[19] Kuncova-Kallio, J., Kallio, P. J., *28th IEEE EMBS Annual International Conference*, New Yourk City 2006.

[20] Lee, G. B., Chen, S. H., Huang, G. R., Sung, W. C., Lin, Y. H., *Sensors and Actuators B-Chemical* 2001, *75*, 142-148.

[21] Grass, B., Neyer, A., Johnck, M., Siepe, D., Eisenbeiss, F., Weber, G., Hergenroder, R., *Sensors and Actuators B-Chemical* 2001, *72*, 249-258.

[22] Brown, L., Koerner, T., Horton, J. H., Oleschuk, R. D., *Lab on a Chip* 2006, *6*, 66-73.

[23] Wang, J., Pumera, M., Chatrathi, M. P., Escarpa, A., Konrad, R., Griebel, A., Dorner, W., Lowe, H., *ELECTROPHORESIS* 2002, *23*, 596-601.

[24] Muck, A., Wang, J., Jacobs, M., Chen, G., Chatrathi, M. P., Jurka, V., Vyborny, Z., Spillman, S. D., Sridharan, G., Schoning, M. J., *Anal. Chem.* 2004, *76*, 2290-2297.

[25] Galloway, M., Stryjewski, W., Henry, A., Ford, S. M., Llopis, S., McCarley, R. L., Soper, S. A., *Anal. Chem.* 2002, *74*, 2407-2415.

[26] Chen, Z., Yu, Z. Y., Chen, G., *Talanta* 2010, *81*, 1325-1330.

[27] Duan, H. T., Zhang, L. Y., Chen, G., *Journal of Chromatography A* 2010, *1217*, 160-166.

[28] Qu, S., Chen, X. H., Chen, D., Yang, P. Y., Chen, G., *ELECTROPHORESIS* 2006, *27*, 4910-4918.

[29] Kuo, J. S., Zhao, Y. X., Ng, L. Y., Yen, G. S., Lorenz, R. M., Lim, D. S. W., Chiu, D. T., *Lab on a Chip* 2009, *9*, 1951-1956.

[30] Rogers, C. I., Pagaduan, J. V., Nordin, G. P., Woolley, A. T., *Anal. Chem.* 2011, *83*, 6418-6425.

[31] Liu, J., Sun, X., Lee, M. L., *Anal. Chem.* 2007, *79*, 1926-1931.

[32] Fischer, D. J., Hulvey, M. K., Regel, A. R., Lunte, S. M., *Electrophoresis* 2009, *30*, 3324-3333.

[33] Nandi, P., Desai, D. P., Lunte, S. M., *ELECTROPHORESIS* 2010, *31*, 1414-1422.

[34] Lin, M. C., Yeh, J. P., Chen, S. C., Chien, R. D., Hsu, C. L., *Int. Commun. Heat Mass Transf.* 2013, *42*, 55-61.

[35] Chien, R.-D., *Int. Commun. Heat Mass Transf.* 2006, *33*, 645-653.

[36] Zhu, X. L., Liu, G., Guo, Y. H., Tian, Y. C., *Microsyst. Technol.* 2007, *13*, 403-407.

Chapter Four:

Integration of a Carbon Electrode into Thermoplastic Microchip for Electrochemical Detection

4.1 Introduction

Electrochemistry (EC) is an ideal detection mode for microfluidic devices for many reasons [1-5]. Electrodes can be miniaturized without loss of sensitivity, and many biological compounds are electrochemically active. Carbon electrodes are of special interest due to their large potential window, facile kinetics for the oxidation of organic compounds, and minimal fouling with biological samples [6]. For these reasons many different methods have been developed to integrate carbon electrodes into polymers, so that microfluidic devices can be made inexpensively.

Carbon-based electrodes have been employed previously in polydimethylsiloxane (PDMS) microfluidic devices [7, 8]. With PDMS, electrodes can be placed directly into or on the electrode substrate because the polymer is soft enough to conform to small raised features of micron thickness, which occurs with rigid electrode materials like a carbon fiber [9]. Carbon ink can be employed in a similar manner [10]. The ink is deposited on a surface using either a mold or screen printing process [11, 12].

However, integrating carbon electrodes into rigid substrates, like polymethylmethacrylate (PMMA) or glass, can be problematic. If electrodes are deposited on top of the surface of the substrate and not imbedded in the substrate, fabrication problems can occur. Most microfluidic devices are fabricated by bonding two substrates together; one substrate containing the three walls of the microfluidic channels and the other substrate creates the fourth wall, to complete the channel. If the surfaces of the two substrates cannot be placed in flush contact, then the bonding will fail. In fact, it has been shown that even small aerosol particles can interfere with the bonding of glass [13].

Martin's group overcame this issue by placing a glassy carbon and/or carbon fiber in liquid epoxy. After the expoxy hardened it could be polished to expose the electrode surface. Using this approach, it is possible to produce a substrate that contains one or multiple electrodes of different materials. In these studies, a PDMS substrate containing the microfluidic channels was used as the other layer, forming a complete microchip [14]. A disadvantage of this approach is that the electrodes are quite large, and PDMS was still used for three on the four walled microfluidic channel.

Carbon paste and ink, which are soft materials, have also been successfully integrated into rigid microfluidic devices. Most carbon paste electrodes (CPEs) are composed of a carbon source (*e.g.* graphite or carbon nanotubes) and a binding agent [15]. The resulting mixture is malleable and, therefore, can conform to a feature etched in a rigid plastic substrate [16]. CPEs can contain additives that can be used to chemically modify the surface or reduce the electrical resistance of the paste [17, 18]. The addition of metal ions to the bulk electrode material has also been show to increase conductivity and can act as a redox mediator. There are too many additives and binders to list fully here, but mineral oil and organic solvents are most commonly employed [19]. These CPE electrodes can be very sensitive and selective [20]. However, they can also suffer from mechanical instability. Hydrodynamic flow can disrupt the carbon paste due to increased shear stress, and erode the CPE [21, 22].

Carbon paste has been integrated into PDMS previously by fabricating an electrode channel and packing the channel with a carbon paste that uses paraffin oil as the binder [23]. Recently, the same fabrication method was used but uncured PDMS was added to the paste as a binder. During fabrication, the carbon paste was malleable, but after being packed into the channel the PDMS was hardened, which produced a more mechanically stable electrode.

However, the electrode surface must be oxidized with plasma before it can be used for electrochemical detection [24]. Again, these methods require the use of PDMS substrates.

In 2008, Dai *et al.* reported the development of an electrode material similar to CPE that was produced by mixing monomethlymethacrylate (MMA) with graphite powder. The MMA was then polymerized in a glass capillary to produce a graphite/PMMA composite. These electrodes were shown to be quite versatile and were employed for the detection of vitamin C using electrogenerated chemiluminescence [25], amperometric detection of NADH [26], and the oxidation of guanine or adenine for quantitation of single-stranded DNA [27].

This chapter describes a simple and inexpensive method to fabricate graphite/PMMA composite electrodes (GPCEs) into a rigid PMMA substrate is described. Fabrication parameters for the production of GCPEs were optimized and the effect of electrode composition on the electrochemical response for dopamine was also evaluated using CV. These optimized GPCEs were then fabricated directly in a PMMA substrate to produce an all-PMMA microchip used for flow-injection analysis. The PMMA/GPCE substrates were also evaluated for microchip electrophoresis (ME) with electrochemical detection using PDMS as the channel substrate and catechol and dopamine as model compounds. The addition of the redox modifiers copper (II) hexacyanoferrate and cobalt (II) hexacyanoferrate was also investigated by cyclic voltammetry (CV) for the selective detection of several electroactive analytes including dopamine, nitrite, ascorbic acid and hydrogen peroxide. These metal complexes are Prussian blue analogues and have been shown to reduce the overpotential of electrodes [28]; however the modifications did not improve the electrode performance and were not used in the optimal electrode composite.

4.2 Materials and methods

4.2.1 Materials

Dopamine, ascorbic acid, sodium nitrite, potassium chloride (KCl), catechol, 2-(N-morpholino) ethanesulfonic acid (MES), copper(II) sulfate pentahydrate, cobalt (II) sulfate heptahydrate, graphite powder, and 2,2 dimetoxy-2-phenylacetophenone (DMPA) were purchased from Sigma-Aldrich (St. Louis, MO, USA). Colloidal silver was received from Ted Pella, Inc. (Redding, CA, USA). PMMA was acquired from McMaster-Carr (Elmhurst, IL, USA). Acetone, acetonitrile, sulfuric acid, nitric acid, hydrochloric acid, Parafilm, paraffin oil, hydrogen peroxide (30%) and Kim-Wipes were obtained from Fischer Scientific (Waltham, MA, USA). Monosodium phosphate monohydrate was received from Acros (Geel, Belgium) and dibasic sodium phosphate heptahydrate was obtained from Mallinckrodt AR (Phillipsburg, NJ, USA). PDMS monomer and curing agent (Dow Corning, Elizabethtown, KY, USA) were also used in microchip fabrication. All aqueous buffers and solutions were prepared with 18.2 MΩ water (Millipore, Kansas City, MO, USA). Stock solutions of 10 mM dopamine, nitrite, ascorbic acid and hydrogen peroxide and catechol were made fresh daily in water. Sample solutions for modified GPCEs were made from the stock solutions in 1 M KCl. All other sample solutions were prepared from the stock solutions in 50 mM sodium phosphate buffer at pH 7, unless otherwise indicated.

4.2.2 Cobalt (II) and copper (II) hexacyanoferrate synthesis

Cobalt (II) and Copper (II) hexacyanoferrate were both synthesized in house using a procedure described by Li et. al [29]. Briefly, equimolar aqueous solutions of either copper (II) sulfate pentahydrate or cobalt (II) sulfate pentahydrate and potassium ferricyanide (III) were mixed. The resulting precipitate was placed in an oven at ~ 60°C until all of the water was removed. Any excess reagent, both very soluble in water, was removed by rinsing the precipitate

with water and vacuum filtered (0.22 μm). The resulting crystals were ground into a powder using a mortar pestle and added to the graphite powder in a 7:3 graphite to metal hexacyanoferrate powder ratio.

4.2.3 Graphite composite electrode fabrication

A solution of PMMA was created by dissolving solid PMMA in either acetone or acetonitrile in varying concentration. At room temperature the PMMA was completely dissolved in ~ 2 days. That time was increased by using sonication. When using sonication the container was covered by Parafilm (for safety reasons, do not heat/sonicate a tightly sealed container of any volatile liquid) and any volume lost to evaporation was added before use. Graphite powder was used as received or mixed with cobalt (II) hexacyanoferrate (or copper (II) hexacyanoferrate). A graphite composite solution (GCS) was prepared by mixing different ratios of graphite powder and different concentrations of the PMMA solution. Care was taken to minimize solvent evaporation during mixing.

Initial electrode fabrication was accomplished using the following procedure:

1) Using Corel Draw and a CO_2 laser with 0.8% speed, 3% power, and 1000 dpi settings (Universal, Scottsdale, AZ, USA) trenches were lased into solid PMMA. The process was repeated three times while varying the position of the laser by 0.01 in to create a smooth trench ~100 μm × ~100 μm.

2) The trenches were filled with carbon composite using a syringe.

3a) The excess paste was removed from the surface using Kim-Wipes and acetone. The resulting electrodes were placed in an oven at 95°C overnight.

The optimized composite electrode fabrication method replaced step 3a with the following process: 3b) The excess paste was removed from the surface using Kim-Wipes and

acetone and the finished electrodes were placed in an oven at 110°C for at least 10 min, the temperature was increased to 160°C and held for 2 h; the oven was then cooled to 80°C over 1–2 h.

This new step 3b annealed the GCPE and the PMMA substrate, which reduced the internal strain. The entire process, shown in Figure 4.1, took approximately 6 hours start to finish to make 1–50 electrodes. Four hours of that time was dedicated to heating and cooling the electrodes, so the number of electrodes that can be made in 6 hours was dictated mostly by the oven and substrate size.

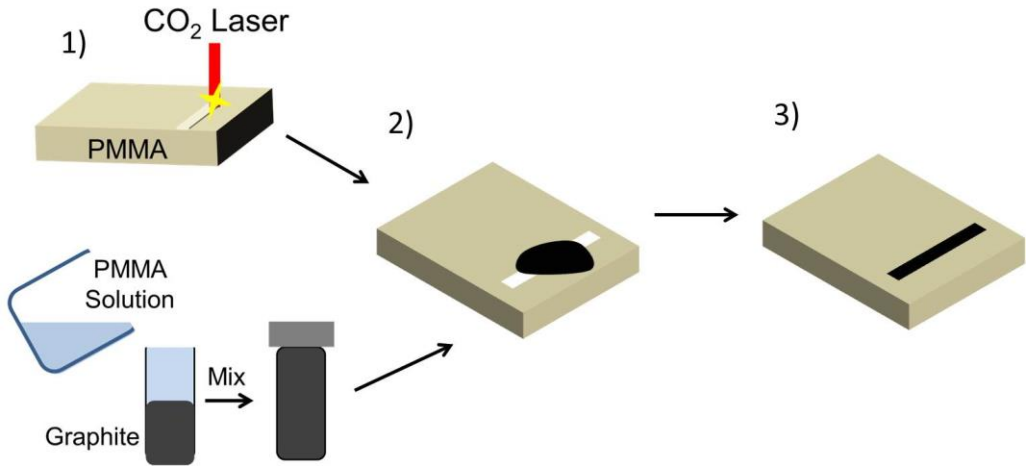

Figure 4.1: A diagram of the GPCE fabrication process. 1) A channel is cut into a PMMA substrate using a CO_2 laser and the GCS is prepared by mixing the graphite and PMMA solution 2) The channel is filled with GCS 3) The electrode is dried in an oven at 110°C for at least 10 min, the temperature was increased to 160°C, held for 2 h, then cooled to 80°C.

4.2.4 Electrochemical measurements

Cyclic voltammetry and amperometric detection measurements were performed using an 812c potentiostat (CH Instruments, Inc., Austin, TX, USA). The electrochemical detection cell consisted of a GPCE working electrode (unless otherwise noted), a platinum wire auxiliary electrode, and an Ag/AgCl reference electrode (Bioanalytical Systems, Inc., West Lafayette, IN, USA). All cyclic voltammograms were performed scanning the potential from 0 to 1 V, at a scan rate of 100 mV/s. Peak height and peak potential were determined from the CVs using Origin 8.6 software (OriginLab, Northampton, MA, USA) following baseline subtraction. Amperometric detection for the microchip electrophoresis experiments was performed using an electrically isolated potentiostat (Pinnacle Technology, Lawrence, KS, USA) with an Ag/AgCl reference electrode (Bioanalytical Systems) and a GPCE working electrode. A 3 mm diameter glassy carbon electrode (Bioanalytical Systems was used as a working electrode; it was prepared by polishing the surface with an alumina slurry (Bioanalytical Systems) then sonicating in water (18.2 MΩ) for at least 10 s to remove residual alumina. The electrophoretic separation was accomplished using a high voltage power supply (Ultravolt Inc., Ronkonkoma, New York, USA) that was controlled using Labview hardware and software (National Instruments, Austin, TX, USA). All Labview software was written in-house. Resistance of the optimized GPCE's was determined using the following procedure: Six electrodes were constructed from the optimal graphite composite (8 mg/mL PMMA in acetone and 20:1 graphite to PMMA by weight). Electrodes were submerged in 18.2 MΩ purified water (Millipore, Kansas City, MO, USA) so that any voltage drop was due only to the electrode material. Measurements were acquired using a RadioShack voltmeter (Lawrence, KS, USA).

4.2.5 PMMA flow injection device

The fabrication procedure for the PMMA flow injection device is shown in Figure 4.2.A. A flow channel cut into a piece of PMMA flow cell was created using the same laser ablation process as electrode trench, resulting in a channel 0.7 in long, ~ 100 µm wide, and ~100 µm deep. An inlet was made using a 35 gauge needle, and an outlet (6 mm diameter) was cut using a CO_2 laser. The "channel PMMA" plate and the "electrode PMMA" plate were bonded together using the following procedure:

1) The two PMMA pieces were placed together and 1–2 drops of a solvent (75% IPA and 25% acetone) were placed at the seam of the interface. This allowed capillary action to create a thin layer of solvent between the two pieces. The two layers were aligned without allowing the solvent to evaporate and then placed between two pieces of glass.

2) Pressure was applied using a C-clamp, and the assembly was placed in an oven at 110°C for at least 15 min. Nanoports (Upchurch Scientific, Oak Harbor, WA, USA) were then affixed using epoxy (Quick Set Locktite, Ace Hardware, Lawrence, KS, USA). Electrical connection to the graphite/PMMA composite electrode was accomplished using copper wire and colloidal silver. Flow injection experiments were conducted using a syringe pump (Harvard Apparatus, Holliston, MA, USA) at flow rate of 20 µL/min. The analysis buffer was 50 mM sodium phosphate (pH 7). Samples were injected using a 5 µL sample loop and a six port Rheodyne 7725i valve (Bioanalytical Systems) into the flow cell. The working electrode was set at 500 mV vs. Ag/AgCl.

4.2.6 Fabrication and operation of the hybrid PDMS/PMMA ME-EC device

The fabrication of a simple "T" PDMS microchip has been described in detail elsewhere [23]. Briefly, a solution of 20 parts PDMS monomer and 1 part curing agent by weight was

prepared and mixed. The pre-polymer was then poured onto a silicon wafer with raised SU-8 micro-channel features The PDMS was allowed to degas and harden on the wafer for 8 h. The resulting polymerized PDMS with recessed channels 40 μm wide and 40 μm deep was peeled from the wafer; reservoirs were created with biopsy punches (Harris Uni-core, Ted Pella). The PDMS channel layer was reversibly bonded to the substrate containing the graphite/PMMA composite electrode (GPCE) [12]. A diagram of the simple T microchip with the length of the side arms at 0.75 cm and the separation channel 3.5 cm (Figure 4.2 A). The electrode (~100 μm wide) was placed partly in-channel and partly end-channel (Figure 4.2 B). The PDMS channels were then conditioned sequentially with 0.1 M NaOH, water, and 10 mM MES pH 6 buffer solutions. Samples were introduced into the separation channel using a gated injection scheme [33, 34]. A field strength of 77 V/cm was used for all separations. PDMS does not bond to PMMA as strongly as it does to glass. Thus, leaking along the electrode can occur, especially if the reference electrode is jarred, this can, in turn, push the PDMS reservoir. In order to solve this problem, Super Glue® was applied to the electrode PDMS junction on the outside of the microchip. The glue has a very low viscosity and flows into any gaps in the electrode/PDMS interface *via* capillary action. However, this does not allow for the electrode to be re-used.

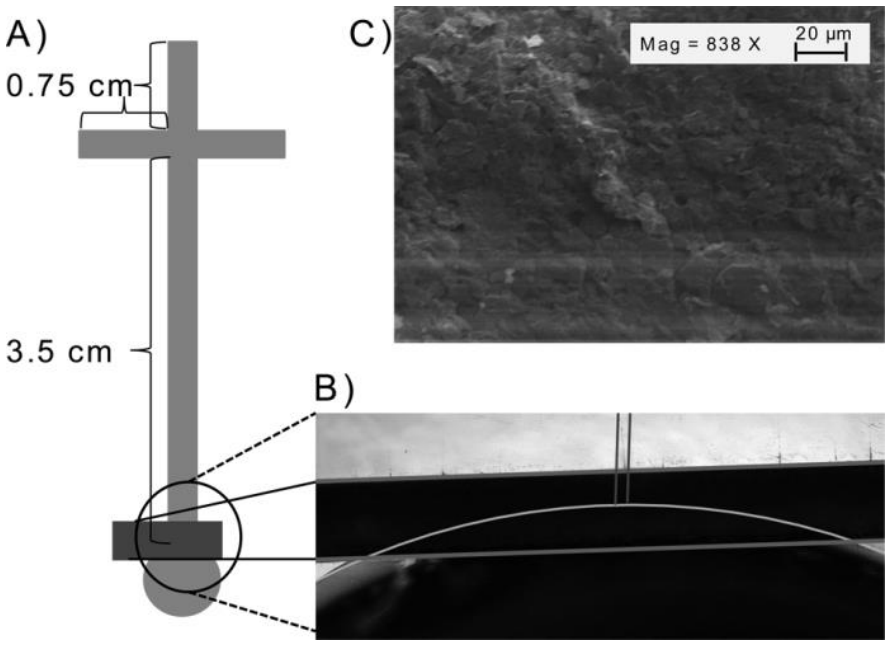

Figure 4.2: A) A diagram of the PDMS microchip for ME-EC showing the dimensions of the channels and the placement of the GPCE. B) A micrograph of the GPCE highlighting the electrode placement in the microchip. C) An SEM of the surface of the optimized GPCE.

4.3. Results and Discussion

4.3.1 Graphite/PMMA composition optimization

4.3.1.1 Modified vs. unmodified graphite

The role of a redox modifier is to lower the potential at which an analyte will oxidize. Using multiple test analytes including dopamine, nitrite, ascorbic acid and hydrogen peroxide the average (n=3) oxidation peak potential was determined with cyclic voltammetry for GCPEs using unmodified graphite, graphite with copper(II) hexacyanoferrate , and graphite with cobalt(II) hexaycanoferrate, shown in Table 4.1.

The addition of copper (II) hexacyanoferrate yielded a lower apparent oxidation peak potential for both dopamine and ascorbic acid. However, nitrite could not be detected over the potential range of 0 – 1 V. Cobalt (II) hexacyanoferrate lowered the apparent oxidation potential of nitrite but did not affect that of dopamine or ascorbic acid. The addition of the redox modifiers significantly increases both the cost and fabrication time for each GPCEs and thus all further experiments were performed using unmodified graphite.

Table 4.1: Peak potential of modified and unmodified GPCEs

Analyte	Unmodified (mv)	Copper(II) Hexacyanoferrate (mV)	Cobalt(II) Hexacyanoferrate (mV)
Dopamine	300	250	300
Nitrite	850	Not detected	800
Ascorbic Acid	250	200	250
Hydrogen peroxide	Not detected	Not detected	Not detected

4.3.1.2 Optimization of PMMA and graphite concentration

Cyclic voltammetry was used to determine the peak current (i_p) and peak potential (E_p) for the anodic ($E_{p,a}$, $i_{p,a}$) and cathodic peaks ($E_{p,c}$, $i_{p,c}$) of 2 mM dopamine in a 50 mM phosphate pH 7 background electrolyte, unless otherwise stated. To determine the optimal PMMA solution concentration, the graphite: PMMA ratio was held constant at 20:1 (w/w) and the PMMA solution concentration (mg PMMA/mL acetone) was varied (n = 3 for each concentration). The electrochemical results for those electrodes are shown in shown in Figure 4.3 A.

Electrodes prepared using PMMA solution concentrations of 8 and 10 mg/mL exhibited the lowest average anodic peak potential (~ 320 mV) and the highest peak current (~1.31 μA) for dopamine and were not statistically different from each other. However, the standard deviation for the peak current of the 10 mg/mL concentration was almost 2× higher than the 8 mg/mL concentration. This is probably due to the fact that the 10 mg/mL concentration was more viscous and, thus, there was incomplete mixing of the graphite. Therefore, the 8 mg/mL PMMA solution concentration was considered optimal and used for future experiments.

Using the optimal PMMA solution concentration, the ratio of graphite: PMMA (w/w) was then varied. These results are shown in Figure 4.3 B. The 20:1 graphite: PMMA ratio exhibited the lowest peak oxidation potential for dopamine and, more importantly, the highest oxidation current, (1.30 ± 0.2 μA); this was more than 2.5 times higher than the 30:1graphite: PMMA ratio, which was the next highest. Therefore, the optimal electrode composition was determined to be a PMMA concentration of 8 mg/mL with a graphite/PMMA ratio of 20:1. This resulted in an average $i_{p,a}$ of 1.30 ± 0.2 μA and an $E_{p,a}$ of 300 ± 30 mV. All further electrode

characterization was performed with GPCEs prepared using 20:1 graphite: PMMA ratio and 8 mg/mL PMMA solution.

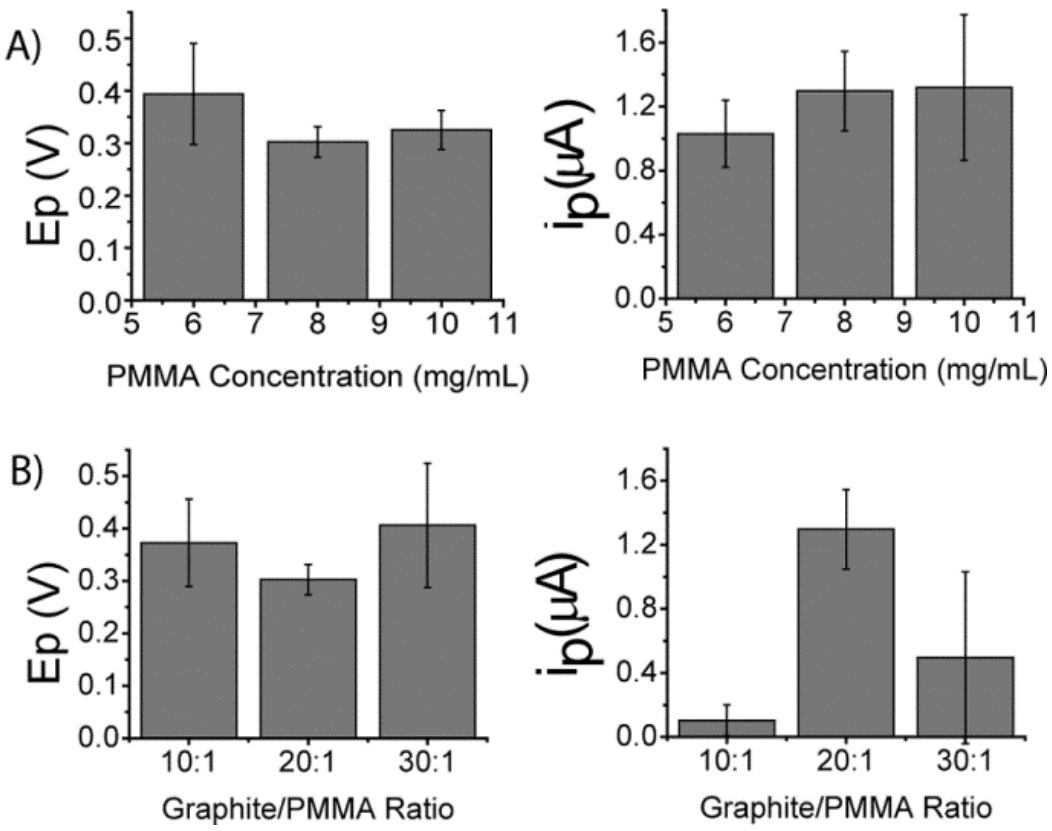

Figure 4.3: Data obtained from baseline-subtracted response for the oxidation of 2 mM dopamine. A) The potential (E_p) and the current (i_p) for electrode composites with 20:1 graphite: PMMA ratio (g:g) and varying PMMA solution concentration. B) The potential (E_p) and the current (i_p) for electrode composites with a constant PMMA solution concentration of 8 mg/mL and varying graphite: PMMA ratio.

Lastly, the performance of the GPCE was compared to that of the most commonly used carbon material, glassy carbon. Since dopamine exhibits a chemically reversible oxidation, the ΔE_p, or difference in the anodic and cathodic peak potential, was measured for both electrode types. The ΔE_p for glassy carbon and the optimized GPCE were 0.21 ± 0.03, and 0.15 ± 0.03 V, respectively, using the same experimental conditions. The lower ΔE_p suggests that the GPCEs are less resistive and have more facile reduction and oxidation kinetics [42].

4.3.2 GCPE characterization

4.3.2.1 Conductivity and of GPCE

Three resistance measurements were taken for six different electrodes. The within electrode RSD was less than 6.3% and the electrode-to-electrode variability was 2.6%.

The conductivity was calculated using Equations 4.1 and 4.2:

$$\rho = R * \frac{A}{l} \qquad \textbf{Eq. 4.1}$$

$$\sigma = 1/\rho \qquad \textbf{Eq. 4.2}$$

where ρ is resistivity, R (Ω) is resistance, A (m^2) is cross-sectional area, l (m) is length, and σ (S/m) is conductivity.

The depth of an electrode was variable due to the rastering of the laser and, therefore, the cross-sectional area was not consistent throughout a specific electrode. Thus, the values for conductivity were calculated using an exaggerated minimum (75 μm x 175 μm) and maximum (200 μm x 175 μm) cross-sectional area. Using the minimum and maximum cross-sectional

areas, the possible range of conductivities were calculated to be 9.0×10^2 (S/m) and 3.4×10^2 (S/m), respectively.

4.3.2.2 Reconditioning of the electrode surface

It was found that if noise increases occurred during the use of the electrode, either due to fouling or excess current, the electrode can be re-conditioned by performing cyclic voltammetry. The following re-conditioned parameters were used: voltage sweep from -0.4-1.4 V, 0.5 V/s scan rate and 12 sweeps. It should be noted, however, that each time the electrode is reconditioned the efficacy of the recondition decreases, as shown in Figure 4.4.

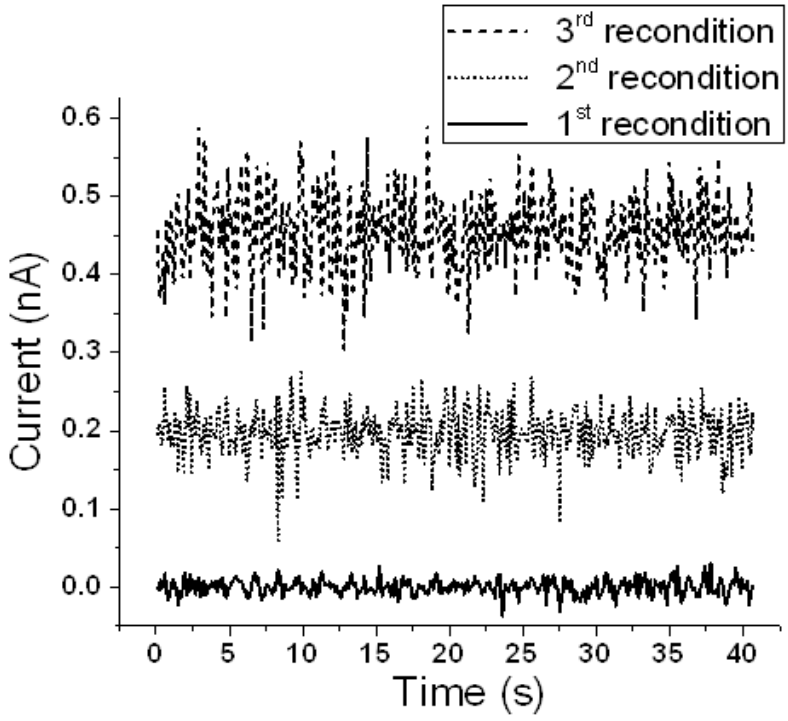

Figure 4.4: The effect of three re-conditioning procedures on the baseline noise.

4.3.2.3 Detection of dopamine using flow injection analysis

Three separate optimized GPCE electrodes were evaluated by flow injection analysis using PMMA flow cells and dopamine as the test analyte. Figure 4.5 shows the calibration curve for the best electrode that was obtained using five standard solutions ranging in concentration from 50 to 500 nM. All the electrodes fabricated during this study exhibited excellent linearity, with R^2 values not less than 0.90. However, the dynamic range varied from electrode to electrode. The sensitivities of the three electrodes varied within an order of magnitude, ranging from 30–300 pA/μM. The noise varied over three orders of magnitude (pA–nA), which led to calculated limits of detection (LOD) (S/N >3) ranging from 14 μM–50 nM. The inset in Figure 4.5 shows the response obtained from the best of the three electrodes for a solution containing 250 pmol of dopamine (S/N = 5).

The surface of the GCPE, shown in Figure 4.2 C, is very rough, which leads to an increase in the surface area. This may be the major contributing factor to such low limits of detection, which agrees with other published reports [27]. The variations in both the surface and the internal structure of the electrode, such as different amounts of graphite on the surface and trapped microair bubbles, respectively, may be the reason for such a large amount of variation in the noise. These defects are most likely due to the fact that each electrode is made by hand one at a time. However, the cost in both money (< $0.10 per electrode on a 2 × 2 in substrate) and time (> 50 electrodes fabricated per day, start to finish) is small; thus, electrodes with unacceptable noise levels can be discarded.

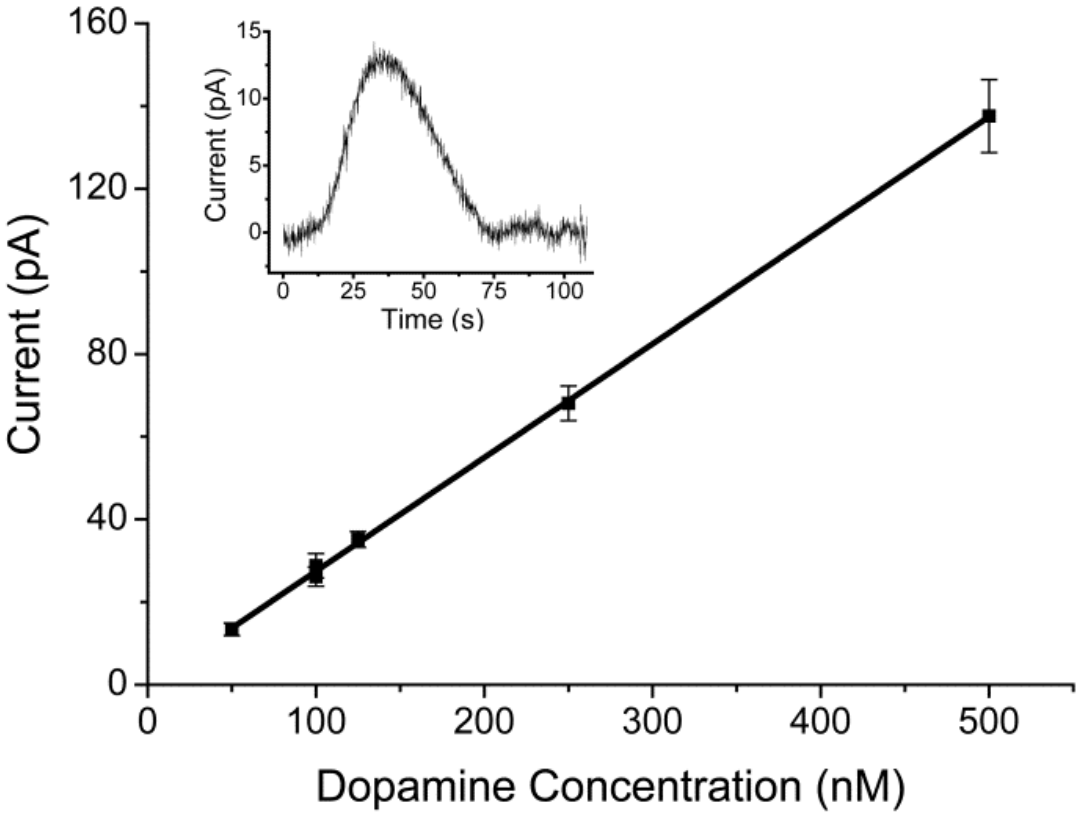

Figure 4.5: A calibration curve ($R^2 = 0.999$) for flow injection analysis using the all-PMMA flow microchip with an integrated GPCE. (Inset: 50 nM dopamine peak using the all-PMMA flow microchip and integrated GPCE with flow-injection analysis.)

4.3.2.4 Electrophoretic separation

Using a PDMS microchip reversibly sealed on a GPCE PMMA substrate, ME was performed with amperometric detection. Due to the relatively large size of the electrode (~100 μm wide) in comparison with the separation channel (40 μm wide), the electrode placement was both in- and–end-channel, as shown in Figure 4.2 B. The resulting electropherogram for 100 μM dopamine and catechol is shown in Figure 4.6. The baseline noise was significantly higher for the electropherogram then the flow-injection analysis. Since the electric field and electrode are not decoupled, due to the in-channel alignment, all of the flicker noise generated by the high voltage power supply also affects the baseline noise. Although the separation and detection conditions were not optimized, the electropherogram demonstrates that this electrode can be used for ME-EC. It was stable under electroosmotic flow conditions, and the same electrode was used with multiple PDMS microchips over several days.

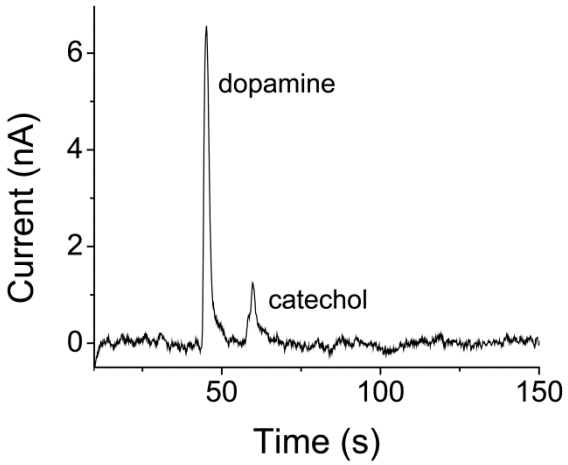

Figure 4.6: Separation and detection of 100 μM dopamine and catechol using ME-EC.

4.4 Conclusion

In this chapter, the fabrication of an inexpensive graphite/PMMA composite electrode that can be integrated into an all-PMMA microfluidic device is reported. In addition, the use of the electrode in a PMMA/PDMS hybrid microchip for ME is also demonstrated. These inexpensive, simple to fabricate electrodes can exhibit low LODs and low noise. Also, these GPCE are stable and can withstand high flow rates (20 µL/min) and electrophoretic fields. However, each electrode must be individually evaluated and calibrated, due to electrode-to-electrode variability. Future work will concentrate on integrating GPCEs into all-PMMA device capable of ME. In the next chapter the development of a microchip capable of interfacing with and sampling from microdialysis flow is described.

4.5 References

[1] Vilela, D., Anson-Casaos, A., Martinez, M. T., Gonzalez, M. C., Escarpa, A., *Lab on a Chip* 2012, *12*, 2006-2014.

[2] Matysik, F. M., *Microchim. Acta* 2008, *160*, 1-14.

[3] Ghanim, M. H., Abdullah, M. Z., *Talanta* 2011, *85*, 28-34.

[4] Fischer, D. J., Hulvey, M. K., Regel, A. R., Lunte, S. M., *Electrophoresis* 2009, *30*, 3324-3333.

[5] Vandaveer, W. R., Pasas-Farmer, S. A., Fischer, D. J., Frankenfeld, C. N., Lunte, S. M., *Electrophoresis* 2004, *25*, 3528-3549.

[6] McCreery, R. L., *Chem. Rev.* 2008, *108*, 2646-2687.

[7] Omiatek, D. M., Santillo, M. F., Heien, M. L., Ewing, A. G., *Anal. Chem.* 2009, *81*, 2294-2302.

[8] Ding, Y., Ayon, A., García, C. D., *Anal. Chim. Acta* 2007, *584*, 244-251.

[9] Gawron, A. J., Martin, R. S., Lunte, S. M., *ELECTROPHORESIS* 2001, *22*, 242-248.

[10] Mecker, L. C., Filla, L. A., Martin, R. S., *Electroanalysis* 2010, *22*, 2141-2146.

[11] Kovarik, M. L., Torrence, N. J., Spence, D. M., Martin, R. S., *Analyst* 2004, *129*, 400-405.

[12] Wang, J., Pumera, M., Chatrathia, M. P., Rodriguez, A., Spillman, S., Martin, R. S., Lunte, S. M., *Electroanalysis* 2002, *14*, 1251-1255.

[13] Chiem, N., Lockyear-Shultz, L., Andersson, P., Skinner, C., Harrison, D. J., *Sensors and Actuators B: Chemical* 2000, *63*, 147-152.

[14] Johnson, A. S., Selimovic, A., Martin, R. S., *Electrophoresis* 2011, *32*, 3121-3128.

[15] Adams, R. N., *Anal. Chem.* 1958, *30*, 1576-1576.

[16] Rossier, J. S., Schwarz, A., Reymond, F., Ferrigno, R., Bianchi, F., Girault, H. H., *ELECTROPHORESIS* 1999, *20*, 727-731.

[17] Shiddiky, M. A., Won, M. S., Shim, Y. B., *Electrophoresis* 2006, *27*, 4545-4554.

[18] Oshea, T. J., Lunte, S. M., *Anal. Chem.* 1994, *66*, 307-311.

[19] Svancara, I., Vytras, K., Kalcher, K., Walcarius, A., Wang, J., *Electroanalysis* 2009, *21*, 7-28.

[20] Li, X. C., Chen, Z. G., Zhong, Y. W., Yang, F., Pan, J. B., Liang, Y. J., *Anal. Chim. Acta* 2012, *710*, 118-124.

[21] Kalcher, K., Kauffmann, J. M., Wang, J., Svancara, I., Vytras, K., Neuhold, C., Yang, Z., *Electroanalysis* 1995, *7*, 5-22.

[22] Mikysek, T., Svancara, I., Kalcher, K., Bartos, M., Vytras, K., Ludvik, J., *Anal. Chem.* 2009, *81*, 6327-6333.

[23] Martin, R. S., Gawron, A. J., Fogarty, B. A., Regan, F. B., Dempsey, E., Lunte, S. M., *Analyst* 2001, *126*, 277-280.

[24] Sameenoi, Y., Mensack, M. M., Boonsong, K., Ewing, R., Dungchai, W., Chailapakul, O., Cropek, D. M., Henry, C. S., *Analyst* 2011, *136*, 3177-3184.

[25] Dai, H., Wu, X., Wang, Y., Zhou, W., Chen, G., *Electrochim. Acta* 2008, *53*, 5113-5117.

[26] Dai, H., Xu, H., Lin, Y., Wu, X., Chen, G., *Electrochem. Commun.* 2009, *11*, 343-346.

[27] Dai, H., Lin, Y., Xu, H., Yang, C., Chen, G., *Analyst* 2010, *135*, 2913-2917.

[28] Garjonyt, R., Malinauskas, A., *Sensors and Actuators B: Chemical* 1998, *46*, 236-241.

Chapter Five:

Continuous–flow Sampling with Microchip Electrophoresis and Electrochemical Detection

5.1 Introduction

In order to understand the biochemical basis of neurological diseases as well as to develop pharmacological interventions, it is important to be able to simultaneously monitor biological analytes (i.e. neurotransmitters, second messengers) and behavior in near real-time. Nitric oxide (NO) has been identified as a neurotransmitter [1-3], neuromodulator [4], and is associated with oxidative stress resulting in neurodegeneration [5]. This small molecule is a gas at standard temperature and pressure and has a short physiological half-life [6]. Thus nitrite, which is one of the degradation products of NO, is commonly used for the indirect detection of nitric oxide (NO) [7, 8].

Microdialysis (MD) sampling, discussed in Section 2.2.2, is a powerful *in vivo* sampling technique that can be employed to continuously monitoring compounds in the extracellular space of the brain and other tissues [9-12]. Coupling microdialysis sampling to microchip electrophoresis (ME) creates a separation-based sensor that can monitor several compounds in the extracellular space simultaneously in near real-time [13, 14]. In order to be compatible with our autonomous system that can be used on an awake and freely roaming animal this separation-based sensor needs to use electrochemical detection.

Scott *et al*. developed a method to detect nitrite in microdialysis samples using an on-line MD-ME system with a glass microchip and an integrated platinum electrode [15]. However, these microchips were very expensive due to both raw materials (such as high quality glass and metal) and instrumentation needed to fabricate the devices (such as a metal deposition system and high temperature ovens). Also, the fabrication process limits the type of electrode material that can be used to metal.

In a separate report, Gunasekara *et al*. investigated the generation of NO from the degradation of diethylammonium (Z)-1-(N,N-diethylamino)diazen-1-ium-1,2-diolate (DEA/NO)

and 1-(hydroxyl-NNO-azoxy)-l-proline disodium salt (PROLI/NO) by monitoring the amount of nitrite that was produced using microchip electrophoresis with amperometric detection at a platinum electrode. They used a hybrid microchip that consisted of a simple-T polydimethylsiloxane (PDMS) microchip reversibly sealed to a glass substrate containing the platinum electrode. By using a reversibly sealed PDMS microchip, the cost per microchip was greatly reduced compared to an all-glass microchip because the platinum electrode could be re-used by simply peeling the old microchip off the glass and putting on a new one. However, this type of reversibly bonded microchip could not be coupled to microdialysis sampling using our double-T design (discussed in Section 2.4.2) because the pressure generated by the microdialysis hydrodynamic flow causes delamination of the PDMS from the glass substrate.

Both these approaches for the detection of nitrite used a platinum working electrode, but it has been shown that under certain conditions, such as high oxidation potentials and/or high pH, an oxide layer will form on the platinum surface[16]. The oxide layer then hinders the electron transfer, shown in Equation 5.1, from nitrite to the electrode surface [17], which can lead to poor limits of detection (LOD).

$$NO_2^- \rightarrow NO_2 + e^- \qquad \textbf{Eq. 5.1}$$

The use of carbon electrodes are many times preferable to metal because they have larger potential windows and are thus less susceptible to oxide formation[18]. Carbon electrodes have also been shown to exhibit a good response to catechol like neurotransmitters such as dopamine and serotonin [19].

In order to develop a prototype microchip capable of using amperometric detection with our previous double-T design, described in Section 2.4.2 that couples MD to ME, a PDMS microchip was developed, due to the low cost and ease of fabrication. Carbon electrodes have

been routinely used with PDMS microchips for amperometric detection following microchip electrophoresis. Carbon fiber [20-22], ink [23, 24], paste [25, 26], glassy carbon [27] and pyrolyzed photoresist films (PPF) [28, 29] have all been used. Previous work done in our lab has shown that PPF electrodes have excellent sensitivity and low noise [29], due to their low capacitance and low internal resistance [30].

This chapter describes the fabrication and characterization of a hybrid glass/PDMS double-T microchip. This microchip is capable of interfacing with MD flow and has a carbon PPF electrode for amperometric detection of nitrite. Negative polarity was used by reversing the electroosmotic flow (EOF) with the positively charge surfactant tetradecyltrimethylammonium bromide (TTAB).

5.2 Materials and Methods

5.2.1 Reagents

All reagents were analytical grade or better. All deionized (DI) water had 18.3 MΩ purity (Millipore, Kansas City, MO, USA). The following were used as received: S1818 positive photoresist and Microposit 351 developer (Microchem Corp., Newton, MA, USA); SU-8 10, SU-8 2 negative photoresist and SU-8 developer (MicroChem Corp., Newton, MA, USA); 100 mm and 127 mm Si wafers (Silicon, Inc., Boise, ID, USA); and high temperature fused silica glass plates (4 in. × 2.5 in. × 0.085 in.; Glass Fab, Inc., Rochester, NY, USA). Tetratrimethylammonium bromide (TTAB), 2-(N-morpholino) ethanesulfonic acid (MES), sodium citrate, boric acid, sodium nitrite, magnesium chloride ($MgCl_2$) and calcium chloride ($CaCl_2$) were obtained from Sigma Aldrich (Saint Louis, MO, USA). Sodium phosphate dibasic heptahydrate and sodium phosphate monobasic were purchased from Acros and Mallinckrodt, respectively. Acetonitrile, isopropanol, sodium hydroxide, potassium chloride (KCl) and sodium

chloride (NaCl) were from Fischer Scientific. Artificial cerebral spinal fluid (aCSF) was made to contain 148 mM NaCl, 3 mM KCl, 1.4 mM $CaCl_2$, 0.8 mM $MgCl_2$ and 0.9 mM phosphate at pH 7.4 in DI water. All solutions were filtered using a syringe 0.22 μm nylon filter (Fischer Scientific, Fair Lawn, NJ, USA) before use.

5.2.2 Pyrolyzed photoresist film (PPF) electrode fabrication

Pyrolyzed photoresist electrodes were fabricated based on a previously published procedure [31] and a schematic of the process is shown in Figure 5.1. Positive photoresist (S1818) was spin coated (100 rpm for 5 s then 3500 rpm for 30 s) on a fused silica glass plate. The photoresist coated plate was prebaked at 100 °C for 1 min on a hotplate prior to UV exposure (7 s at 21.5 mW/cm^2). The plate was developed for 30 s in Microposit 351 developer, diluted 1:3.5 (v_{Devl}:v_{H20}) with DI H_20, then rinsed with DI water and dried under N_2. A final postbake was performed for 10 min at 115 °C.

A Lindberg/Blue M Three-Zone Tube Furnace (Cole-Parmer, Vernon Hills, IL, USA) was utilized for pyrolysis. The furnace was continuously flushed with nitrogen gas at 5 psi to provide an inert atmosphere. The temperature of the furnace started under ambient conditions and was increased at the rate of 5.5 °C/min to 925 °C, held for 1 h, and then allowed to cool to room temperature. The width of the resulting PPF electrodes was 40 μm and the height was determined with a surface profiler to be 0.6 μm. Colloidal silver paste (Ted Pella Inc., Redding, CA, USA) was used to provide electrical contact between a copper wire and the electrical contact pads.

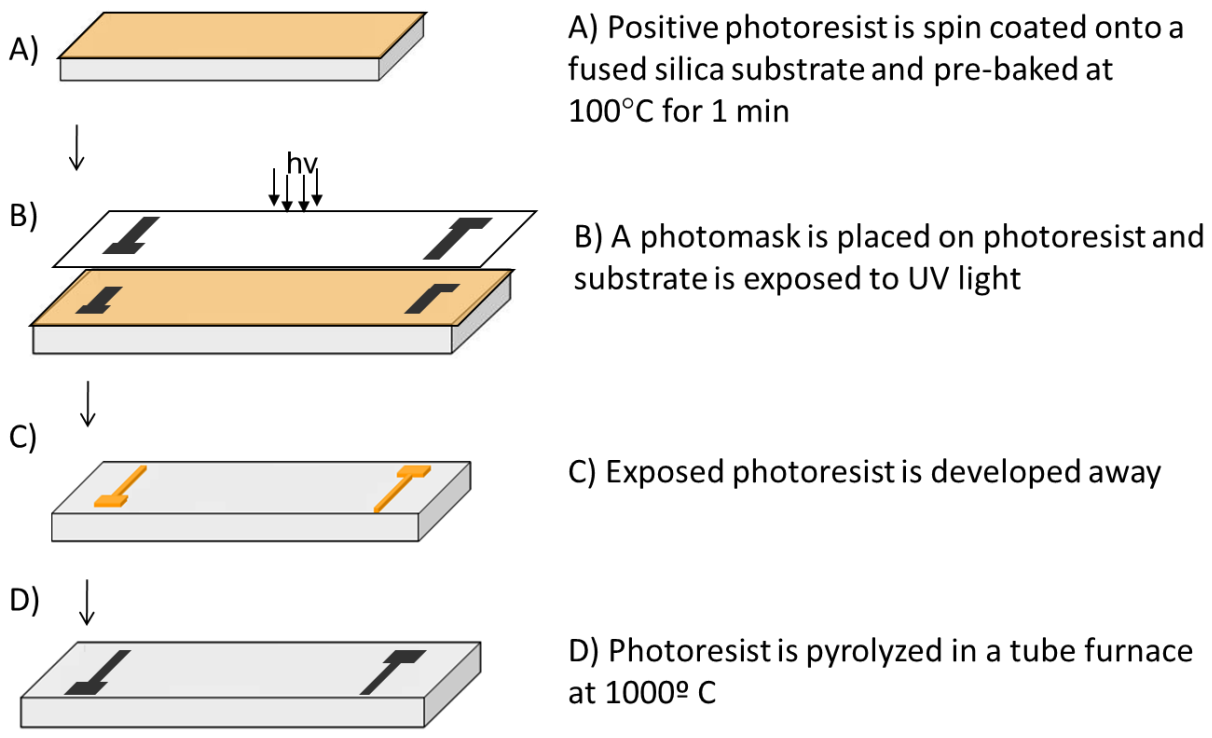

Figure 5.1: The fabrication procedure of PFF electrodes.

5.2.3 Simple-T microchip fabrication and operation

Simple-T PDMS microchips, shown in Figure 5.2, were fabricated using the procedure detailed in section 2.2.3. Briefly, PDMS monomer and curing agent (Sylagard184, Dow Corning, Midland, MI, USA) were mixed in a 10:1 ratio and de-gassed in a vacuum to eliminate any bubbles and poured over a simple-T silicon wafer/SU-8 10 master. The PDMS was cured on the master in an oven at 85°C for not less than 3h. Once cured the PDMS was allowed to cool then peeled off of the master. Access reservoirs were created using a biopsy punch (Harris Uni-Core, Redding, CA, USA). The microchip was then placed on the fused silica substrate with the PPF electrode and aligned with the electrode using the in-channel configuration.

The PDMS channels were prepared for use by flushing with 0.1 N NaOH for 3-5 min, then rinsed with DI water and filled with background electrolyte (BGE) (40 mM MES, 2 mM TTAB, pH 6.3) by applying a vacuum. Electrophoresis was performed using a Jenway Microfluidic Power Supply (Dunlow, Essex, U.K.). High voltage was applied to the BGE reservoir (-1400 V) and sample reservoir (-1200 V), while the sample waste and detection reservoirs were grounded, as shown in Figure 5.2. For all simple-T data presented, a gated injection method (described in Section 2.4.2) was used for introduction of the sample plug and was achieved by floating the high voltage at the BGE reservoir for the duration of the injection before it was returned to -1200 V

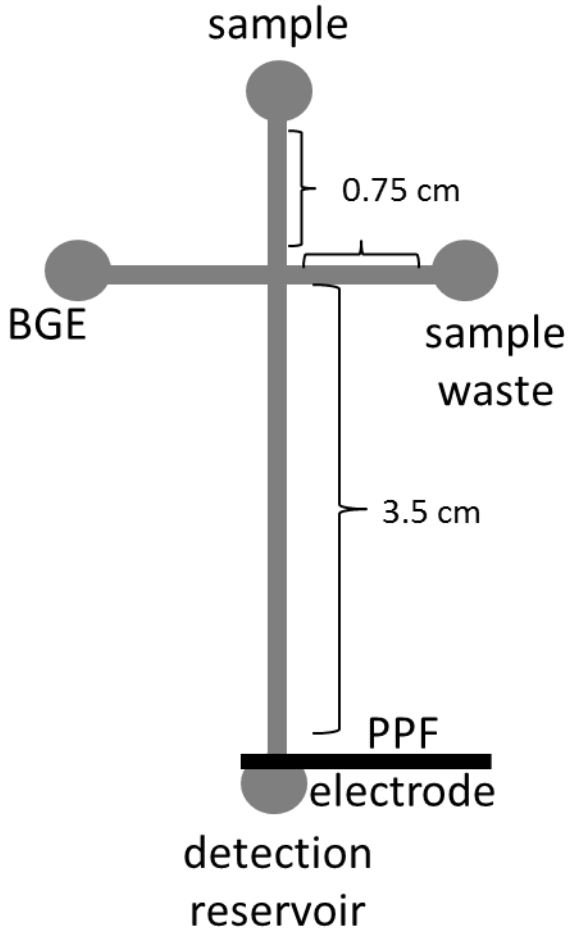

Figure 5.2: Simple-T microchip with in-channel alignment of PPF electrode

5.2.4 Double-T PDMS microchip fabrication

Microchannels were fabricated in PDMS using the same methods described in Section 3.6. Briefly, a silicon wafer/SU-8 10 master was fabricated according to the procedure detailed in Section 3.3.1, with feature depths of 25 μm. PDMS monomer and curing agent (Sylagard184, Dow Corning, Midland, MI, USA) were mixed in a 20:1 ratio and de-gassed in a vacuum to eliminate any bubbles. The mixture was poured onto the master, placed in an oven at 90°C and evaluated every 1-2 min by placing metal tongs on the surface and pulling it away. The wafer was taken out of the oven when the PDMS no longer pulled away with the tongs. The PDMS was then cooled to room temperature and removed from the master. Once removed, the channel containing PDMS layer had access reservoirs punched into it with a biopsy punch (Harris Uni-Core, Redding, CA, USA) except the sample flow reservoir , which was addressed with a 20-gauge luer stub. The channel layer was then placed channel side down on the quartz glass/electrode substrate using in-channel alignment, taking care that no air bubbles were trapped between the two pieces. The completed PDMS microchip with PPF electrode was then heated overnight at 80°C to completely cure the PDMS.

5.2.5 Double-T microchip operation

The separation channel was conditioned through sequential flushing of the channels with 0.1 N NaOH, DI water, and BGE for 2 min each using vacuum. The high voltage power supply (HV Rack, Ultravolt Inc., Ronkonkoma, NY, USA) was controlled using a Labview (National Instruments, Austin, TX, USA) program written in-house. Hydrodynamic sample flow (0.5 μL/min) was produced with a syringe pump (102 CMA, Holliston, MA, USA) and interfaced to the microchip sample inlet with the 20-gauge luer stub adapter. The EOF was produced by

applying -1200 V to the BGE reservoir and grounding the separation and side arm channels as shown in Figure 5.3 A.

Sample injection, shown in Figure 5.3 B, for the double-T microchip was achieved by floating the high voltage for 0.4 s, which allowed sample to fill the interface. The high voltage was then re-applied, which reestablished the gate at the interface and injected a sample plug into the separation channel.

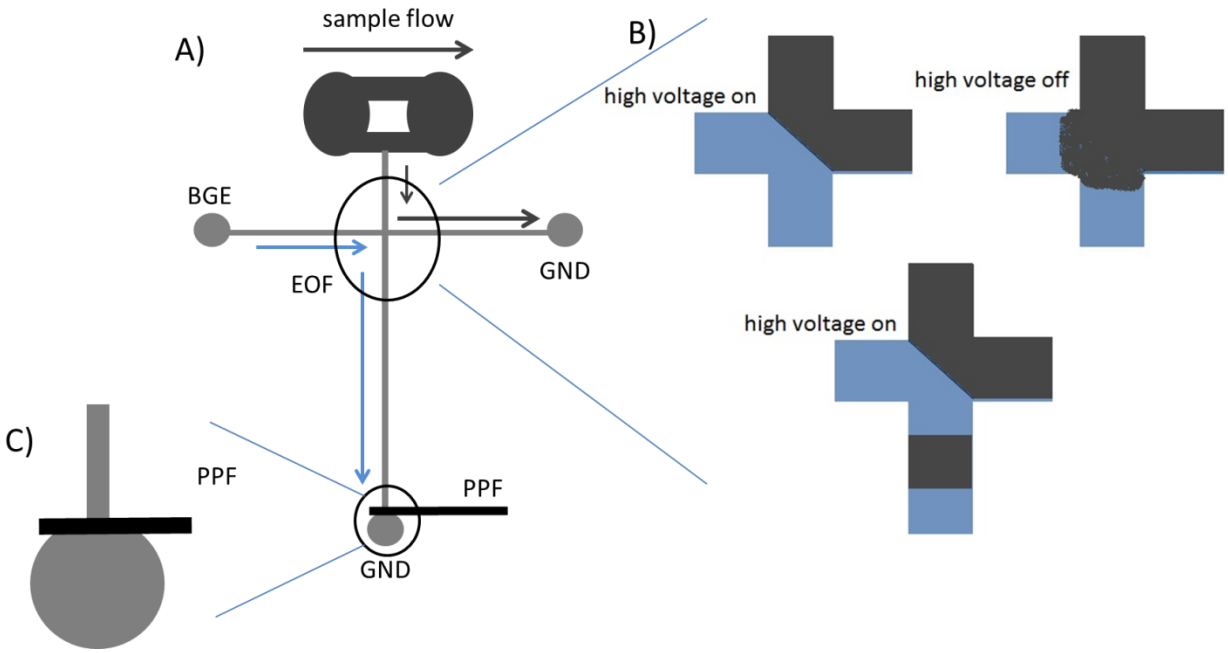

Figure 5.3: A schematic of A) a double-T microchip with a 2.5 cm separation channel, B) the sample injection procedure and C) the in-channel electrode alignment.

5.2.6. Electrochemical detection

5.2.6.1 Cyclic voltammetry

Cyclic voltammetry (CV) was performed using an 812c potentiostat (CH Instruments, Inc., Austin, TX, USA*).* The electrochemical detection cell consisted of a 1.6 mm diameter platinum or a 3 mm diameter glassy carbon working electrode (Bioanalytical Systems, Inc., West Lafayette, IN, USA), a platinum wire auxiliary electrode, and an Ag/AgCl reference electrode (Bioanalytical Systems, Inc., West Lafayette, IN, USA). All cyclic voltammograms employed a scan rate of 100 mV/s using a 1 mV sampling rate. Peak height and peak potential were determined for the oxidation of nitrite, shown in Equation 4.1, from the CVs using Origin 8.6 software (OriginLab, Northampton, MA, USA) following baseline subtraction.

Working electrodes were cleaned prior to each use. The glassy carbon electrode was prepared by polishing the surface with alumina slurry (Bioanalytical Systems) then rinsing with DI water to remove residual alumina. The platinum electrode was polished sequentially using a series of diamond slurries (Bioanalytical Systems) with 6 μm, 3 μm, and 1 μm particle sizes, then rinsed with DI water. Three different BGEs with 1 mM nitrite were evaluated with cyclic voltammetry (CV) A) 25 mM sodium citrate, 2 mM TTAB at pH 4.5, B) 25 mM phosphate, 2 mM TTAB at pH 7.2, and C) 25 mM boric acid, 2 mM TTAB at pH 9.2.

5.2.6.2 Amperometric detection

Amperometric detection for the microchip electrophoresis experiments was performed using an electrically isolated two-electrode potentiostat (Pinnacle Technology, Lawrence, KS, USA) with a 5 Hz sampling rate. The working electrode was a 40 μm wide PPF and a Ag/AgCl reference electrode (Bioanalytical Systems) was used. Electrodes were aligned in-channel, shown in Figure 5.3 C, and a constant potential of +700 mV VS. Ag/AgCl reference electrode

was applied unless otherwise specified. The working electrode was aligned in-channel, as shown in Figure 5.3 C. The background electrolyte (BGE) consisted of 40 mM MES and 2 mM TTAB at pH 6.44 in DI. Nitrite stock (10 mM) was prepared in DI water. Nitrite standards were diluted into BGE or aCSF from the stock.

5.3 Results and Discussion

5.3.1 Electrochemical detection optimization

To determine what type of electrode material, metal or carbon, and what BGE would produce the lowest oxidation potential and the highest oxidation current for nitrite, cyclic voltammetry (CV) was used. The current generated by the oxidation of nitrite for three different BGEs was determined for both platinum and glassy carbon electrodes. The current was normalized for electrode area, as shown in Figure 5.4 A. At both low and high pH conditions, the current response for glassy carbon was better than platinum. At the more neutral pH of 7.2, platinum generated a better current response. This indicates that an oxide may be forming on the surface at the low and high pH conditions but not under the neutral conditions [16]. The oxidation potential for nitrite was also determined. Figure 5.4 B shows that the pH of the BGE had little effect on the oxidation potential, but in all cases a higher potential was needed to oxidize nitrite on platinum than glassy carbon. This implies that glassy carbon is a better material for the oxidation of nitrite than platinum. However, glassy carbon is not easily integrated into a planer microchip. Therefore, pyrolyzed photoresist film (PPF) electrodes were used with a 25 mM sodium citrate, 2 mM TTAB at pH 4.2 BGE, which has been shown to be structurally similar to glassy carbon [18].

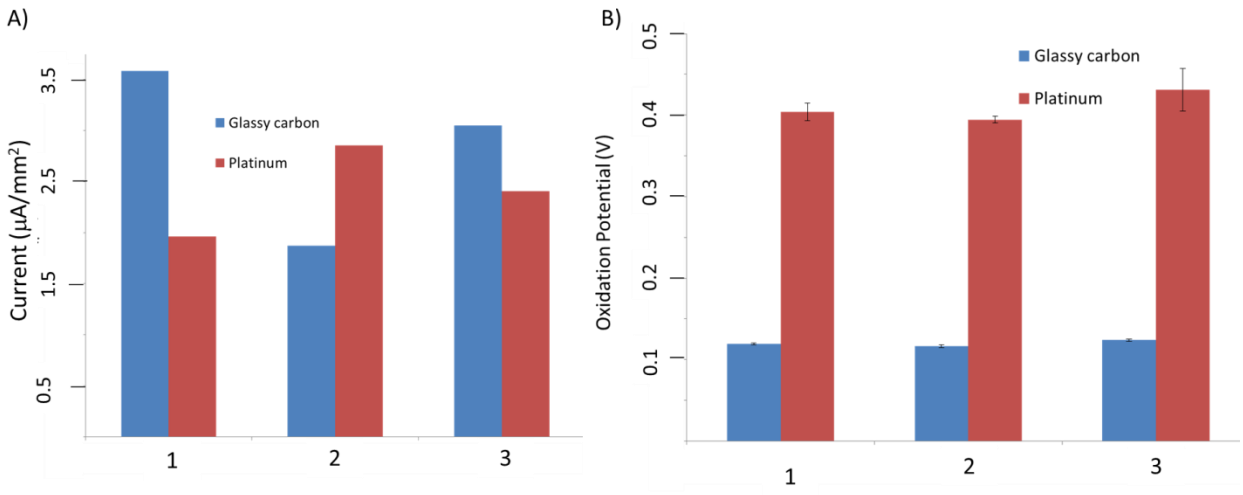

Figure 5.4: A) The oxidation current (normalized to electrode area and B) and peak oxidation potential of 1 mM nitrite in 1) 25 mM sodium citrate, 2 mM TTAB at pH 4.5, 2) 25 mM phosphate, 2 mM TTAB at pH 7.2, and 3) 25 mM boric acid, 2 mM TTAB at pH 9.2 for glassy carbon and platinum electrodes.

In-channel electrode alignment, discussed in Section 2.5.2, affects the apparent potential of the working electrode. This alignment scheme does not decouple the potential applied by the potentiostat from the potential induced by the electrophoretic voltage. Therefore, the actual potential at the working electrode is the sum of the applied potential and the potential induced by the field [32, 33]. Thus, the optimal electrode potential for nitrite was determined experimentally by generating a hydrodynamic voltammogram (HDV) with a simple-T microchip using PPF electrode with in-channel alignment and a 25 mM sodium citrate, 2 mM TTAB at pH 4.2 BGE. As the detection potential is increased, the current generated should also increase until a current limiting plateau is reached. However, the HDV, shown in Figure 5.5 A, had a sharp decline in current after the applied potential reached 0.85 V. The PPF electrode was inspected with a microscope and a portion of it has disintegrated, shown in Figure 5.5 B, which is the probable cause of the abnormal HDV.

To determine if this effect was BGE dependent a separation voltage was applied to a new microchip with the PPF electrode held at 1 V for < 1 min. using a BGE of 10 mM boric acid, 2 mM TTAB at pH 9.2. The same electrode deterioration was observed. Thus, it was hypothesized that PPF electrodes cannot withstand large amounts of current. This means that as higher potentials are applied the PPF becomes smaller due to disintegration. This would explain why there is such a sharp decrease in signal at 0.85 V, as shown in the HDV (Figure 5.5), when there should be an increase or plateau for current response as potential is increased.

In order to lower the amount of current the PPF electrodes were exposed to a lower conductivity BGE (40 mM MES, 2 mM TTAB at pH 6.44) was used, the working electrode potential was reduced to 0.7 V vs. Ag/AgCl and the electrode was aligned so that only a small

portion (< 2 μm) of the electrode was in the channel. Using these low current conditions the PPF electrodes were indeed stable and did not deteriorate with use.

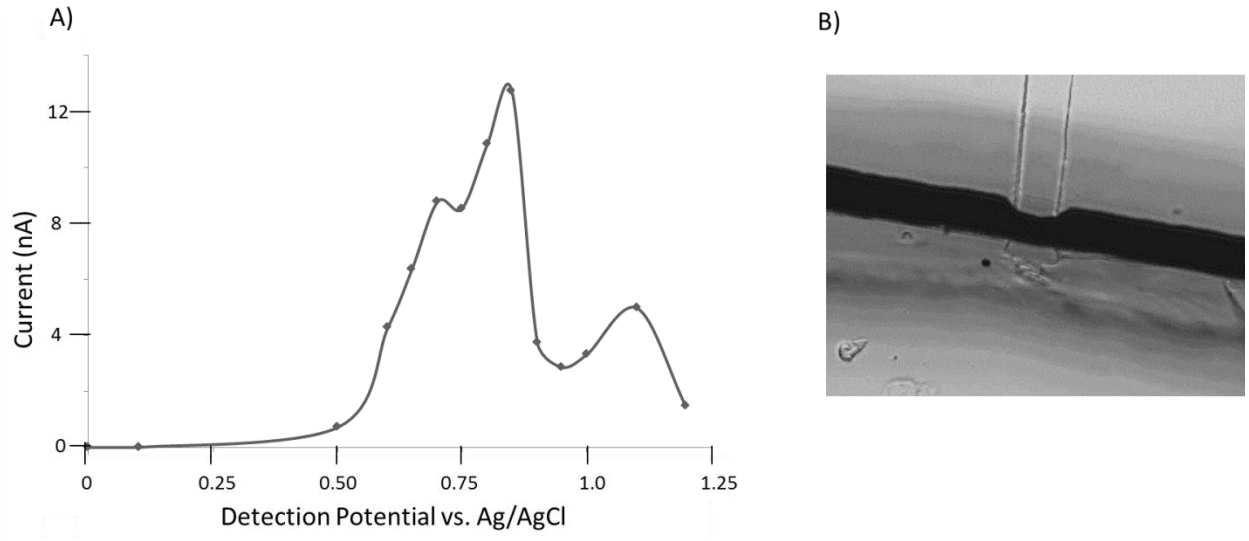

Figure 5.5: A) An HDV of 500 μM nitrite in 25 mM sodium citrate, 2 mM TTAB at pH 4.5 and B) the PPF electrode after use.

5.3.2 Analysis of a continuous hydrodynamic flow using ME-EC

The on-line system, shown in Figure 5.6, was then evaluated using a syringe pump containing nitrite dissolved in BGE (100 μM final concentration). A gate was established using a sample flow rate of 0.5 μL/min with -1200 V applied to the BGE reservoir. The gating was stable over a flow rate range of 0.2 - 0.5 μL/min. However, at the lower flow rates the pulsing produced by the syringe pump was more noticeable. At flow rates higher than 0.5 μL/min too much pressure was created in the sample flow channel and delamination of the PDMS from the glass occurred.

The electropherogram in Figure 5.7 was generated using baseline subtraction (4.6, Origin 8.6 software) and shows three injections of the 100 μM nitrite standard in BGE (40 mM MES, 2 mM TTAB at pH 6.44) . The 0.4 s injections of sample resulted in nitrite migrating at 22 s ± 2 with 1.4 s ± 0.1 peak widths. A sample of 100 μM nitrite in aCSF was then used in order to simulate a microdialysis sample. However, this caused the injection gate to be very unstable and sample to continuously leak into the separation channel. The high conductivity of the aCSF also caused joule heating, which damaged the PDMS, as shown in Figure 5.8.

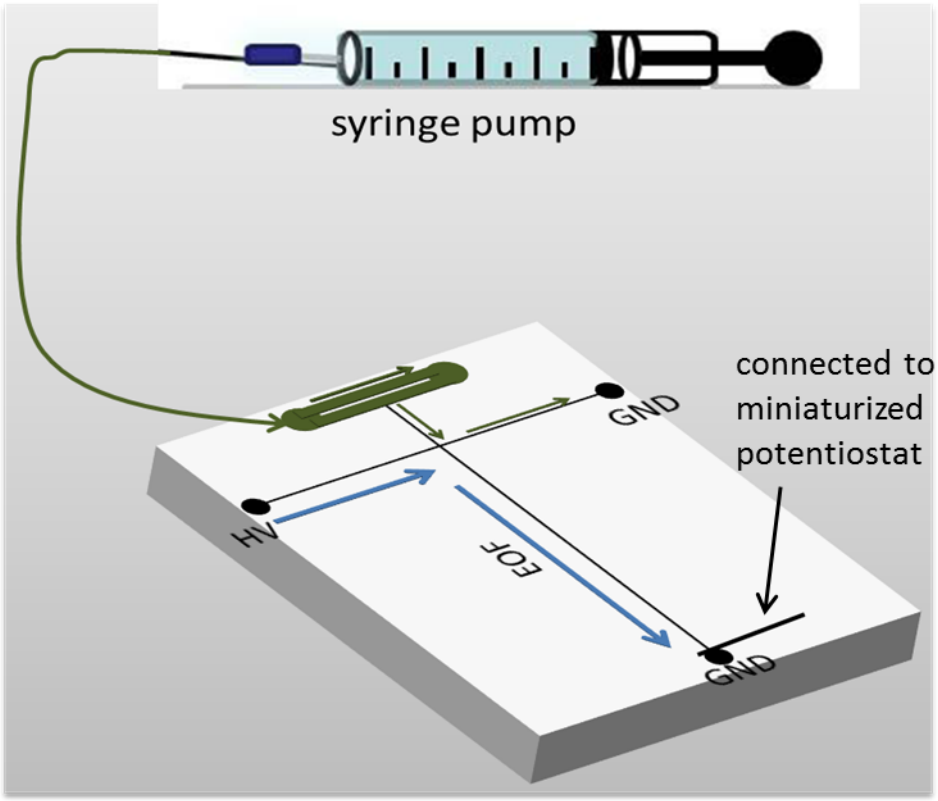

Figure 5.6: A schematic of the on-line system were the syringe holds the sample (100 μM nitrite in BGE) with a flow rate at 0.5 μL/min and -1200 V applied to the high voltage (HV) reservoir. The PDMS microchip was placed over a PFF electrode aligned in-channel.

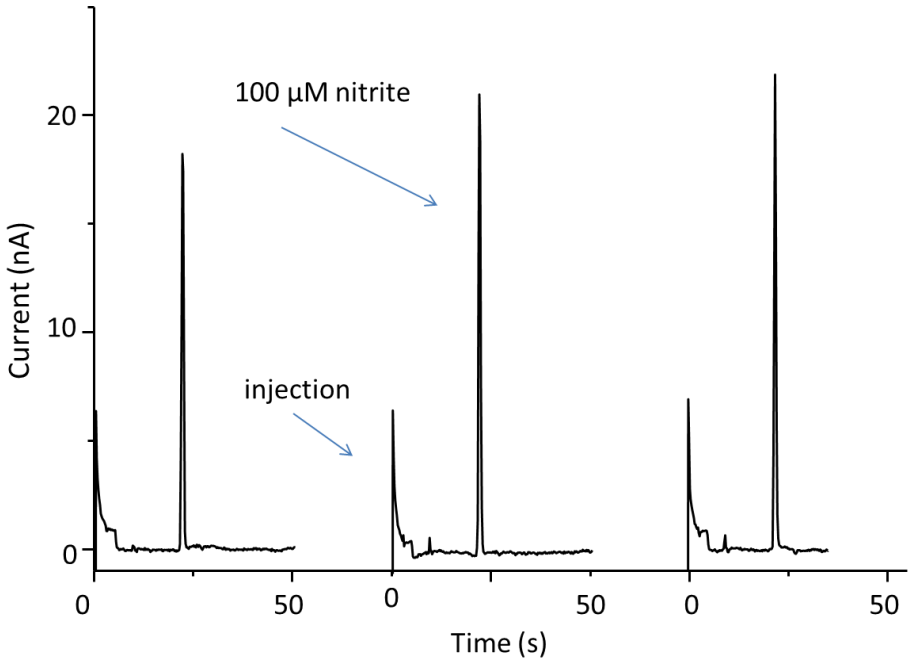

Figure 5.7: Electropherogram of three injections (0.4 s) of 100 µM nitrite in BGE (40 mM MES 2 mM TTAB pH 6.44) using a 0.5 µL/min sample flow rate and -1200 V applied separation voltage. The working electrode was at 0.7 V VS. Ag/AgCl.

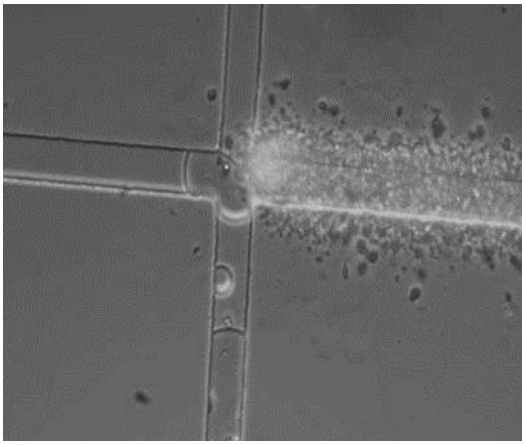

Figure 5.8: Micrograph of PDMS damaged by joule heating.

5.4 Conclusions

The total amount of current that PPF electrodes are exposed to during microchip electrophoresis affected their stability and therefore low conductivity buffers should be used with these electrodes. The altered PDMS monomer to curing agent ratio created a strong bond between the PDMS and the glass layers and prevented leaking, even when used with hydrodynamic flow. The hybrid PDMS/glass PDMS double-T microchip was coupled to a syringe pump to monitor the composition of a standard nitrite solution diluted in BGE.

This method has the ability to couple the hydrodynamic microdialysis flow to ME with electrochemical detection using carbon electrodes, as long as the sample and BGE solutions have similar conductivities. However, in the case of high conductivity samples, the sample injection process needs to be modified. This is based on the fact that nitrite diluted into aCSF, which is commonly used for MD studies, resulted in unstable leaky injections and "burning" of the PDMS layer. The development of a new microchip design capable of correcting the injection problem is described in Chapter 6.

5.5 References

[1] Bult, H., Boeckxstaens, G. E., Pelckmans, P. A., Jordaens, F. H., Vanmaercke, Y. M., Herman, A. G., *Nature* 1990, *345*, 346-347.

[2] Snyder, S. H., *Science* 1992, *257*, 494-496.

[3] Obrenovitch, T. P., Sarna, G. S., Millan, M. H., Lok, S.-Y., Kamauchi, M., Ueda, Y., Symon, L., in: Krieglstein, J., Oberpichler, J. (Eds.), *Pharmacology of Cerebral Ischemia*, Wissenschaftliche Verlagsgesellschaft, Stuttgart 1990, pp. 23-31.

[4] Garthwaite, J., *Trends in Neurosciences* 1991, *14*, 60-67.

[5] Coyle, J. T., Puttfarcken, P., *Science* 1993, *262*, 689-695.

[6] Hakim, T., Sugimori, K., Camporesi, E., Anderson, G., *Physiological Measurement* 1996, *17*, 267-277.

[7] Kikura-Hanajiri, R., Martin, R. S., Lunte, S. M., *Anal. Chem.* 2002, *74*, 6370-6377.

[8] Kang, S.-M., Kim, K.-N., Lee, S.-H., Ahn, G., Cha, S.-H., Kim, A.-D., Yang, X.-D., Kang, M.-C., Jeon, Y.-J., *Carbohydrate Polymers* 2011, *85*, 80-85.

[9] Klinker, C. C., Bowser, M. T., *Anal. Chem.* 2007, *79*, 8747-8754.

[10] Li, H., Wang, H., Chen, J. H., Wang, L. H., Zhang, H. S., Fan, Y., *Journal of Chromatography B* 2003, *788*, 93-101.

[11] Bowser, M. T., Kennedy, R. T., *ELECTROPHORESIS* 2001, *22*, 3668-3676.

[12] Lanckmans, K., Sarrea, S., Smoldersa, I., Michotte, Y., *Talanta* 2008, *74*, 458-469.

[13] Cellar, N. A., Kennedy, R. T., *Lab on a Chip* 2006, *6*, 1205-1212.

[14] Sandlin, Z. D., Shou, M., Shackman, J. G., Kennedy, R. T., *Anal. Chem.* 2005, *77*, 7702-7708.

[15] Scott, D. E., Grigsby, R. J., Lunte, S. M., *ChemPhysChem* 2013, *14*, 2288-2294.

[16] Piela, B., Piela, P., Wrona, P. K., *Journal of The Electrochemical Society* 2002, *149*, E357-E366.

[17] Piela, B., Wrona, P. K., *Journal of The Electrochemical Society* 2002, *149*, E55-E63.

[18] McCreery, R. L., *Chem. Rev.* 2008, *108*, 2646-2687.

[19] Fang, H., Pajski, M. L., Ross, A. E., Venton, B. J., *Analytical Methods* 2013, *5*, 2704-2711.

[20] Martin, R. S., Gawron, A. J., Lunte, S. M., Henry, C. S., *Analytical Chemistry* 2000, *72*, 3196-3202.

[21] McDonald, J. C., Duffy, D. C., Anderson, J. R., Chiu, D. T., Wu, H., Schueller, O. J. A., Whitesides, G. M., *Electrophoresis* 2000, *21*, 27-40.

[22] Vandaveer IV, W. R., Pasas-Farmer, S. A., Fischer, D. J., Frankenfeld, C. N., Lunte, S., M., *Electrophoresis* 2004, *25*, 3528-3549.

[23] Hulvey, M. K., Genes, L. I., Spence, D. M., Martin, R. S., *Analyst* 2007, *132*, 1246-1253.

[24] Hulvey, M. K., Martin, R. S., *Anal. Bioanal. Chem.* 2009, *393*, 599-605.

[25] Sameenoi, Y., Mensack, M. M., Boonsong, K., Ewing, R., Dungchai, W., Chailapakul, O., Cropek, D. M., Henry, C. S., *Analyst* 2011, *136*, 3177-3184.

[26] Martin, R. S., Gawron, A. J., Fogarty, B. A., Regan, F. B., Dempsey, E., Lunte, S. M., *Analyst* 2001, *126*, 277-280.

[27] Johnson, A. S., Selimovic, A., Martin, R. S., *Electrophoresis* 2011, *32*, 3121-3128.

[28] Vandaveer, W. R., Pasas-Farmer, S. A., Fischer, D. J., Frankenfeld, C. N., Lunte, S. M., *Electrophoresis* 2004, *25*, 3528-3549.

[29] Fischer, D. J., Hulvey, M. K., Regel, A. R., Lunte, S. M., *Electrophoresis* 2009, *30*, 3324-3333.

[30] Hebert, N. E., Snyder, B., McCreery, R. L., Kuhr, W. G., Brazill, S. A., *Anal. Chem.* 2003, *75*, 4265-4271.

[31] Fischer, D. J., Vandaveer, W. R. I. V., Grigsby, R. J., Lunte, S. M., *Electroanalysis* 2005, *17*, 1153-1159.

[32] Gunasekara, D. B., Hulvey, M. K., Lunte, S. M., *ELECTROPHORESIS* 2011, *32*, 832-837.

[33] Martin, R. S., Ratzlaff, K. L., Huynh, B. H., Lunte, S. M., *Anal. Chem.* 2002, *74*, 1136-1143.

Chapter Six:

Microchip Design for Electrokinetic Sampling of Microdialysis Flow

6.1 Introduction

Microdialysis sampling for *in vivo* animal studies requires the use of high conductivity perfusate such as Ringer's solution or artificial cerebral spinal fluid (aCSF) in order to maintain physiological relevance [1]. This is especially important for long-term awake and freely moving animal studies [2]. Conversely, the use of a low conductivity background electrolyte (BGE) is necessary for microchip electrophoresis with amperometric detection to minimize joule heating and background current (noise), and to obtain good limits of detection [3]. The lower the joule heating the higher the field strength that can be applied, leading to better separation efficiencies [4, 5].

The ability to injection discreet sample plugs into a separation channel for electrophoresis from a continuous flow is not trivial. Small portions of the sample must either be removed from the hydrodynamic microdialysis flow (without stopping it) or the flow must be diverted into the separation channel for a controlled amount of time. Also, the pressure exerted by the hydrodynamic flow can cause microchips that are not well sealed to leak.

Several approaches have been reported in the literature for the injection of small plugs of microdialysis sample into the electrophoresis separation channel, some of which are addressed in Section 2.4. The Martin group was able to inject a small plug of the sample hydrodynamically by integrating pressure driven valves into PDMS microchips. The valves are pneumatically actuated by compressed gas and diverting the sample either into the separation channel or to sample waste as shown in Figure 2.12, Chapter 2 [6, 7]. Another approach for diverting small amounts of sample flow into a separation channel was described by Buettgenbach *et al.* This approach is shown in Figure 6.1 A. In this case, a passive valve connected a large sample channel with the separation channel. The default position for the valve was closed. To inject

sample into the separation channel, the outlet of the sample channel outlet was blocked. This increased the pressure on the valve and forced it into an open position, causing sample to flow into the separation channel. The injection was complete when the outlet of the sample channel was opened which reduced the pressure and closed the valve [8]. The use of hydrodynamic pressure in these applications eliminates the injection bias that is commonly seen in electrokinetic injections. This second method has not yet been employed for microdialysis. If it were to be used, the pressure and flow rate of the perfusate would change during each injection, making it difficult to determine recovery.

Electrokinetic injections often use electroosmotic flow (EOF) to divert hydrodynamic sample flow out of the separation channel. When a sample injection is needed, the EOF is reduced or stopped, and the hydrodynamic force will once again divert the sample into the separation channel. An example of such an injection method was published by Attiya *et al.*, who designed a sample injection interface (shown in Figure 6.1 B) that used a small channel to connect a large sample flow to the separation channel [9]. Since the sample flow channel had a much larger (800x) internal volume than the connecting channel, the pressure that the sample flow exerted on the separation channel interface was greatly reduced. Thus, the force generated by the EOF during a separation was enough to keep the sample flow out of the separation channel. When a sample injection was needed, the EOF was turned off, and the sample flow was allowed to enter the separation channel. This approach of reducing the hydrodynamic force present at the sample injection interface has been integrated into other microchip designs, including the double-T microchip design described in Figure 2.13 [10-12].

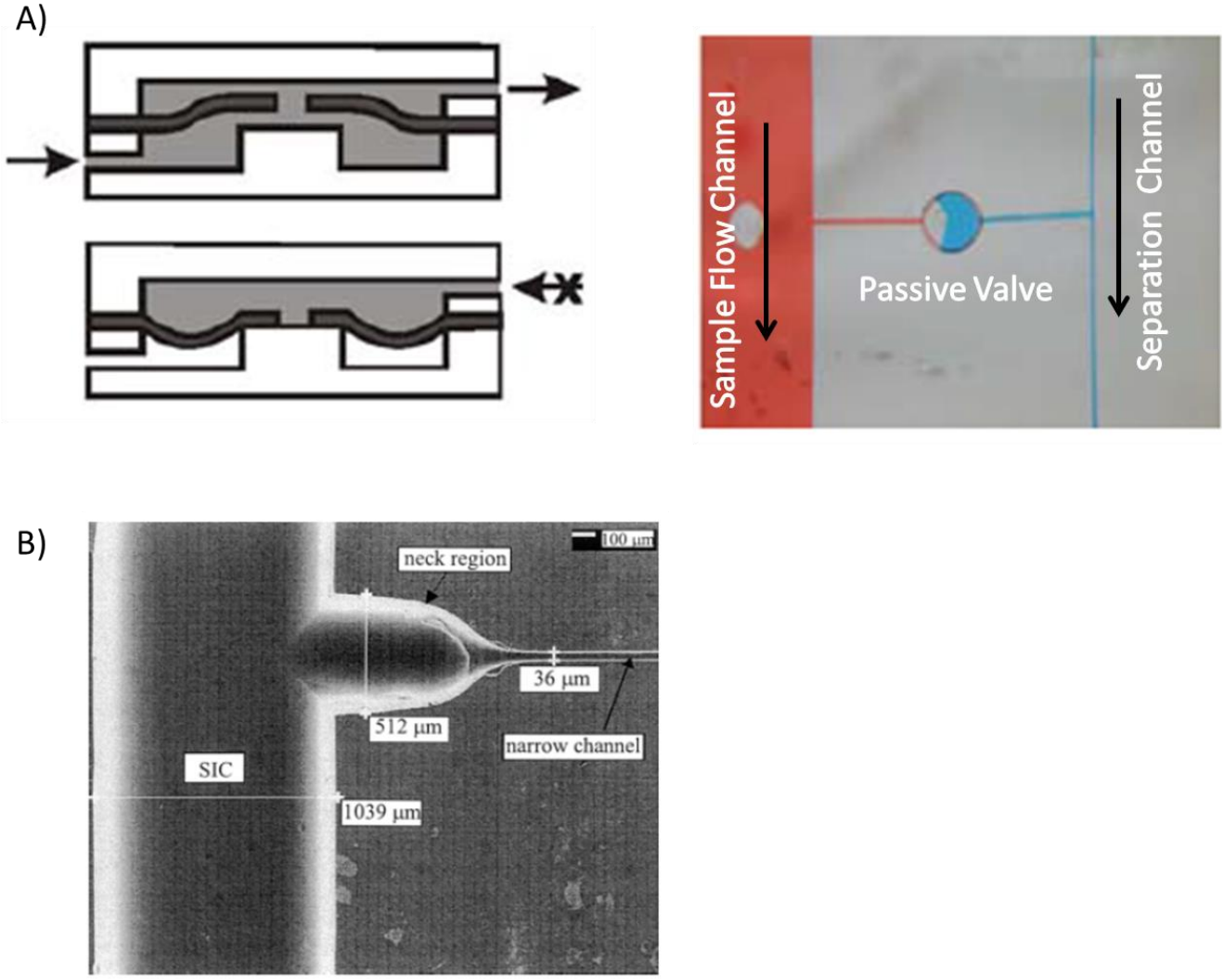

Figure 6.1: A) Schematic (cross-sectional view) and photograph (top view) of the integrated passive valve. The schematic shows the two possible states of the check valve: open (top) and blocked (bottom). Dye was added to the water to allow better viewing clarity (adapted with permission from [8]) B) Electron micrograph of the sample introduction channel (SIC) 1 mm wide and 300 µm deep intersection with the electrokinetic injection channel etched to 36 µm width and 10 µm depth. The neck region was caused by under-etching in some masking procedures (reproduced with permission from [9])

Our lab has used the double-T microchip design to couple microdialysis flow to microchip electrophoresis (ME) as described in Section 5.2.5. Those studies all used BGEs with conductivities that were similar to that of the microdialysis perfusate. However, when the conductivities of the sample flow and the BGE differ significantly, the injection gate becomes very unstable and problems with sample leaking into the separation channel occur. A similar unstable electrokinetic injection due to the sample flow and BGE conductivities being different has been previously described in the literature [13]. Wu *et al*. attempted to perform on-line sampling and analysis of the extracellular fluid (ECF) of rat organotypic hippocampal slices cultured in aCSF using electroosmotic (EO) pumping and ME, as shown in Figure 6.2. However, when trying to inject the high conductivity sample into a separation channel filled with a low conductivity BGE using a gated injection no sample was injected. In order to understand this injection failure, Wu and coworkers employed a finite element modeling program, COMSOL, to simulate the injection process [13]. COMSOL has also been used to model electroosmotically facilitated push-pull sampling [14], heat transfer in microchannels for microfluidic devices [15], and sample transport in electrokinetic injections [16].

In this chapter, the finite element modeling program COMSOL was used to model the double-T injection in order to better understand why using significantly different conductivities for the sample and BGE created an unstable injection. In addition, a novel bow-microchip design was developed and the injection process simulated and compared with the existing double-T design. The new design was then evaluated experimentally using fluorescein to visualize the sample flow at the injection interface.

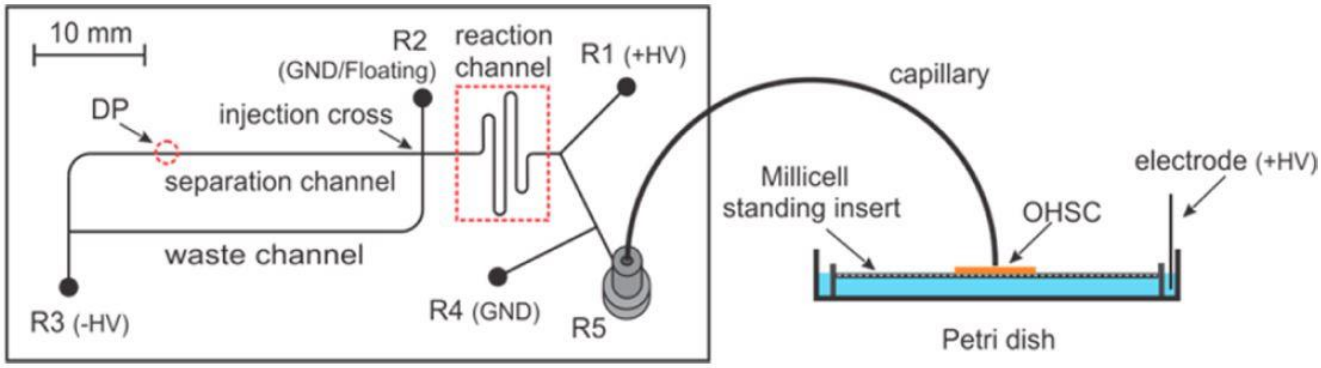

Figure 6.2: The EO sampling of brain slices coupled to microchip electrophoresis. Reproduced with permission from [13].

6.2 Materials and Methods

6.2.1 Materials

All reagents were analytical grade or better and used as received. All solutions were prepared with deionized (DI) water with 18.3 MΩ resistances (Millipore, Kansas City, MO, USA). Tetradecyltrimethylammonium bromide (TTAB), 2-(N-morpholino) ethanesulfonic acid (MES), magnesium chloride ($MgCl_2$), calcium chloride ($CaCl_2$) and sodium fluorescein were obtained from Sigma Aldrich (Saint Louis, MO, USA). Sodium phosphate dibasic heptahydrate and sodium phosphate monobasic were purchased from Acros and Mallinckrodt (St. Louis, MO, USA), respectively. Acetonitrile, isopropanol, potassium chloride (KCl) and sodium chloride (NaCl) were obtained from Fisher Scientific. Artificial cerebral spinal fluid (aCSF) was consisted of 148 mM NaCl, 3 mM KCl, 1.4 $CaCl_2$, 0.8 mM $MgCl_2$ and 0.9 mM phosphate at pH 7.4. The background electrolyte (BGE) for the electrophoresis separations consisted of 10 mM MES, 2 mM TTAB and 1% (v/v) acetonitrile in deionized water.

6.2.2 Microchip fabrication

PDMS microchips were fabricated using a semi-cure method that has been described elsewhere [17]. Briefly, a silicon wafer/SU-8 10 master was fabricated according to the procedure detailed in Section 3.3.1, with feature depths of 25 μm. PDMS monomer and curing agent (Sylagard184, Dow Corning, Midland, MI, USA) were mixed in a 20:1 ratio and de-gassed in a vacuum to eliminate any bubbles. The mixture was poured onto the master, placed in an oven at 90°C and evaluated every 1-2 min by placing a metal tongs on the surface and pulling it away. The wafer was taken out of the oven when the PDMS no longer pulled away with the tongs. A blank piece of PDMS was prepared in the same manner, except that blank silicon wafer was used instead of a master. The channel and blank PDMS were prepared concurrently and

allowed to cool completely before they were removed from the wafers. Once removed, the channel containing PDMS substrate had access reservoirs punched into it using a biopsy punch (Harris Uni-Core, Redding, CA, USA). The microdialysis sample flow inlet was accessed by inserting a 20-gauge luer stub at the beginning of the sample flow channel. The channel containing PDMS layer was then placed channel side down on the blank PDMS layer. Great care was taken so that no air bubbles were trapped between the two pieces of PDMS. The completed PDMS microchip was then heated in an oven overnight at 80°C to create an irreversible bond between the two substrates.

6.2.3 COMSOL parameters

The conductivity values for the BGE (2.11×10^{-2} S/m) and aCSF (2.873 S/m) were calculated using Peakmaster 5.3 software [18]. Using experimental values determined by Cocke *et al.* for a glass surface with 2 mM TTAB at pH6 , the EOF was defined as - 2×10^{-4}($cm^2 * V^{-1} * s^{-1}$) [19]. The conductivities of the channels were defined by Equation 6.1.

$$Conductivity = BGE * \left(\frac{C1}{C1+C2}\right) + Sample * \left(\frac{C2}{C1+C2}\right) \quad \textbf{Eq. 6.1}$$

In this equation, *BGE* is the conductivity (S/m) of the BGE, *Sample* is the conductivity of the sample, *C1* is the concentration of BGE and *C2* is the concentration of the sample.

All simulations were performed using 3D models and geometries for channels having widths of 40 μm and depths of 25 μm, unless otherwise indicated. Channels with hydrodynamic flow had fluid velocity of zero at the surface boundary (no-slip conditions) and both EOF and hydrodynamic flow were calculated using laminar flow with inertial terms disregarded (Stokes flow). Figure 6.3 A-B shows the double-t and bow microchip designs with the flow rates (1 μL/min) and voltages (-2000 V) used in the simulation. In order to reduce the computational time needed for the calculations, channel lengths were modeled $1/20^{th}$ to scale but the widths and

depths of the channels were not changed. The voltages and flow rates were also scaled to preserve pressure and voltage drops, but for clarity only the original values are shown.

6.2.4 PDMS bow-design microchip operation

Hydrodynamic sample flow was generated with a syringe pump (102 CMA, Holliston, MA, USA) and interfaced to the microchip sample inlet, shown in Figure 6.3 B, with the luer stub adapter. The high voltage power supply (HV Rack, Ultravolt Inc., Ronkonkoma, NY, USA) was controlled using a Labview (National Instruments, Austin, TX, USA) program written in-house and applied to reservoir 1, as in Figure 6.3 B. Two different experimental conditions were investigated. The first employed a low conductivity sample with low conductivity BGE. In this case, a solution of 10 mM MES, 2 mM TTAB and 1% acetonitrile was used for both the BGE and the sample. A gate was established with a 1.4 μL/min sample flow rate and -2000 V applied to reservoir 1, as shown in Figure 6.3. The second parameter conditions used a low conductivity BGE and a high conductivity aCSF for the sample. A gate was established using 1.5 μL/min flow rate and -1000 V applied to reservoir 1, as shown in Figure 6.3. Sample injection for the bow-microchip was achieved using the following procedure: 1) gate was established, 2) high voltage was floated for 1.5 s, which allowed sample to fill the interface, and 3) high voltage was re-applied, which reestablished the gate at the interface and injected a sample plug into the separation channel. Micrographs were taken using a CCD camera (CoolSnap, Photometrics, Tucson, AZ, USA).

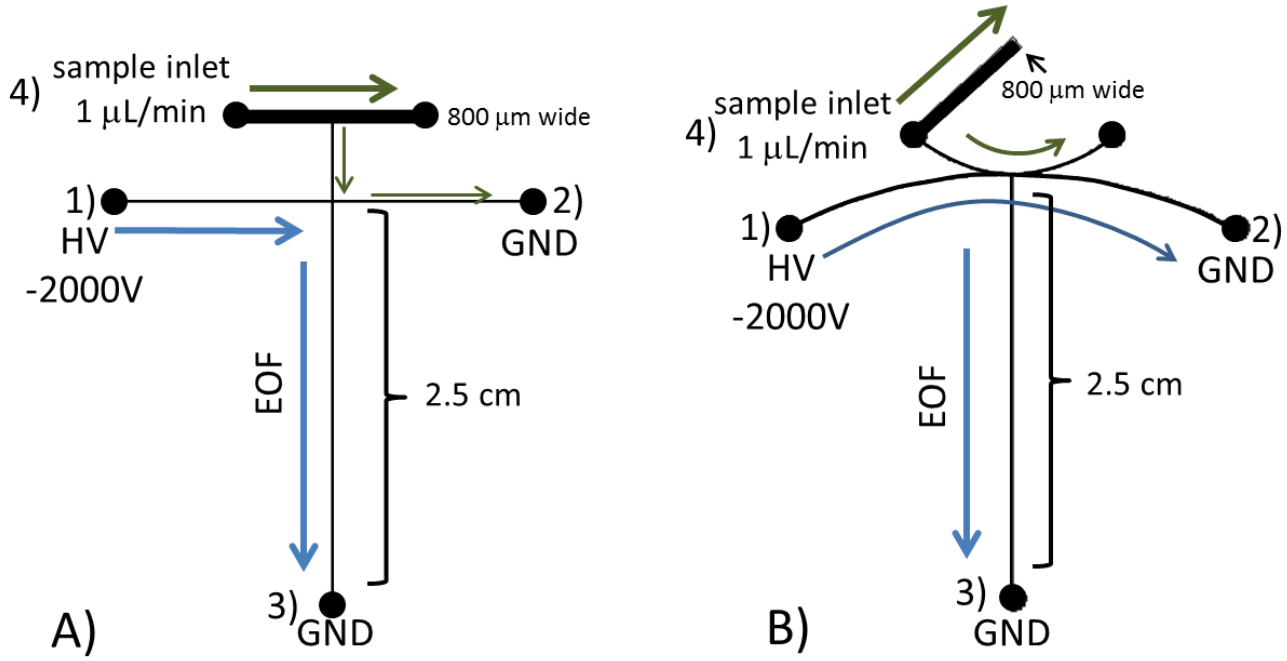

Figure 6.3: A schematic of the A) double-T and B) bow microchip design. Hydrodynamic flow was interfaced at the sample inlet and is represented by the green arrows. High voltage was applied to reservoir 1 and the resulting EOF is represented by the blue arrows.

6.3 Results and Discussion

6.3.1 COMSOL modeling double-T microchip injection

The double-T microchip design used for COMSOL modeling is shown in Figure 6.3 A. In these simulations, the potential was defined by -2000 V at reservoir 1 and reservoirs 2 and 3 held at ground. A laminar inlet flow of 1 μL/min was used for the sample (microdialysis) flow channel at inlet 4. Figure 6.4 A shows the COMSOL simulation of a successfully formed gate with the sample concentration (100 μM of uncharged particles) shown in red. Both the BGE and the sample have identical (low) conductivity values. The corresponding electric potential diagram (Figure 6.4 B) shows a linear voltage drop across the side arms. The current density (A/m^2), shown by the color plot, and the flow velocity, represented by the black arrows, in Figure 6.4 C both have the largest magnitude leading into the T-junction. This means that the sample flow will be swept towards the sample waste side arm and away from the separation channel.

When the sample conductivity was significantly higher than the BGE, the potential drop across the channels was not linear and dependent the conductivity of a mixture of high conductivity sample flow and the low conductivity BGE flow. Figure 6.5 A1-C1 shows the three different phases of how a gate is formed in a double-T microchip and their corresponding simulated sample concentration, potential and current density and velocity. Figure 6.5 A1 shows the concentration of the sample before it enters the injection T, Figure 6.5 B1 when the sample enters the injection T, and Figure 6.5 C1 when the sample fills the side arm.

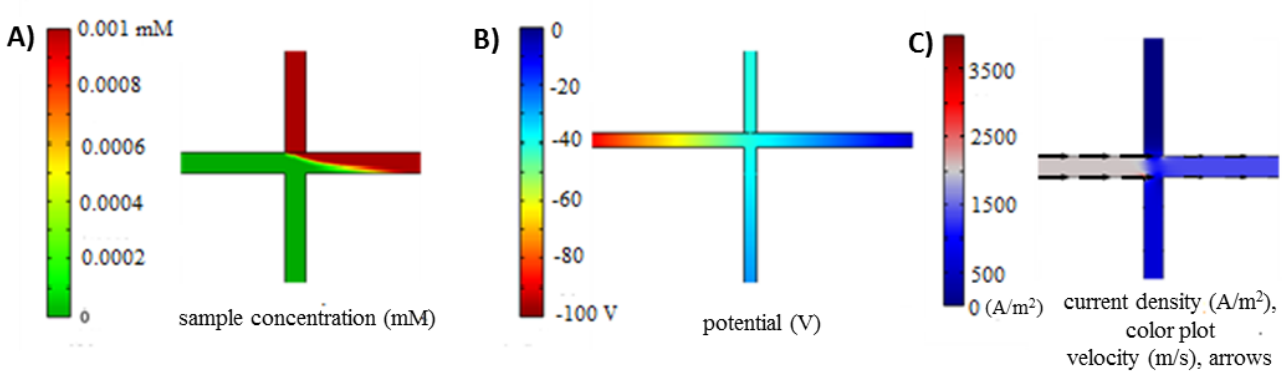

Figure 6.4: The injection area of the double-T microchip for low conductivity sample and BGE conditions; A) The sample concentration in a gating position, B) the potential voltage drop across the microchip and C) the resulting current (color plot) and velocity (arrows).

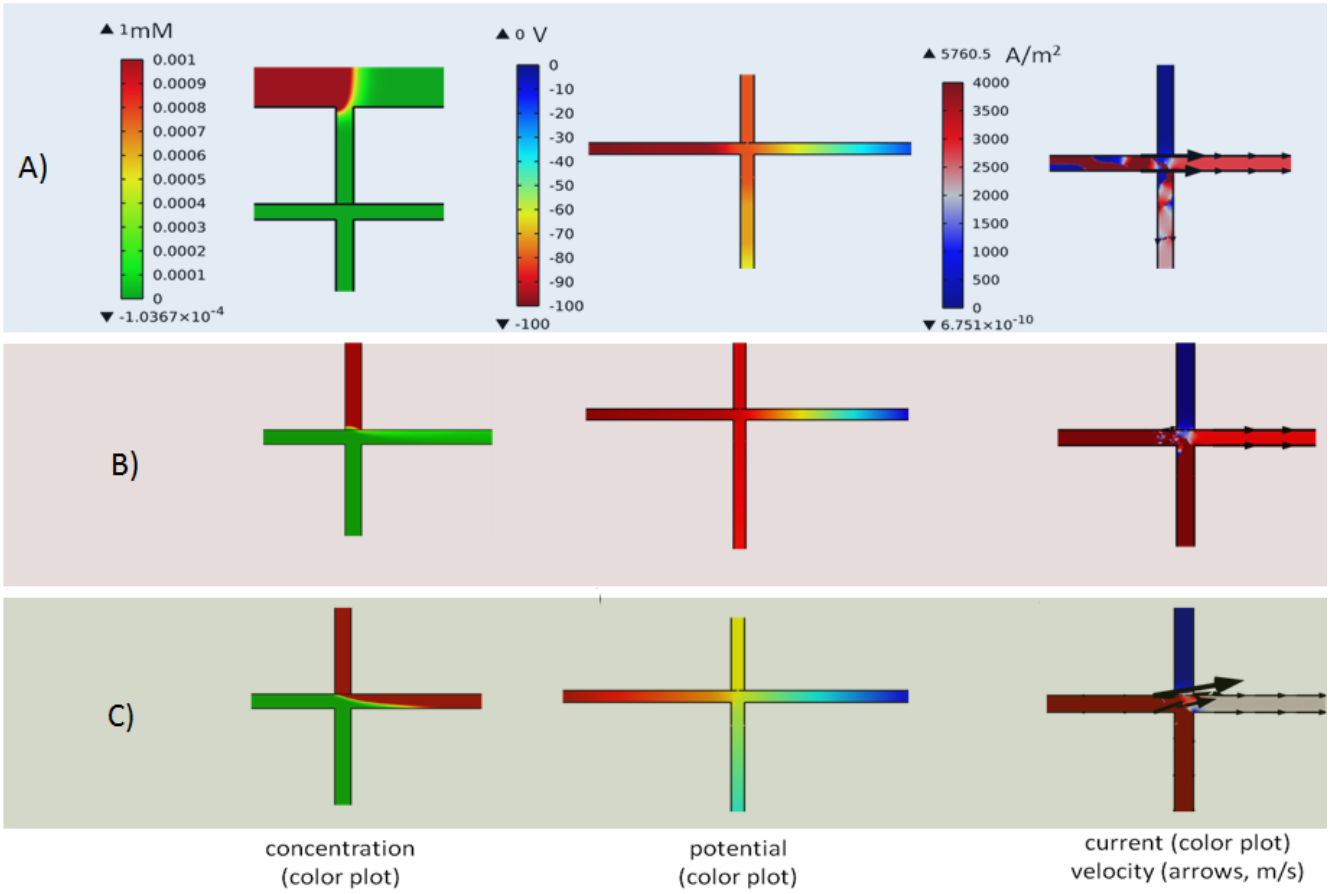

Figure 6.5: The high conductivity sample, low conductivity BGE parameters modeled when the T-junction has different concentrations of sample.

As the sample moves into the T-junction the potential, resulting current density and flow velocity change. In order for a gate to form, the sample flow velocity would also need to be adjusted to compensate for the fluctuating EOF. Additionally, any disturbance in the flow, such as that caused by an injection, would disrupt the flow equilibrium and the gate would fail. Another issue with this design is the large amount of current that is generated in the separation channel. The current density in the separation channel for the low conductivity parameters (low conductivity sample flow and low conductivity BGE) was simulated to be 670 A/m^2. The high conductivity parameters (high conductivity sample and a low conductivity BGE) had a simulated current density in the separation channel a thousand fold higher (67,000 A/m^2).

6.3.2 COMSOL modeling of bow– microchip injection

In order to obviate the problems associated with the double-T microchip design regarding the injection of high ionic strength samples, a new design, called a bow design, shown in Figure 6.3 B, was evaluated using COMSOL. In these simulations, the potential was defined by -2000 V at reservoir 1 and 0 V (ground) at reservoirs 2 and 3. A laminar inlet flow of 1 μL/min was used for the sample (microdialysis) flow channel at inlet 4. Hydrodynamic sample flow passes through the top bow and electroosmotic flow passes through the bottom bow. The separation channel bisects the two bows where they meet at the sample interface. This design limits the amount of sample entering the channels where EOF is the predominant flow mechanism. Thus, it was hypothesized that the potential drop across the bottom bow would be more stable than that of the side arm used for sample waste in the double-T design. Also, the voltage is not grounded through any sample solution which should lower the overall current.

The COMSOL simulations shown in Figure 6.6 A1-C1 are for the high conductivity sample, low conductivity BGE parameters. Columns A-B show three different sample

concentrations in red, which represent how a gate is formed, and the corresponding potential, current density and velocity. Column A, B, and C show that as the high conductivity sample enters the sample injection interface the potential across the same area changes only slightly when the sample first enters the interface. The potential shifted so that a larger drop occurred right before the sample interface. This asymmetry caused the velocity to change only slightly while the current density increased significantly at the sample interface. However, once the sample channel was filled, the potential drop across the interface became more symmetric, and the band of high current density dissipated.

The COMSOL model revealed an unanticipated result: the sample flow volume was reduced at the sample interface. The force generated by the EOF pushed the sample flow up at the interface, which caused a lower than expected conductivity in that area. In order to emphasize this, the analyte concentration scale was changed in Figure 6.6 C. This in turn is why the potential and resulting current density and velocity are so stable, even with a high conductivity sample. This design also exhibits a lower simulated current density (690 A/m^2) in the separation channel, even when a high conductivity sample was being used.

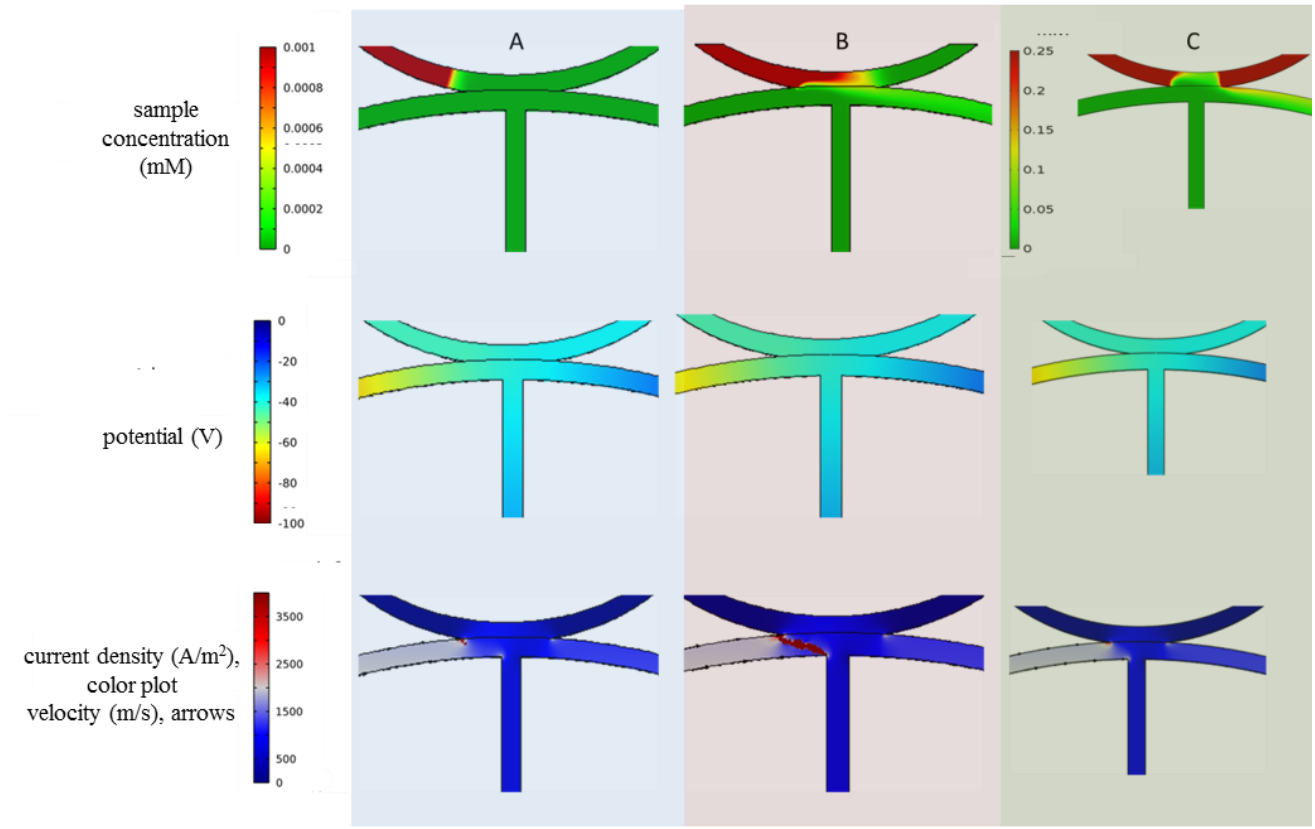

Figure 6.6: Columns A-C show the concentration of the high conductivity sample in the bow–design microchip and the rows show the corresponding potential, current and velocity.

6.3.3 COMSOL modeling of double-T and bow– microchip sample plug

The shape of a sample plug can affect the separation efficiency and resolution, but it is difficult to determine plug shape from micrographs. For this reason, the injection of sample into the separation channel was simulated using COMSOL for both the double-T and bow microchip designs using the low conductivity sample, low conductivity BGE parameters. Figure 6.7 shows the concentration of analyte as a function of time for both the (A) double-T and (B) bow microchip designs. Both injection methods produced an asymmetric plug shape due to the amount of time it takes for the sample flow in the left (buffer) side arm to move across the separation channel and enter the right (sample waste) side arm.

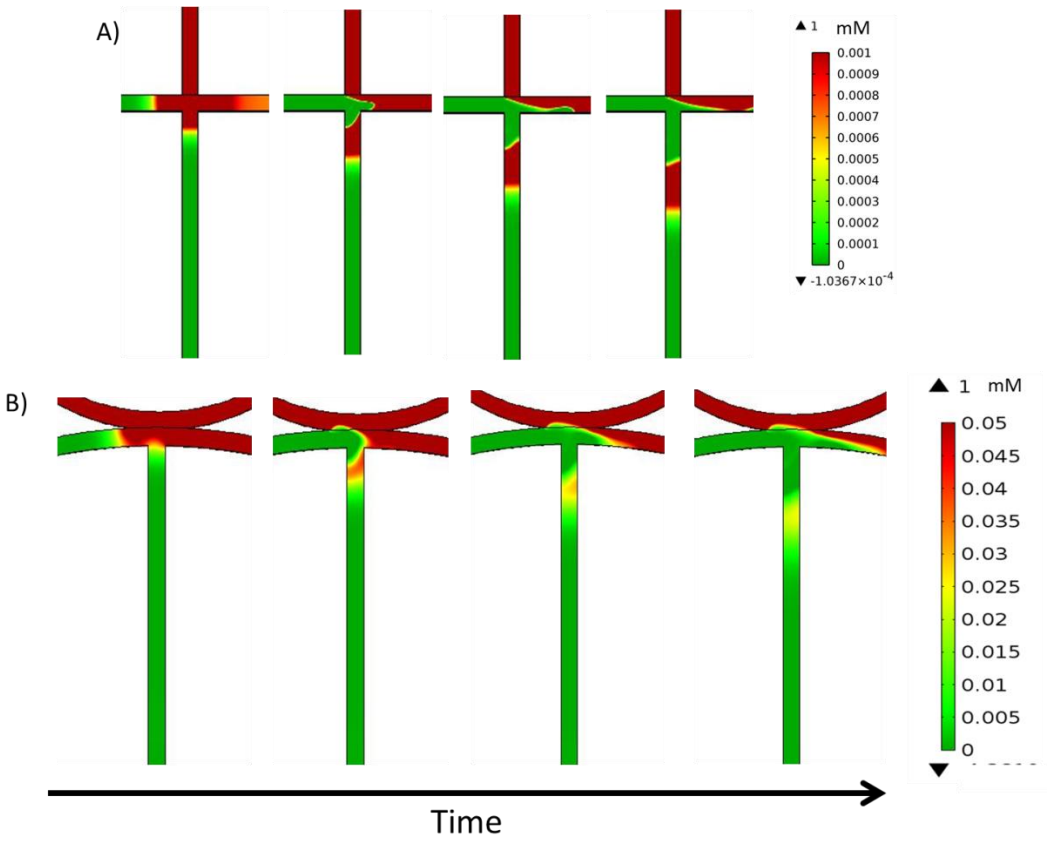

Figure 6.7: The concentration of sample as an injection plug enters the separation channel for A) the double-T design and B) bow design.

6.3.4 Experimental sample injections with bow–microchip design

The bow design was fabricated in PDMS and the two sample conductivity parameters were investigated experimentally. Using the low conductivity sample with low conductivity BGE condition a stable injection gate (n=20) was established using 1.4 μL/min sample flow rate and -2000 V applied voltage and is shown in Figure 6.8. The resulting current in the separation channel was 10 μA. The flow rates needed to establish a stable gate were slightly different between the COMSOL model and the experimental results. However, the COMSOL model used a no-slip boundary for the hydrodynamic flow but did not account for how the material (in this case PDMS) would affect the flow. As PDMS is very hydrophobic, the resistance to hydrodynamic flow of the aqueous solution, even with 1% acetonitrile and TTAB, may account for the difference in flow rates for a successful gate between the model and the experimental.

The same microchip was then used with the high conductivity sample and low conductivity BGE conditions. A successful gate was established using 1.5 μL/min sample flow rate and -1000V applied voltage. This applied potential is lower than that used for the COMSOL model to achieve successful gating. This may be due to the amount of sample that enters the bottom bow after an injection as shown in the COMSOL model Figure 6.7 B. This would increase the conductivity at the sample interface and cause a larger potential drop to occur in that area. Thus, increasing the force exerted by the EOF at the gate.

A series of micrographs are shown in Figure 6.9, which show a single injection (of 20 total injections) of 100 μM fluorescein in aCSF. The resulting current in the separation channel was 10 μA, but the field strength used was half that of the low conductivity parameters. This small increase in the current being generated was probably due to sample that had entered the

bottom bow. Despite this, the bow-microchip design was able to repeatedly inject (n=20) high conductivity samples with a low conductivity BGE.

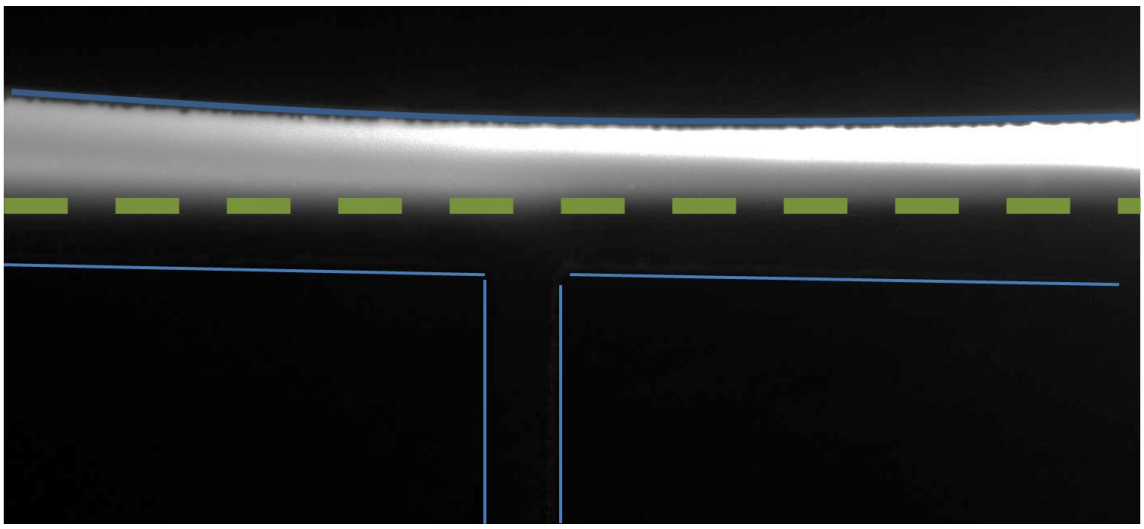

Figure 6.8: A micrograph of the injection interface for the bow design microchip. The bright/white color is 100 μM fluorescein in the sample. The channels of the microchip are outlined by blue lines and the gate is highlighted with the green dashed line.

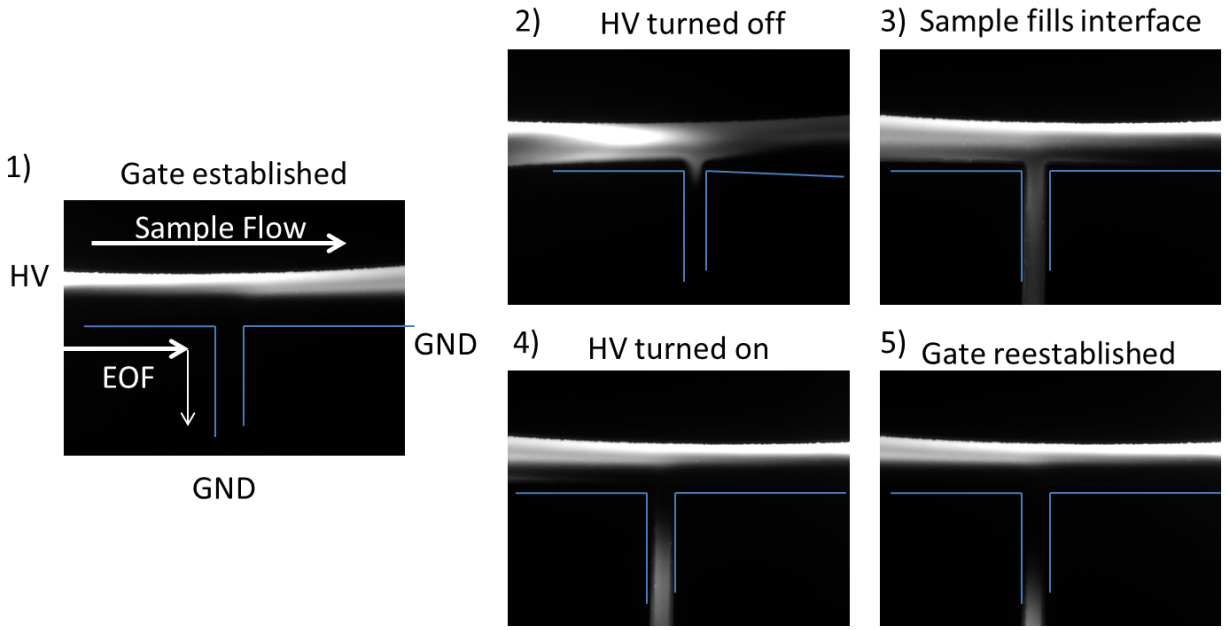

Figure 6.9: Micrographs of an injection of 100 μM fluorescein diluted in aCSF

6.4 Conclusions

The finite element analysis software COMSOL was used to investigate why the double-T design microchip cannot be used when the sample and BGE have significantly different conductivities. A new bow−microchip design for on-line microdialysis-microchip electrophoresis was evaluated and compared with the double-T design using COMSOL. The simulations predicted a stable injection with lower background current for this design. The experimental data for the bow microchip design did indeed have a stable injection and low background current. The ability to use a low conductivity BGE in conjunction with microdialysis sampling should improve the sensitivity of microchip electrophoresis with electrochemical detection for neurotransmitters by lowering the background current, improving separation efficiency, and minimizing joule heating. Additionally, the simplicity of the on-line method, which only a power supply and syringe pump, will allow for this system to be portable, which makes it compatible with an on-animal system. The last chapter gives a summary and the future directions of this thesis.

6.5 References

[1] de Lange, E. C. M., de Boer, A. G., Breimer, D. D., *Advanced Drug Delivery Reviews* 2000, *45*, 125-148.

[2] Stenken, J. A., *Anal. Chim. Acta* 1999, *379*, 337-357.

[3] O'Shea, T. J., Greenhagen, R. D., Lunte, S. M., Lunte, C. E., *Journal of Chromatography* 1992, *593*, 305-312.

[4] Cao, J., Cheng, P., Hong, F., *Sci. China Ser. E-Technol. Sci.* 2009, *52*, 3477-3490.

[5] Zhu, Y., Nahavandi, S., Bui, A., Petkovic-Duran, K., 2005, 603612-603612.

[6] Li, M. W., Martin, R. S., *ELECTROPHORESIS* 2007, *28*, 2478-2488.

[7] Mecker, L. C., Martin, R. S., *Anal. Chem.* 2008, *80*, 9257-9264.

[8] Büttgenbach, S., Wilke, R., *Anal. Bioanal. Chem.* 2005, *383*, 733-737.

[9] Attiya, S., Jemere, A. B., Tang, T., Fitzpatrick, G., Seiler, K., Chiem, N., Harrison, D. J., *ELECTROPHORESIS* 2001, *22*, 318-327.

[10] Sandlin, Z. D., Shou, M., Shackman, J. G., Kennedy, R. T., *Anal. Chem.* 2005, *77*, 7702-7708.

[11] Lin, Y.-H., Lee, G.-B., Li, C.-W., Huang, G.-R., Chen, S.-H., *Journal of Chromatography A* 2001, *937*, 115-125.

[12] Chen, S. H., Lin, Y. H., Wang, L. Y., Lin, C. C., Lee, G. B., *Anal. Chem.* 2002, *74*, 5146-5153.

[13] Wu, J., Xu, K., Landers, J. P., Weber, S. G., *Anal. Chem.* 2013, *85*, 3095-3103.

[14] Rupert, A. E., Ou, Y., Sandberg, M., Weber, S. G., *ACS Chemical Neuroscience* 2013, *4*, 849-857.

[15] Koşar, A., *International Journal of Thermal Sciences* 2010, *49*, 635-642.

[16] Kovarik, M. L., Lai, H. H., Xiong, J. C., Allbritton, N. L., *ELECTROPHORESIS* 2011, *32*, 3180-3187.

[17] Nandi, P., Desai, D. P., Lunte, S. M., *ELECTROPHORESIS* 2010, *31*, 1414-1422.

[18] Gaš, B., Jaroš, M., Vlastimil, H., Zuskova, I., Štědrý, M., *LC-GC Europe* 2005, *18*, 282-288.

[19] Cocke, D. L., Schennach, R., Yu, Z. H., *J. Chromatogr. Sci.* 2002, *40*, 187-190.

Chapter Seven:

Thesis Summary and Future Direction

7.1 Thesis Summary

This thesis describes the development of microfluidic devices that are capable of interfacing with microdialysis sampling, performing electrophoretic separations with electrochemical detection. It also describes the development of an integrated graphite/PMMA composite electrode for electrochemical detection in polymer chips. Chapter 2 contains background information on microdialysis, microchip electrophoresis and electrochemical detection. It also discusses approaches for coupling microdialysis to microchip electrophoresis. In Chapter 3, methods that can be employed for the fabrication of polymer microfluidic devices are described. Specifically, the advantages, disadvantages, relative costs and the appropriateness of each method for specific applications are discussed. It was found that a PDMS microchip fabricated using silicon wafers with SU-8 10 features was the best method for rapid production of microfluidic devices. Therefore, that method was often used to prototype new microchip designs.

Chapter 4 describes the fabrication and integration of a graphite/PMMA composite electrode (GPCE) into a PMMA substrate. The GPCE was optimized for the electrochemical detection of dopamine. The electrodes were evaluated using cyclic voltammetry, flow-injection analysis with amperometric detection, and microchip electrophoresis with amperometric detection. These electrodes exhibited low noise and low LOD for dopamine, but showed high electrode-to-electrode variability. Thus, each electrode must be individually calibrated.

In chapter 5, a microchip capable of interfacing the hydrodynamic flow from microdialysis sampling with microchip electrophoresis with electrochemical detection was developed. However, a problem with this interface was found, for the analysis of high ionic

strength samples such as those used for *in vivo* sampling. The microdialysis sample failed to inject into the separation channel when the sample and background electrolyte had significantly different conductivities. Chapter 6 addressed this problem using COMSOL modeling, and a new microchip design was developed. Both the old and new designs were evaluated using computational and experimental methods. The new bow-microchip design was able to inject highly conductive artificial cerebral spinal fluid into a separation channel filled with the low conductivity buffer MES.

7.2 Further Optimization of Bow-microchip Design

The bow−microchip design could be improved in two ways 1) increasing the field strength in the separation channel without changing the applied voltage and 2) reducing the number of physical grounds. The current design, shown in Figure 6.3, requires the use of two physical grounds and has a significant voltage drop before the separation junction, which decreases the field strength in the separation channel. If the injection interface is moved closer to the voltage source the field strength in the separation channel will increase without changing the applied voltage. Also, if one of the side arm channel's dimensions is decreased and connected to the separation channel's ground than only one physical ground will be necessary, but the overall electrical resistance in the side arm channel will not change. This proposed microchip design is shown in Figure 7.1.

The flow splitter employed in the current design has the majority of the microdialysis sample flow being shunted to waste. An alternative to the current design is to interface a portion of this sample to a droplet generator, similar to those described in Section 2.4.1. The droplets could then be collected and analyzed at a later date using either derivatization and fluorescence

detection or mass spectrometry. The use of additional analytical methods for one microdialysis study could be used to confirm the electrochemical data or to detect analytes that are not electroactive.

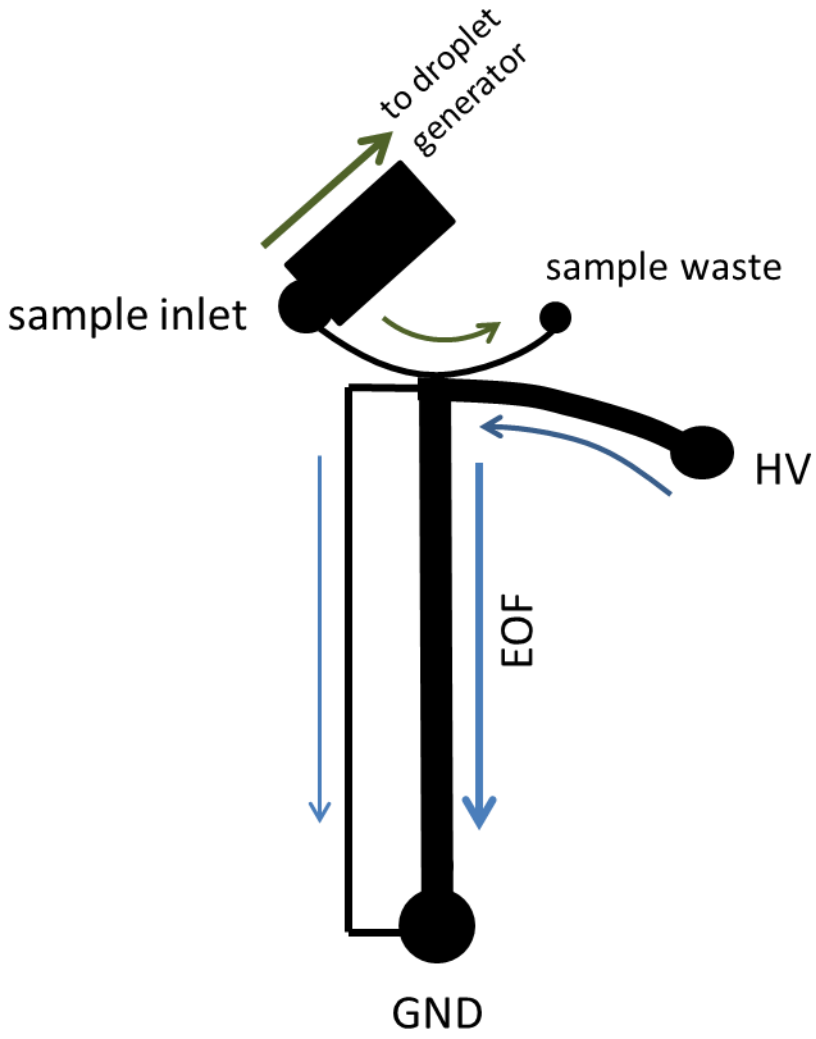

Figure 7.1: Schematic of proposed bow microchip design to both simplify and increase functionality.

7.3 Improving Electrochemical Detection

While the studies performed in Chapter 5 of this thesis describe a simple method for the construction of a low noise carbon electrode fabricated in PMMA, there are modifications that may improve the limits of detection. It has been shown that using an array of narrow electrodes (< 25 μm), instead of one large electrode, lowers the LOD [1-3]. The dimensions of the electrodes in the present design are limited to 100 microns, due to the size of trench that can be etched using the CO_2 laser system. A different fabrication method to make the trenches, such as a computer numerical control (CNC) machine, would make it possible to fabricate an array (2-5) of smaller (10-25 μm wide) electrodes

The addition of ionic liquids (IL) to increase the conductivity of PMMA has been investigated by others for applications of energy storage [4]. ILs have also been used with carbon paste to improve electron transfer rates [5-9]. The addition of an ionic liquid to the graphite/PMMA composite developed in Chapter 5, may lead to an improvement of the electrode's performance.

7.4 Microdialysis with Bow-microchip and an Integrated Graphite/PMMA Composite Electrode

Once the bow-microchip design has been optimized and the GPCEs have been fabricated to be an array, the next step would be to optimize the electrophoretic separation of microdialysis samples for nitrite. Preliminary on-animal experiments will be conducted by affixing a nitroglycerin patch to the skin of a sheep. The nitroglycerin will be absorbed into the skin and generate nitric oxide, which will degrade into nitrite. A linear MD probe will be implanted subcutaneously in a sheep. The resulting microdialysate will be interfaced to the bow-microchip,

analytes will be separated and detected using ME and amperometric detection, all on animal with our miniaturized system, shown in Figure 2.7. By using a subcutaneous probe these preliminary experiments can evaluate the system without needing to sacrifice the animal.

Once the system has been proven with the nitroglycerin patch, the next experiments will involve detection of dopamine and its metabolic pathway in the brain. Optimization of the separation of of L-tyrosine, L-3, 4-dihydroxyphenylalanine (DOPA), homovanillic acid (HVA), 3, 4-dihydroxypenylacetic acid (DOPAC), and dopamine (DA) using ME-EC is currently being done in our lab. Once the separation is optimized, the proven on-animal system can be used with cannula MD probes implanted in the sheep brain. Initially, L-DOPA will be administered to the animal and the change in dopamine will be monitored concurrently with behavior.

7.5 References

[1] Holcomb, R. E., Kraly, J. R., Henry, C. S., *Analyst* 2009, *134*, 486-492.

[2] Amatore, C., Da Mota, N., Sella, C., Thouin, L., *Anal. Chem.* 2008, *80*, 4976-4985.

[3] Johnson, A. S., Selimovic, A., Martin, R. S., *Electrophoresis* 2011, *32*, 3121-3128.

[4] Kim, H. S., Kum, K. S., Cho, W. I., Cho, B. W., Rhee, H. W., *J. Power Sources* 2003, *124*, 221-224.

[5] Zheng, J. B., Zhang, Y., Yang, P. P., *Talanta* 2007, *73*, 920-925.

[6] Wang, Y., Xiong, H. Y., Zhang, X. H., Wang, S. F., *Microchim. Acta* 2010, *169*, 255-260.

[7] Ensafi, A. A., Rezaei, B., Krimi-Maleh, H., *Ionics* 2011, *17*, 659-668.

[8] Svancara, I., Walcarius, A., Kalcher, K., Vytras, K., *Cent. Eur. J. Chem* 2009, *7*, 598-656.

[9] Maleki, N., Safavi, A., Tajabadi, F., *Anal. Chem.* 2006, *78*, 3820-3826.